Title
Expression and function of microRNAs during Xenopus development

Author
McGann, James Christopher

Publication Date
2009

Peer reviewed|Thesis/dissertation

Expression and function of microRNAs during Xenopus development

by

James Christopher McGann

A dissertation submitted in partial satisfaction
of the requirements for the degree of
Doctor of Philosophy
in
Molecular and cell biology
in the
Graduate division
of the
University of California, Berkeley

Committee in charge:

Professor Richard M. Harland
Professor Sharon L. Amacher
Professor Michael A. Levine
Professor Marvalee H. Wake

Fall 2009

Expression and function of microRNAs during *Xenopus* development

! 2009

by

James Christopher McGann

Abstract

Expression and function of microRNAs during *Xenopus* development

By

James Christopher McGann

Doctor of Philosophy in Molecular and Cell Biology

University of California, Berkeley

Professor Richard M. Harland, Chair

MicroRNAs are approximately 22-nucleotide non-coding RNAs that are important regulators of diverse biological processes. I have developed and adapted methods to study the precise function of individual microRNAs during embryonic development of the African frog, *Xenopus*. I began by developing an in situ hybridization protocol to study the spatiotemporal expression patterns of microRNAs during embryogenesis. Using digoxigenin-labeled probes complementary to the primary microRNA sequence I was able to determine tissue-specific expression patterns. These included numerous conserved expression patterns between *Xenopus* and other vertebrates, including *miR-9* and *miR-124* (central nervous system), *miR-1* and *miR-133* (muscle), and *miR-10c* (posterior mesoderm), as well as novel expression patterns for conserved microRNAs such as *miR-23b* and *miR-24a*. This method can also distinguish the unique expression patterns for different members of a microRNA family.

From this analysis, I selected two microRNAs for further functional studies. *miR-24a* is expressed in the neural retina during its development, and blocking the function of *miR-24a* with an antisense morpholino results in a small eye phenotype. I show that this reduction in eye size is not due to changes in patterning, specification, differentiation, or proliferation, but is due instead to an increase in programmed cell death (apoptosis). I have identified two genes important for apoptosis, *caspase9* and *apaf1*, that are regulated targets of *miR-24a*. Caspase9 protein levels are increased when *miR-24a* is knocked down, *caspase9* inhibitors can specifically rescue the knockdown phenotype, and *miR-24a* is able to rescue *caspase9*-induced apoptosis. These data strongly suggest that *miR-24a* is required in the developing neural retina to repress apoptosis by regulating *caspase9* and *apaf1*.

The second microRNA that I have done extensive functional studies on is *miR-133b*, which is expressed in somitic mesoderm and developing hypaxial myoblasts. Knockdown of *miR-133b* causes a reduction in markers of hypaxial muscle differentiation without affecting specification, migration, or proliferation. At late stages, embryos lacking *miR-133b* function have increased levels of apoptosis in hypaxial domains and a severe reduction in body wall and head muscles derived from hypaxial myoblasts. Overexpression of *miR-133b* causes premature differentiation but has no effect on myoblast proliferation. Animal caps injected with the myogenic factor *myoD* or *activin* can induce *miR-133b* and may be useful as a

secondary experimental system to identify *miR-133b* targets. Several computationally predicted targets are identified and discussed.

While computational predictions have become the standard method for identifying potential microRNA targets, the algorithms used to make these predictions are flawed in many ways. To ensure that I was investigating biologically relevant targets, I have attempted several different biochemical purification techniques aimed at isolating microRNA:mRNA duplexes *in vivo*. I have had little success with microRNA-directed RT-PCR or digoxigenin-labeled pre-microRNA immunopurification, but I am encouraged by results using biotin-labeled mature microRNAs for purification. Future refinements to this protocol must be completed before a screen for *miR-133b* targets is initiated.

To everyone who inspired my curiosity

Table of Contents

List of Figures

Acknowledgements

No words can adequately express the amount of gratitude I have for everyone who helped make this experience challenging, fulfilling, and successful.

I am extremely grateful to:

Maggie

My #1 Fan. My #1 Critic. I needed both.

P.S. I love you

My family

For all the love and support

My advisor

For the freedom to follow my instincts, and the advice to make it work

My labmates

For rigorous scientific discussions and equally rigorous merriment

My friends

For bringing balance to my life

Chapter 1

Introduction

When I began this project, next to nothing was known about microRNAs during vertebrate development except that they existed and were likely important. Exploring the functions of this fascinating class of genes seemed both a large challenge and an enormous opportunity. Both these predictions have been borne out. We now know that microRNAs (miRNAs) are important regulators of numerous developmental processes in all metazoans. Yet despite years of effort, we have only just uncovered the tip of the iceberg. I hope that the groundwork I have helped to lay provides for many future discoveries.

MicroRNA history

The first miRNA was identified in *C. elegans* from a forward genetic screen for developmental timing mutations (Lee et al., 2004). A single allele was isolated of *lin-4* that caused larval tissues to endure at the expense of adult structures being formed. This was in contrast to another developmental timing gene, *lin-14*, a transcription factor whose loss-of-function alleles conferred the opposite phenotype, with lineages skipping larval stages and going directly to adult cell types. *Lin-14* also had gain-of-function alleles that phenocopied the *lin-4* mutation, and these were all found to be deletions of the 3' untranslated region. Genetic analysis found that *lin-14* was epistatic to *lin-4* and could rescue the defects caused by *lin-4* mutations. Several years of effort at cloning the *lin-4* gene resulted in a functional fragment of only 22 bases that was found to be complementary to several sites in the *lin-14* 3'UTR. This initial report of a small, non-coding regulatory RNA was thought to be worm-specific, because no *lin-4* homologues were found outside the nematodes.

Another screen for developmental timing mutants in *C. elegans* turned up a second miRNA, *let-7*, which is highly conserved throughout Metazoa (Ruvkun et al., 2004). This opened the floodgates for investigating the extent to which small, noncoding RNAs were expressed and regulating various biological processes. This coincided with the sequencing of several animal genomes, notably the human genome, and bioinformatics searches for the characteristic secondary RNA structure revealed the presence of many hundreds of possible miRNA genes in each species (Griffiths-Jones, 2006).

MicroRNA biogenesis

Most animal miRNAs, like protein-coding genes, are transcribed by RNA polymerase II from promoters that are regulated by the transcription machinery and various transcription factors. These transcripts, called primary microRNAs (pri-miRNA), can have more than one mature miRNA located in them, and several clusters of miRNAs are expressed in this way (He et al., 2005). The most salient feature of these transcripts is the presence of an RNA secondary structure called a 'stem-loop,' in which the mature

miRNA forms imperfect Watson-Crick pairs with down- or up-stream sequences (the stem) with a bulge of 4-10 unpaired nucleotides in between (the loop) (Bartel, 2004). This structure is recognized by the RNAse-III enzyme Drosha, which cleaves away all but the stem-loop of the pri-miRNA into an approximately 70-bp preliminary microRNA (pre-miRNA) with a two-nucleotide 3' overhang(Lee et al., 2002). Several intronic miRNAs (miRtrons) have been shown to bypass processing by Drosha because the splicing machinery also can produce a pre-miRNA(Ruby et al., 2007). Pre-miRNAs are exported from the nucleus into the cytoplasm by Exportin5, where they are then cleaved by another RNAse-III enzyme, Dicer, which removes the loop and leaves an imperfectly double-stranded RNA with two-nucleotide overhangs on both 3' ends that is between 21 and 25 nucleotides in length (Hutvagner et al., 2001; Lund et al., 2004). From this duplex, usually only one strand is incorporated into the RNA-induced silencing complex (RISC), and the mature miRNA is almost always the strand with the less stable 5' end (Khvorova et al., 2003).

Regulatory mechanisms of microRNAs

While much is known about the biogenesis of miRNAs, there is still a great deal of controversy surrounding the mechanism by which they regulate their target mRNAs. In plants, the entire length of microRNAs is perfectly complementary to 3'UTR sequences of their targets, and the RISC complex hydrolyzes both the microRNA and the mRNA (Bartel, 2004). This also occurs in animals when completely perfect target sites exist, but this is rare. Most animal mRNA targets experience imperfect base-pairing with nucleotides 2-8 of the miRNA, the so-called 'seed region' (Bartel, 2009). It is thought that the more complementary a target site is, the more likely it will form a miRNA:mRNA duplex and direct RISC activity. However, several studies have shown that exact seed region pairing is not necessarily required (Brennecke et al., 2005; Vella et al., 2004). Most target sites are located in the 3'UTR of mRNA, but some examples of 5'UTR or coding target sites have been identified (Lytle et al., 2007; Place et al., 2008). Once the miRNA directs the RISC to its target mRNA, protein synthesis is inhibited by repressing translation or by deadenylation and degradation of the transcript, or both. There appears to be no correlation between the extent of microRNA:mRNA complementarity and the mechanism of repression.

A critical component of the RISC complex is a member of the Argonaute (Ago) family of proteins (He and Hannon, 2004). This family is defined by the presence of a PAZ and a Piwi domain, and mutations in *Ago* genes abolish miRNA-induced repression (Carmell et al., 2002). GW182 proteins are also present in RISC and are necessary for miRNA-induced repression, interacting directly with Ago proteins (Liu et al., 2005). Both Ago and GW182 proteins repress protein synthesis when artificially tethered to the mRNA 3'UTR, suggesting that these components are the effectors of translational repression, while the miRNAs provide the target specificity (Rehwinkel et al., 2005).

Several mechanisms by which the RISC represses translation have been put forward by different groups (He and Hannon, 2004). Originally, it was found that *lin-4* caused *lin-14* to be found in polysomes, which argued that repression occurs post-initiation (Olsen and Ambros, 1999). This could be due to inhibition of elongation, premature termination, or by degradation of nascent polypeptides. More recently, the

preponderance of data suggests that repression occurs instead by blocking initiation of the ribosome (Humphreys et al., 2005; Pillai et al., 2005). These studies find that miRNA repression requires the 5' cap but not polyadenylation, and does not inhibit IRES-directed translation. Therefore inhibiting recognition of the 5' cap or preventing the interaction with the 60S subunit are possible hypotheses for the mechanism of initiation repression. Any or all of these mechanisms might contribute to miRNA-mediated translational repression, and it remains to be seen whether and how they are context-dependent.

In addition to repressing translation, miRNAs have been shown to function by causing deadenylation and therefore higher turnover of their target mRNAs (Bagga et al., 2005; Giraldez et al., 2006; Wu et al., 2006). This function is thought to explain their presence in P-bodies, cytoplasmic foci responsible for storing or degrading nontranslated mRNAs. Both Ago and GW182 proteins are found in P-bodies, and several P-body components have been implicated in miRNA-mediated repression (Liu et al., 2005). miRNAs have been shown to recruit deadenylation and decapping enzymes, which leads to degradation of the target mRNA by ubiquitous exonucleases (Eulalio et al., 2008). miRNA-directed deadenylation and degradation does not require translation (Eulalio et al., 2009). Because the converse is also true (miRNA-directed translational repression does not require polyadenylation) (Kiriakidou et al., 2007), it appears these two mechanisms are independent of one another, though further investigations into what regulates the decision between the two (cell context, mRNA characteristics, miRNA, etc.) are ongoing.

MicroRNAs are necessary for embryogenesis

Once the role of Dicer as a critical enzyme in the maturation of all microRNAs was appreciated, *dicer1* knockouts were made in mouse. *Dicer1* is required for viable mouse embryonic stem cells, and embryos null for *dicer1* die early in development and are depleted of stem cells (Bernstein et al., 2003). These results indicate that microRNAs are required for stem cell survival and early embryogenesis. Subsequent conditional *dicer1* knockouts have shown that microRNAs are necessary for angiogenesis, limb morphogenesis, skeletal muscle development, germline development, pancreatic islet cells, lymphocyte development, neuronal differentiation, and many more developmental processes (Bernstein et al., 2003; Davis et al., 2008; Koralov et al., 2008; Lynn et al., 2007; Murchison et al., 2007; O'Rourke et al., 2007; Yang et al., 2005). MicroRNA expression cloning and in situ hybridization patterns during early mouse development suggest functional roles for individual microRNAs in numerous developing tissues, including the liver, brain, lung, skeletal muscles, and heart (Kloosterman et al., 2006; Sempere et al., 2004).

The maternal-zygotic *dicer* mutant characterized in zebrafish did not have as severe a phenotype as that in mice, resulting in normal axis formation and tissue regionalization of brain segments, pigment cells, hatching gland, heart, notochord, somites, and blood (Giraldez et al., 2005). However, gastrulation, somitogenesis, brain development, and heart development were severely impaired, and the embryos dyed shortly after hatching. Though one microRNA (*miR-430*) was able to rescue the brain morphogenesis defects, other microRNAs must be essential for the remaining processes still perturbed in the *dicer* mutant. Expression studies in zebrafish also strongly suggest

functional roles for individual microRNAs during development (Kloosterman et al., 2006).

Many subsequent publications have demonstrated the important functions that microRNAs have during embryonic development in mouse and fish. In order to study the evolution of microRNAs, however, an additional system is necessary. The African frog, *Xenopus*, has been a model system for developmental biology for over a century and represents an evolutionary step between fish and mammals, and is therefore well-suited to comparative studies of microRNA function. Furthermore, novel investigations of microRNA functions have been carried out in *Xenopus* that demonstrate the value and effectiveness of pursuing microRNA studies in this model system.

Xenopus microRNA studies

Very few reports concerning miRNA function in *Xenopus* had been published when I began my studies. The first was an article by Watanabe et al., which cloned small RNAs from oocytes and embryonic stages up to tadpole stages (Watanabe et al., 2005). They found many conserved miRNAs and were the first to suggest that developmentally specific expression might equate to specific functions during embryogenesis. This report was the springboard for my subsequent studies because it showed me not just that miRNAs were differentially expressed in *Xenopus*, but that they were experimentally tractable.

Since then, *Xenopus* miRNA studies have continued to focus on their functional roles during embryogenesis. *Xenopus* was used to show that the muscle-specific phenotype for *miR-133* and *miR-1* overexpression was conserved from the mammalian cell culture system the authors used for the majority of their analysis (Chen et al., 2006). The role for miRNA regulation in the induction of Spemann's organizer early in development was explored by Martello et al., who found that miR-15 and miR-16 target the Nodal receptor, Acvr2a, limiting the size of the organizer (Martello et al., 2007). Remarkably, knocking down *miR-15* and *miR-16* was able to induce an organizer in a completely ventralized embryo, suggesting that miRNAs play a key role in the proper specification and patterning of the embryo.

Both this investigation and a more extensive genomics-level analysis by Tang and Maxwell reported differences in the expression pattern of a pri-miRNA and its mature miRNA, indicating that miRNA processing can be regulated by the embryo (Tang and Maxwell, 2008). How widely this process occurs, at what biochemical stage, and by what mechanism, are all very much open questions. However, this observation does indicate that care must be taken to accurately describe expression patterns regardless of the method used to generate them. Tang and Maxwell also provided the first computational search for miRNAs in the *X. tropicalis* genome and EST databases, which significantly increased the number of potential miRNAs available for functional study (Tang and Maxwell, 2008).

Reports then emerged investigating the role of miRNAs during *Xenopus* eye development. Decembrini et al. inactivated Dicer in the retina and found that this delayed cell cycle exit and differentiation gene activation, leading to apoptosis and a smaller, disorganized eye (Decembrini et al., 2008). *MiR-196* overexpression also causes eye defects (Qiu et al., 2009), although because *miR-196* is not expressed in the eye, the

results of this study do not reflect in vivo organogenesis. As an organ whose specification, patterning, and differentiation are highly regulated, whose function is not required for viability, and whose phenotypes can be morphologically obvious, the eye remains a strong candidate for functional miRNA studies.

The most abundant miRNA in early *Xenopus* development is *miR-427*. Rosa et al. suggest that this miRNA targets both *nodal* antagonists (*leftyA* and *leftyB*) and agonists (*xnr5* and *xnr6b*) (Rosa et al., 2009). However, inhibition of *miR-427* resulted in the inhibition of general mesoderm induction, especially repressing dorsal mesoderm, suggesting that the more important in vivo targets are the nodal antagonists. To prove that this was the primary role of *miR-427*, they blocked the putative target sites on both the *lefty* transcripts, which recapitulated the knockdown of *miR-427*. These data contrast with another group that has studied the effects of *miR-427* knockdown; Lund et al. suggest that *miR-427* is the functional equivalent in *Xenopus* of the zebrafish *miR-430* (Lund et al., 2009). The zebrafish *miR-430* miRNA plays a global role in degrading maternal transcripts after the maternal-to-zygotic transition (MZT) (Giraldez et al., 2006). Lund et al. find that *miR-427* is required for the deadenylation of *cyclinA1* and *cyclinB2* transcripts after MZT in *Xenopus*, and hypothesize that it regulates many other maternal mRNAs in the same manner. While these roles for *miR-427* are not necessarily irreconcilable (an early role for maternal mRNA clearance, a later role for the control of *nodal* signaling), I have noticed knockdown phenotypes can be interpreted differently by different groups depending on the mechanistic interest of the lab. A possible explanation for this phenomenon may be that computational predictions of putative targets for any given miRNA can contain hundreds of transcripts (Griffiths-Jones et al., 2006). Verification of these putative targets must necessarily rely on some subjective selection criteria, leading to potential target bias. To avoid this bias, biochemical techniques are needed, a subject that is addressed in Chapter 6.

The most recent publication concerns the role of *miR-30* during kidney development. Agrawal et al. show that *miR-30a* is expressed in the kidney and its knockdown results in pronephric defects, including abnormal patterning, delayed differentiation, and edema (Agrawal et al., 2009). They find that *miR-30a* regulates *xlim1* and is necessary for its proper degradation during late kidney development.

This brief review of work in *Xenopus* demonstrates that much like transcription factors, miRNAs as a gene class can regulate a wide variety of developmental processes, including cell cycle regulation, apoptosis, tissue specification, terminal differentiation, etc., depending upon the identity of their targets (He et al., 2007b; Hino et al., 2007; Rosa et al., 2009). And just as *Xenopus* has proved to be a useful system for the study of transcription factors during development, these and other studies show it has the potential to be just as useful for exploring the roles of miRNAs.

Goals of this thesis

The first goal of this thesis was to identify tissue-specific expression patterns for miRNAs during embryogenesis in *Xenopus*. The second goal was to characterize the developmental function of a subset of these genes. To fulfill these goals, I have adapted previous molecular techniques to the particularities of miRNAs, including *in situ* hybridization, antisense morpholino oligonucleotide knockdown, and RNA

overexpression. In Chapter three, I discuss the protocol that I have developed for *in situ* hybridization on pri-miRNAs to identify tissue-specific expression patterns, showing miRNAs with conserved and novel expression patterns. In Chapter four, I show that miR-24a is required to prevent programmed cell death in the neural retina by targeting the pro-apoptotic genes *caspase9* and *apaf1*. Chapter five focuses on the role of *miR-133b* during hypaxial muscle development, where it regulates the terminal differentiation of the migrating myoblasts of the trunk and head. Finally, Chapter six describes my preliminary investigations into several methods for the biochemical isolation of miRNA targets.

Chapter 2

Methods

General *Xenopus* methods

Xenopus laevis embryos were generated and cultured by standard methods (Sive et al., 2000). Embryos were allowed to develop in 1/3X Marc's Modified Ringer (MMR) solution and staged according to the normal table of Nieuwkoop and Faber (1967). *Xenopus tropicalis* embryos were generated and cultured as described in http://tropicalis.berkeley.edu/home. *X. tropicalis* embryos were allowed to develop in 1/9X MMR and staged according to the normal table of Nieuwkoop and Faber (1967).

Whole-mount in situ *hybridization (Chapters 3-5)*

Embryos were allowed to develop until the desired stage and then fixed for two hours in MEMFA (0.1M MOPS pH7.4, 2mM EGTA, 1mM $MgSO_4$, 3.7% v/v Formaldehyde) (Sive et al., 2000). *In situ* hybridizations were carried out with RNA probes labeled with digoxigenin-UTP using a multibasket technique previously described (Sive et al. 2000).

Whole-mount antibody staining (Chapters 4 and 5)

Embryos were allowed to develop until the desired stage and then fixed for two hours in MEMFA. The anti-phospho-histone3 antibody (Upstate Biotechnology) was used at a 1:1000 dilution in 10% goat serum in 2mg/ml BSA in PBS plus 0.1% TritonX-100 (PBST). A goat anti-rabbit IgG secondary conjugated to HRP (BioRad) was used at a dilution of 1:1000 in PBST. The muscle-specific 12/101 monoclonal antibody was used to visualize differentiated skeletal muscle (Kintner and Brockes, 1984) (Harland Lab). Monoclonal hybridoma cell supernatant was diluted 1:1 into PBST following a standard immunohistochemistry procedure (Sive et al. 2000). Either a goat anti-mouse IgG conjugated to HRP (BioRad) or a fluorescent moiety (AlexaFluor555, Invitrogen) was used as a secondary antibody at a 1:500 dilution. In cases where both *in situ* hybridization and 12/101 staining were carried out on embryos, *in situ* staining was performed first, followed immediately by immunohistochemistry.

Whole-mount TUNEL staining (Chapters 4 and 5)

TUNEL staining was performed as in Hensey and Gautier (Hensey and Gautier, 1997), using NBT/BCIP (Roche) as the staining substrate.

Microinjection of antisense morpholinos (Chapters 4 and 5)

Antisense and control morpholinos (MOs) were ordered from Gene Tools, LLC designed to block the mature microRNA and the ~5nt of the loop sequence. The following sequences were used: miR-24aMO, 5'CTGTTCCTGCTGAACTGAGCCAGTG3', miR-24ammMO, 5'CTGTTCCTGCTGAACACAGGGAGTG3', and *miR-133b*MO 5'TAGCTGGTTGAAGGGGACCAAACCT3'. Stock solutions were suspended at 2mM in DEPC-treated water. Initially, 10, 20, 40, and 80ng of antisense MO were injected into

1 cell at the 2-cell stage. 20ng was determined to be the optimal dose for miR-24aMO and 15ng was determined to be the optimal dose for *miR-133b* and these were subsequently used for injection.

mRNA synthesis and microinjection (Chapters 4 and 5)

Synthetic mRNA was made using the mMessage mMachine SP6 or T7 kit (Ambion). The synthesized mRNA was resuspended as a stock solution in DEPC-treated water at a concentration of 1mg/ml. Working solutions were diluted in DEPC-treated water so that 10nl would give the concentrations noted. 10nl (of each mRNA solution) was injected into both cells at the two-cell stage using a Picospritzer (General Valve) with. Fluorescent protein, *caspase9*, *myoD*, and *activin* injections were targeted to the animal region of the cell.

Formation and microinjection of duplexed microRNAs (Chapters 4 and 5)

Short RNAs were ordered from Integrated DNA Technologies as miR-24aTop (5'GUGCCUACUGAACUGAUAUCAGU3') and miR-24aBot (5'UGGCUCAGUUCAGCAGGAACAG3'), combined and diluted to a stock concentration of 1μg/μl, heated to 80°C for one minute, and then allowed to cool to room temperature to form duplexes. The same was done for miR-24mmTop (5'GUGGGUACUGAACUGAUAAGAGU3') and miR24mmBot (5'UCUCUCAGUUCAGCACCAACAG3') to get duplexed miR-24a mismatch RNA (miR-24amm), and *miR-133b*Top (5'UUGGUCCCCUUCAACCAGCUA3') and *miR-133b*Bot (5;GCUGGUCAAACGGAACCAAUU3') to get duplexed *miR-133b* RNA. Working solutions were diluted in DEPC-treated water so that 10nl would give the concentrations noted. 10nl of *miR-133b* solution was injected into one cell at the two-cell stage using a Picospritzer (General Valve), targeting the medial-lateral region of the cell. MiR-24a and miR-24amm injections were injected into both cells at the two-cell stage and targeted to the animal region of the cell.

Microinjection of Caspase inhibitors (Chapter 4)

Caspase inhibitors ordered from CalBiochem were Caspase1inhibitor I (Ac-YVAD-CHO), Caspase3 inhibitor II (Z-DEVD-FMK), Caspase inhibitor I (Z-VAD-FMK) and Caspase9 inhibitor III (Ac-LEHD-CMK), all used at 1ng per injection. Stocks were diluted in DMSO or distilled water.

Hydroxyurea treatment (Chapter 4)

Hydroxyurea (Sigma) was diluted in 1/3x MR solution to a final concentration of 15mM and embryos treated from 2 hours post-fertilization until stage 10.5, then fixed in MEMFA (Sive et al., 2000).

RT-PCR (Chapters 4-6)

RT-PCR was performed as in Fletcher and Harland (2008). Photographs were taken by Image-Pro Plus software with a Leica DFC480 camera mounted on a Leica MZFLIII stereomicroscope. The following primers were used: 5'GGACCTGTCCTCTTGTGCC3' and 5'GCTCAAGGGCCCGACTC3' for pri-*miR-24a*, 5'CGGGATGGATTTGTTGCA3' and 5'TTGAACCAGACCTGGACT3' for *otx2*,

5'GTCAATGATGGAGTGTAT3' and 5'TTCCATTCCGCTCTCCTGAG3' for *ornithine decarboxylase* (ODC), 5'CAGAATGCGCTCCTTTCACTTTG3' and 5'AAGTAGCTCACGATTCTCTCTAC3' for *caspase9*, 5'TCTCACTCTCTCTTACAGGGGGAC3' and 5'TCTTGTGCCTTATGTGGTTGGG3' for *pax3*, 5'CTCAAAAGATGCACCACTACAAAC3' and 5'CTAGATAAGCAGTCAAGGCTGG3' for *myf5*, 5'GCCGACAGGAGGAAGGCCGCCAC3' and 5'CTGTAGAAGCTGCTGTCGTAGCTG3' for *myoD*, 5'TTAGGAACAGGAGTAGGAGGGGAG3' and 5'ATCTTGGCTGGGGGCTATTG3' for pri-*miR-133b*, 5'GCTGACAGAATGCAGAAG3' and 5'TTGCTTGGAGGAGTGTGT3'for *cardiac actin*, 5'GTGGCACCCCTCTTAAGGGC3' and 5'TTCCAGTGGGCACAATAGGT3' for *p27(Xic1)*, 5'CAGATTGGTGCTGGATATGC3' and 5'ACTGCCTTGATGACTCCTAG3' for *ef1alpha*, and 5'CAGAAGAACGGCATCAAG3' and 5'GAACTCCAGCAGGACCATGT3' for *dsGFP*.

Vibratome sectioning (Chapter 3)

Whole mount in situ hybridization was performed on embryos before sectioning. Embryos were rehydrated in a step-wise fashion in PBS plus 0.1% Tween-20. Embryos were embedded in a gelatin/albumin mix (PBS, 18% Sucrose w/v, 27% BSA, 0.44% gelatin) that was hardened after addition of 25% glutaraldehyde (30uL per 500ul gelatin mix) (Adapted from Martyn Goulding, Salk Institute). Embryos were sectioned at 100 microns using a vibratome (Technical Products International, Inc.), then mounted on a slide with water and a coverslip.

Cryosectioning (Chapters 4 and 5)

Embryos were fixed in 4% paraformaldehyde in PBS for 2 hours to overnight, rinsed in PBS three times for five minutes, and then incubated overnight in 30% sucrose in PBS. They were then transferred to OCT Compound (Tissue-Tek) in plastic molds and frozen on dry ice and kept at –80°C. Sections were cut using a Microm HM550 cryostat and put on glass slides pre-coated with a Fro-Tissuer pen (Electron Microscopy Sciences) and dried overnight. All sections are 20µm thick unless otherwise noted.

Hematoxylin and eosin staining of cryosections (Chapter 4)

Slides were stained with Hematoxylin and Eosin (H&E) by incubating in Accustain Harris Hematoxylin (Sigma) for five minutes; after rinsing with tap water for one minute, they were incubated in acidic ethanol (2% concentrated HCl) for one minute, tap water for one minute, stained in Accustain Eosin Y (Sigma) for three minutes, and then dehydrated in 75%, 95%, and 100% ethanol for one minute each. Finally, slides were transferred to Histo-clear (Sigma) and mounted with Permount (Fisher). Photographs were taken by Leica Firecam software with a Leica DFC500 camera mounted on a Zeiss Axioplan compound microscope.

Immunohistochemistry on cryosections (Chapter 4)

The 40.2D6 antibody developed by TM Jessell, and the XAP-1 and XAP-2 antibodies developed by DS Sakaguchi and WA Harris were obtained from the Developmental Studies Hybridoma Bank developed under the auspices of the NICHD and maintained by the University of Iowa, Department of Biological Sciences, Iowa City, IA 52242. For phosphorylated histone 3 (Upstate) and islet-1 staining (40.2D6), TBS (155mM NaCl, 10mM Tris-Cl, pH 7.5) was used. For XAP-1 and XAP-2 antibodies, PBS was used. After sectioning, slides were washed three times for five minutes in TBS, then once in TBST (TBS, 0.1% Triton X-100, 2mg/ml BSA). They were then blocked for one hour with 10% goat serum in TBST. Antibody was added to blocking solution at a concentration of 1:1000 overnight at 4°C. Then slides were washed five times for five minutes each in TBST, and incubated in secondary antibody (AlexaFluor goat anti-mouse IgG or IgM (for XAP-1) 488 or 555, Invitrogen) at 1:200 in TBST overnight at 4°C. Slides were then washed five times for five minutes in TBST. DAPI was added in the last wash and then slides were mounted with Aqua Poly/Mount (Polysciences, Inc.). After drying, photographs were taken by Leica Firecam software with a Leica DFC500 camera mounted on a Zeiss Axioplan compound microscope using epifluorescence.

Nuclei counting (Chapter 4)

Cryosection photographs were analyzed for phospho-histone3-positive cells or TUNEL-positive cells by counting all stained nuclei in all areas of the eye in all sections that had undamaged tissue for both uninjected and injected eyes. P values were obtained using the paired student's t-test.

Western Blotting (Chapter 4)

Embryos were injected in both cells at the two-cell stage with 20ng 24aMO or 24ammMO and cultured until stage 28. Heads were dissected away from bodies and homogenized in homogenization buffer (250mM Sucrose, 5mM Hepes 6.8, 1mM EDTA, and 1mM PMSF) and centrifuged three times at 14000rpm, keeping the supernatant. Lysates were stored in 1X Laemmli buffer, run on 10% acrylamide gels, transferred to nitrocellulose using a semi-dry apparatus and blocked with 5% BSA in TBS+0.1%Triton. Anti-Actin antibody (Santa Cruz Biotechnology #H3105) was used at 1:4000 and Anti-Caspase9 antibody (Abcam ab25758) at 1:200 incubated overnight. Secondary antibody (Jackson Immunoresearch, HRP-conjugated donkey anti-rabbit IgG) was used at 1:5000 for 1 hour. Actin runs at ~45kD and full-length Caspase9 at ~47kD.

Northern Blotting (Chapter 6)

Agarose gels were made with 0.9% agarose in 18% formaldehyde buffered with 1x running buffer (200mM MOPS, 8mM sodium acetate, and 1mM EDTA). Samples were mixed with 5X SB loading buffer (Ambion), formaldehyde (5% of final volume), 1ug ethidium bromide (EtBr) and formamide (50% of final volume), loaded into wells, and run overnight at 12V. in 1X running buffer. After soaking the gel in several changes of 0.5M Na_2HPO_4 for two hours, the gel was placed top-down in a glass transfer dish, covered by Hybond membrane, two sheets of Whatman paper, and a two-inch thick stack of paper towels. A glass plate and a moderate weight were placed on top of the stack to transfer overnight.

Polyacrylamide gels were made with 12% acrylamide, bis-acrylamide mixture (29:1) in 1X TBE with 7M urea and polymerized by adding ammonium persulfate and TEMED. Samples were mixed with SB loading buffer (Ambion) and 1 vol of 7M urea before loading and running in 1X TBE at 20V for 4 hours. Transfer to Hybond membrane was made using a semi-dry apparatus at 5V for one hour.

Probe against mature *miR-133b* was synthesized by reacting 5ug *miR-133b*Bot RNA with TdT enzyme (Invitrogen) overnight with P^{32}-labeled dUTP overnight. Probe was then diluted into 20mL hybridization buffer (350mM Na_2HPO_4, 1% BSA, 15% formamide, 7% SDS). Hybond membranes were crosslinked with UV light, them pre-hybridized for one hour at 37°C in hybridization buffer. Membranes were then transferred to probe and hybridized overnight at 37°C. Membranes were then washed three times for thirty minutes in 150mM Na_2HPO_4 and visualized using film (Kodak) overnight at -80°C.

Animal cap explants (Chapter 5)

Embryos were injected at the two-cell stage and cultured in 1/3X MMR at 12°C until stage 9, then cultured in 3/4X NAM for animal cap isolation according to Sive et al. (2000).

Fluorescent protein quantification (Chapters 4 and 5)

Photographs of injected embryos were taken by Image-Pro Plus software with a Leica DFC480 camera mounted on a Leica MZFLIII stereomicroscope separately under blue light (for GFP) and green light (RFP). All photos from a particular experiment were identically batch-processed using Photoshop (Adobe), adjusting only levels. Using the ImageJ1.34S program (Wayne Rasband, NIH, Bethesda, MD), 0.160 square inches of each photograph (roughly $1/8^{th}$ of an embryo) were measured for average pixel intensity of RFP, and this was repeated for nine embryos in each photograph. Then the identical area of each photograph corresponding to the same embryo was measured for the average pixel intensity of GFP. The ratio between GFP and RFP was then used for comparison. All statistical significance tests were done using the unpaired student t-test.

MicroRNA directed RT-PCR

Five *X. tropicalis* embryos were homogenized in 40uL cell fractionation buffer (250mM Sucrose, 5mM Hepes pH 6.8, 1mM EDTA) with protein inhibitors (PMSF, Sigma) and centrifuged at max speed for 10 minutes at 4°C. The supernatant was collected and 4uL of 10% SDS added and placed on ice for one minute. Then 1mL of pre-chilled first-strand reverse transcription mix (SuperscriptIII, Invitrogen) was added and the reaction raised from 4°C to 37°C gradually over 10 minutes, then incubated at 37°C for one hour. After phenol/chloroform extraction and ethanol precipitation, polynucleotides were resuspended in 100uL second-strand reverse transcription mix (Tth DNA polymerase, Promega) at 25°C for 10 minutes, and then incubated at 70°C for 30 minutes. DNA was then run on an agarose gel and purified with a PCR purification kit (Qiagen). Samples were digested with HaeII enzyme (New England Biolabs) and ligated to an adapter oligo, then re-purified. Samples then were PCR amplified with primers complementary to the adapter and identical to *miR-133b*, then amplified again with nested primers and cloned into TOPOII vector using the TOPO TA cloning kit

(Invitrogen). Random colonies were selected and screened with EcoRI for insert incorporation before sequencing.

Digoxigenin-labeled microRNA extracts

Approximately 100 stage 37 embryos were collected and spun at 1000g at room temperature for 2 min to remove water before cell extract buffer (250mM Sucrose, 5mM Hepes pH 6.8, 1mM EDTA + PMSF and 100U rRNasin) was added. Embryos were homogenized with an eppendorf tube and pestle and spun down at max speed for 10 minutes at 4°C, and the supernatant isolated as cell extract. Dig-labeled pre-miRNA was synthesized from *miR-133b* plasmid by using DIG-dUTP (Roche) in a mMessage RNA transcription kit (Ambion). 50ul of extracts were mixed with 10ug of pre-*miR-133b*, and the mixture incubated at 30°C for 60 min. The sample was phenol/chloroform extracted and products prepared for Northern blot analysis as described.

Biotin-labeled microRNA extracts

Approximately 100 stage 37 embryos were washed twice and suspended in 500uL XB buffer (10mM HEPES pH 7.7, 1mM MgCl, 0.1mM CaCl2, 100mM KCl, 50mM sucrose) with 0.01mg/ml of the protease inhibitors leupeptin, pepstatin, and chymostatin. Embryos were homogenized by a pestle and centrifuged at max speed in a microfuge for 15 min. The supernatant was isolated and used as cell extract. 2ug of 133bMRE, mut133MRE, or 24aMRE RNA were incubated in 50uL of cell extract with or without 5'biotin-labeled mature *miR-133b* or scrambled RNA (5'AGCUACCCCUUUGGUUCAACC3') (Integrated DNA Technologies) at 30°C or indicated temperatures for 60 min. 200uL of XB buffer and 20uL of XB buffer-saturated streptavidin agarose beads (bed volume of 10uL) were added and incubated at 4°C overnight with gentle rotation. Extracts were then centrifuged at 5000g for 30 seconds and the supernatant separated. Beads were washed twice with 500uL XB buffer, then heated to 85°C for 10 min and centrifuged at 5000g for 30 seconds. This supernatant (beads) and the previous supernatant (supernatant) were then phenol/chloroform extracted and prepared for RT-PCR as above.

Plasmid Construction

Expression constructs

24aMRE

A full length clone of destabilized green fluorescent protein (GFP) was obtained from Sharon Amacher (Andreatta et al., 2001). The plasmid was digested by BamHI and NotI and subcloned into a BamHI/NotI digested pCS107 vector. A new polylinker containing BglII, SalI MluI and XbaI sites (with sequence 5'GGCCAAGATCTTAAGACTAGTCGACACGCGTCTAGATCGA3') was inserted into the EagI/XhoI-digested plasmid (3' to the stop codon), making pdsGFP+Linker. This plasmid was cut by BglII and SalI and miR-24aMRE inserted (with sequence 5'GATCCTGTTCCTGCTGAACTGAGCCAGCTAGCCTGTTCCTGCTGAACTGAGC CATCGA3') (Harland Lab Plasmid Database #2501).

Mut24aMRE

To create GFP-mut24aMRE, sequential quickchange PCR was performed on 24aMRE using mut24MRE1F (5'TCCTGTTCCTGCTGAACACAGGGAGCTAGCCTGTTCCTGC3') and its reverse complement and mut24MRE2F (5'GCCTGTTCCTGCTGAACACAGGGATCGACACGCGTCTAGA3') and its reverse complement (#2502).

Casp9UTR

An EcoRI cloning site was added to pdsGFP+Linker using quickchange PCR with Linker+EcoRI oligo (5'CAATGTGTAGGCGGCCAAGAATTCTTAAGACTAGTCGACAC5') and its reverse complement to create pdsGFP+EcoLinker. PCR was performed on a *X. laevis* caspase9 clone (IMAGE:7976131) with Casp9UTR1F (5'CGGAAGCGATTTTACTTTAAGACC3') and Casp9UTR1R (5'CACATGCTTATCCCCAGTGAC3') and the products subcloned using the TOPO-TA cloning kit to make TOPO-Casp9UTR. This plasmid was digested with EcoRI and the insert subcloned into an EcoRI-digested pdsGFP+EcoLinker (#2503).

Casp9mutUTR

Sequential quikchange (Stratagene) PCR was performed using C9mutUTR1 (5'GCTGTGGTTGCCTTGCCCTGGTACAGAAGCAC3') and its reverse complement and C9mutUTR2 (5'CTGTGGTTGCCTTGCCCTCCTACAGAAGCACAAAACATC3') and its reverse complement (#2504).

Apaf1UTR

PCR was performed on a *X. laevis* apaf1 clone (IMAGE:5514901) using primers Apaf1UTR1F (5'GTGCTGAAGCTAATAGAGTGATAACG3') and Apaf1UTR1R (5'CACAGTAGTCTATAAATACCGGAATC3') and the resulting PCR product subcloned using the TOPO-TA cloning kit to make TOPO-Apaf1UTR. This plasmid was digested with EcoRI and the insert subcloned into an EcoRI-digested pdsGFP+EcoLinker (#2505).

Apaf1mutUTR

Sequential quickchange PCR was performed on Apaf1UTR plasmid using primers APmutUTR1 (5'CTGTGCCATTAGGTTCCTTACATAATCAGCCATGTGCAAC3') and its reverse complement and APmutUTR2 (5'GGTTCCTTACATAATCAGGGATGTGCAACATT3') and its reverse complement (#2506).

Katushka RFP

A clone for Katushka RFP was obtained from Evrogen. The plasmid was digested with BamHI and NotI and subcloned into a BamHI/NotI digested pCS107 vector (#2432).

133bMRE

pdsGFP+Linker was cut by BglII and SalI and *miR-133b*MRE inserted (with sequence 5'GATCTAGCTGGTTGAAGGGGACCAAGCTAGCTAGCTGGTTGAAGGGGACCAATCGA3' (#2507).

Mut133bMRE

Sequential quickchange PCR was performed on 133bMRE using primers mut133MRE1F (5'TGCCTTAATAGCTGGTTGAAGGCCAGGAAATCGATTAGCTGGTTGAAGG3') and its reverse complement and mut133MRE2F (5'ATCGATTAGCTGGTTGAAGGCCAGGATCGACACGCGTCTAGATC3') and its reverse complement (#2508).

X. laevis miR-133b

Pre-miRNA was made from a *X. laevis miR-133b* clone (IMAGE:4059686) cut with XbaI (#2509).

Caspase9

Caspase9 mRNA was made from a *X. tropicalis* full-length clone (IMAGE:8961007) cut with AscI (#2510).

Probe Constructs

X. tropicalis id4

PCR was done using a stage 30 cDNA preparation as template for *id4* with primers 5'GCCATGAAAGCTGTCAGTCCAG3' and 5'TTGTTCACCACTAAGGCAGC3'. Products were subcloned into pCRII-TOPO using the TOPO TA cloning kit (Invitrogen) (*X. tropicalis* Harland Lab Database #424).

X. tropicalis foxc2

PCR was done using a stage 30 cDNA preparation as template for *foxc2* with primers 5'CCTGAGCGAACAGAACTACTAC3' and 5'GGGCACCTTGACAAAGCACTC3'. Products were subcloned into pCRII-TOPO using the TOPO TA cloning kit (Invitrogen) (#425).

X. tropicalis let-7a

Genomic PCR products for *let-7a* amplified using primers 5'TGGCGTTCCACACTTGTTAAGAC3' and 5'CTCCCCCATCAAAAGCTCAATAAG3' were subcloned into pCRII-TOPO using the TOPO TA cloning kit (Invitrogen) (#426).

X. tropicalis miR-1a-1

Genomic PCR products for *miR-1a-1* amplified using primers 5'GGAAACATCTTACCTTACAGC3' and 5'CGGCATTTCCACGGAGGCAGG3' were subcloned into pCRII-TOPO using the TOPO TA cloning kit (Invitrogen) (#427).

X. tropicalis miR-7-2

Genomic PCR products for *miR-7-2* amplified using primers 5' GGAGAAAGAAGGTACAGTG 3' and 5'GGCTACAAATGATATTGAAGTG3' were subcloned into pCRII-TOPO using the TOPO TA cloning kit (Invitrogen) (#428).

X. tropicalis miR-9a-1

Genomic PCR products for *miR-9a-1* amplified using primers 5'CACACGGGATTCTGGGAATC3' and 5'GATCCAATCAGATGACTATG3' were subcloned into pCRII-TOPO using the TOPO TA cloning kit (Invitrogen) (#429).

X. tropicalis miR-9a-2

Genomic PCR products for *miR-9a-2* amplified using primers 5'GGAATTGTAGTCTGGGTTTTAG3' and 5'GTCACTTTGGACTGGAATGGG3' were subcloned into pCRII-TOPO using the TOPO TA cloning kit (Invitrogen) (#430).

X. tropicalis miR-9-3

Genomic PCR products for *miR-9-3* amplified using primers 5'CACACGGGATTCTGGGAATC3' and 5'GATCCAATCAGATGACTATG3' were subcloned into pCRII-TOPO using the TOPO TA cloning kit (Invitrogen) (#431).

X. tropicalis miR-10c

Genomic PCR products for *miR-10c* amplified using primers 5'TGCCCTTAGCCTTCTGTCCTTATC3' and 5'TAGCCTAAATGTGCCAGCGG3' were subcloned into pCRII-TOPO using the TOPO TA cloning kit (Invitrogen) (#432).

X. tropicalis miR-18a

Genomic PCR products for *miR-18a* amplified using primers 5'GATAATCCCAAGCATCCTAAAC3' and 5'GAGCAAACAGTGAGTGTCC3' were subcloned into pCRII-TOPO using the TOPO TA cloning kit (Invitrogen) (#433).

X. tropicalis miR-23b

Genomic PCR products for *mir-23b* amplified using primers 5'GCCTTCCATCCTTTCTGCTG3' and 5'CACATGATAACTGCTGGGATG3' were subcloned into pCRII-TOPO using the TOPO TA cloning kit (Invitrogen) (#434).

X. tropicalis miR-24a

Genomic PCR products for *miR-24a* amplified using primers 5'CTTAGCTGATTGGTGAACAGTG3' and 5'GGTAACGGAGGGAGAACTGG3' were subcloned into pCRII-TOPO using the TOPO TA cloning kit (Invitrogen) (#435).

X. tropicalis miR-96

Genomic PCR products for *miR-96* amplified using primers 5'CAGCACCACAGAAGAAGAATACTGC3' and 5'TGGAGGATGGATTAAGGGGC3' were subcloned into pCRII-TOPO using the TOPO TA cloning kit (Invitrogen) (#436).

X. tropicalis miR-98

Genomic PCR products for *miR-98* amplified using primers 5'AAGCATCTGAATCCTCTGCTCG3' and 5'GAATACCCCATTTGAACTGAGCC3' were subcloned into pCRII-TOPO using the TOPO TA cloning kit (Invitrogen) (#437).

X. tropicalis miR-124

Genomic PCR products for *miR-124* amplified using primers 5'GGGGATTGGGCAGGTGCGATTG3' and 5'CACTGATGCAGATTTGTGGATAG3' were subcloned into pCRII-TOPO using the TOPO TA cloning kit (Invitrogen) (#438).

X. tropicalis miR-130a

Genomic PCR products for *miR-130a* amplified using primers 5'CCCATGTGCCAAAAAGCATAGC3' and 5 CATGCTCTGTGTATTCTGGGCAG3' were subcloned into pCRII-TOPO using the TOPO TA cloning kit (Invitrogen) (#439).

X. tropicalis miR-133b

Genomic PCR products for *miR-133b* amplified using primers 5'GGAGCTGCTGCACCTTTGTG3' and 5'CCCATTCACCTTTCCCTGCC3' were subcloned into pCRII-TOPO using the TOPO TA cloning kit (Invitrogen) (#440).

X. tropicalis miR-181a-2

Genomic PCR products for *miR-181a-2* amplified using primers 5'GCACACAATATGCTAAGACACTTTC3' and 5'GTAAGGTAACCCAATCCTACAAAAC3' were subcloned into pCRII-TOPO using the TOPO TA cloning kit (Invitrogen) (#441).

X. tropicalis miR-219

Genomic PCR products for *miR-219* amplified using primers 5'GGAAGAGAACTGATGGCAATGACTG3' and 5'GGAAGAGAACTGATGGCAATGACTG3' were subcloned into pCRII-TOPO using the TOPO TA cloning kit (Invitrogen) (#442).

X. tropicalis sharp1(dec2)

PCR was done using a stage 30 cDNA preparation as template for *sharp1(dec2)* with primers 5'GGATTAATGAATGTATCGCTCAGC3' and 5'TCTTTGGCACAGGTCTGGAA3'. Products were subcloned into pCRII-TOPO using the TOPO TA cloning kit (Invitrogen) (#443).

X. laevis apaf1

Probe was made from a full-length *X. laevis apaf1* clone (IMAGE:5514901) cut with SmaI (#2511).

X. laevis caspase9

Probe was made from a full-length *X. laevis caspase9* clone (IMAGE:7976131) cut with SmaI (#2512).

X. laevis foxd2

PCR was done using a stage 30 cDNA preparation as template for *foxd2* with primers 5'GAAGTTCCCCGCCTGGCAGAAC3' and 5'GAGTTCATTGCCCAGGAAAGGG3'. Products were subcloned into pCRII-TOPO using the TOPO TA cloning kit (Invitrogen) (#2513).

X. laevis id2

PCR was done using a stage 30 cDNA preparation as template for *id2* with primers 5'GCAAAACGCCAGTGGATGACCC3' and 5'GGACAAAGGGATTTGCTCTCG3'. Products were subcloned into pCRII-TOPO using the TOPO TA cloning kit (Invitrogen) (#2514).

X. laevis id3

PCR was done using a stage 30 cDNA preparation as template for *id3* with primers 5'CCATGAAAGCCATCAGCCCAG3' and 5'CCCCTTGTGTTGCCAATTCTG3'. Products were subcloned into pCRII-TOPO using the TOPO TA cloning kit (Invitrogen) (#2515).

X laevis *miR-133b*

Probe was made from a *X. laevis miR-133b* clone (IMAGE:4059686) cut with KpnI (#2509).

X. laevis myogenin

PCR was done using a stage 30 cDNA preparation as template for *id4* with primers 5'3' and 5'3'. Products were subcloned into pCRII-TOPO using the TOPO TA cloning kit (Invitrogen) (#2516).

X. laevis serum response factor

PCR was done using a stage 30 cDNA preparation as template for *serum response factor* with primers 5'GTGCCCACCACCTCCACTTCC3' and 5'GGAGGTCATGATGGCTGCAGGC3'. Products were subcloned into pCRII-TOPO using the TOPO TA cloning kit (Invitrogen).

Chapter 3

Expression of microRNAs during embryonic development of *Xenopus tropicalis*

Summary

Several methods are available for characterizing the expression of microRNA transcripts, each with advantages and drawbacks. I have developed a method to use digoxigenin-labeled probes complementary to the primary microRNA transcript for in situ hybridization on *X. tropicalis* embryos. This method allows for unique expression patterns to be distinguished between microRNAs with the same mature sequence but whose primary transcripts are derived from different loci in the genome. In addition, this technique can be used to detect microRNAs that have conserved and novel expression patterns of developmental interest, which will be functionally investigated further.

Introduction

When I set out to determine the expression pattern of miRNAs during *Xenopus* development, there were very few published methods for miRNA detection. One such report was by (Aboobaker et al., 2005), which showed that *in situ* hybridization for the primary transcript of miRNAs was possible in *Drosophila* using standard digoxigenin-labeled probes. Elsewhere in the literature, short labeled DNA cognates called 'locked nucleic acids' (LNAs) were used to detect mature miRNAs by in situ hybridization in zebrafish and mouse (Kloosterman et al., 2006). The first method allows for much longer probes, which can incorporate more labeled nucleotides and theoretically give a stronger signal. It can also distinguish between different members of the same miRNA family, which may have only one (or no) base pair difference in the mature sequence, but have very divergent primary transcripts and potentially different expression (and therefore functions). However, depending on the rate of maturation, the primary transcript is unlikely to be as abundant as the mature transcript, so pri-miRNA levels could fall below the levels of detection. LNAs, on the other hand, hybridize readily and specifically to the mature miRNA, but in addition to being very expensive, anecdotal evidence suggested that they were difficult to optimize (L. Brunet, personal communication). Because my purpose was to do a wide-scale screen for expression patterns of individual miRNAs during development, I decided to try the pri-miRNA detection method based on standard digoxigenin-labeled probes. I made probes to predicted primary miRNA transcripts and used these for in situ hybridization.

My data show conserved tissue-specific expression patterns in the muscle, central nervous system, eye, and posterior mesoderm during embryogenesis. Furthermore, I have identified novel expression patterns for conserved microRNAs during embryogenesis. I also show that this method can differentiate the expression patterns of three microRNAs of the *miR-9* family, as well as confirm co-expression of two miRNAs transcribed from a cluster. The tissue-specificity of many microRNA expression patterns suggests functional roles during development.

Results and Discussion

In order to understand the function of miRNAs during embryogenesis of the developmental model organism *Xenopus*, it is important to know the spatiotemporal expression profiles of these genes throughout development. Though other groups have cloned miRNAs from *X. laevis* embryos (Watanabe et al., 2005), there was as yet no data on the spatiotemporal expression of miRNAs during embryogenesis. Therefore, I generated approximately 1-kb digoxigenin-labeled antisense probes to 60 predicted *Xenopus tropicalis* miRNAs (Griffiths-Jones et al., 2006) and hybridized them to neurula, tailbud, and tadpole stage embryos (Chapter 2 and Appendix I). Probes to 18 of the miRNAs gave spatially distinct patterns above background, and these are shown in Figure 3.1.

Many of the *X. tropicalis* miRNA expression patterns are conserved across animal species. *miR-1a-1* is expressed in muscle tissue in *Drosophila* (Aboobaker et al., 2005; Chen et al., 2006), zebrafish (Chen et al., 2006), and mouse (Zhao et al., 2007b) and expression in *X. tropicalis* can clearly be seen in the trunk mesoderm of the neurula stage embryo and in somites at the tailbud stage (Fig. 3.1B`). Similarly, *miR-133* is expressed in muscle tissue (Chen et al., 2006) (Fig. 3.1O`). Among other conserved expression patterns (Arora et al., 2007; Deo et al., 2006; Mansfield et al., 2004), *miR-124* is highly expressed in the entire central nervous system (Fig. 3.2, N-R), *miR-9* is expressed in the brain (Fig. 3.1, D-F` and Fig. 3.2 A-G), *miR-7* is expressed in the eye (Fig. 3.1C`), and *miR-10* is expressed in the posterior region of the tailbud embryo (Fig. 3.1G). These expression patterns are conserved across large evolutionary distances and at least 600 million years (Erwin and Davidson, 2002).

For the 42 probes that failed to detect distinct patterns of expression above background, I cannot say that this is due to a lack of expression. A negative result could be the result of very rapid processing of the primary transcript, low levels of expression, expression at a different stage of development, or a non-optimized hybridization probe or procedure. Some probes gave ubiquitous expression patterns, but I have not eliminated the possibility that these probes caused non-specific background staining. Probes that gave tissue-specific expression patterns were more enriched for miRNAs that are intergenic (17/18, 94%) than the total collection of probes (48/60, 80%) or the non-tissue specific class (31/42, 74%) perhaps because splicing machinery blocks probe binding or increases the rate of primary microRNA maturation. *miR-133b* is the only intronic miRNA whose expression is investigated here. It is found in the second intron of a homolog of *pkhd1*, whose expression in *Xenopus* is unreported, and where no ESTs have been found among the 1.2 million in Genbank. In mice, however, this gene is expressed in the developing kidney (Nagasawa et al., 2002), a tissue in which I do not detect *miR-133b*.

Using probes for the entire primary-miRNA transcript allowed us to differentiate between the expression patterns of genes that have identical mature miRNA sequences. The three paralogous *miR-9* genes show unique but highly overlapping expression patterns (Fig. 3.1, D-F`). Using staining intensity as a qualitative measure, the most highly expressed at all stages is *miR-9a-1*. *miR-9a-2* has very low levels of expression in the anterior-most portion of the neural plate at the neurula stage, but expression increases at tailbud stages. *miR-9-3* displays intermediate expression levels at both these stages. Interestingly, during the tailbud stage, *miR-9a-2* has a broader expression pattern than the other paralogs, encompassing not just the eye and forebrain, but also the hindbrain. However, by the tadpole stage, all show expression patterns similar to *miR-9a-1* (Fig. 3.2A and data not shown).

A cluster of miRNAs containing *miR-23b* and *miR-24a* is found in the *X. tropicalis* genome, along with *miR-27b* (Griffiths-Jones et al., 2007). Non-overlapping probes to *miR-23b* and *miR-24a* revealed identical expression patterns, first appearing at stage 19 in the eye anlagen and posterior cells around the blastopore (Fig. 3.1, I-J`). This expression pattern has not been described in any species for either or these microRNAs. The neural retina continues to express both miRNAs, as does the posterior-most mesenchyme, and therefore it is likely these miRNAs derive from the same primary transcript.

Many of the miRNAs that gave specific expression patterns are expressed in neuronal tissues. This correlates with previous studies in other vertebrates (Kapsimali et al., 2007), which show that neurons and their progenitors are enriched in the number of expressed miRNAs. In *X. tropicalis*, this includes *let-7a*, *miRs-7*, *-9*, *-18*, *-23*, *-24*, *-96*, *-98*, *-124*, *-130*, *-181*, and *-219* (Fig. 3.1). *miR-429* is expressed in cells of the olfactory placode (Fig. 3.1, R and R`). *miR-9a-1* is expressed broadly in the most anterior portions of the forebrain, where cells are proliferating and differentiation is limited (Papalopulu and Kintner, 1996), and in the mid- and hindbrain it is expressed in the proliferating ventricular zone (Fig. 3.2B-E). *mir-124* is expressed in a complementary pattern, in the medial and lateral areas of the brain and neural tube, where differentiation will take place (Fig. 3.2N-R). This holds true in the eye as well, where *miR-9a-1* is expressed more highly in the marginal zone and *miR-124* is highly expressed in the differentiated neural retina (Figs. 3.2C vs 3.2N, respectively). These results agree with previous observations in mice (Krichevsky et al., 2006; Smirnova et al., 2005).

Overall, the method I selected was very successful in fulfilling my goals, namely to identify tissue-specific expression patterns that would be of interest for further developmental study. However, if one wished to identify a single specific miRNA's expression pattern, this method would have to be optimized and/or supplemented with other methods. Because of the numerous techniques developed in *Xenopus* to study embryogenesis, this organism is well-placed for future studies of microRNA function. I have provided a method for the first step in microRNA studies in *Xenopus*, and have identified several candidate microRNAs for functional experiments.

Figure 3.1 Expression patterns of *X. tropicalis* miRNAs
In situ hybridization for various pri-miRNAs at neurula (A-R, dorsal view) and early tadpole stages (A`-R`, lateral view, anterior to the left).

Figure 3.1

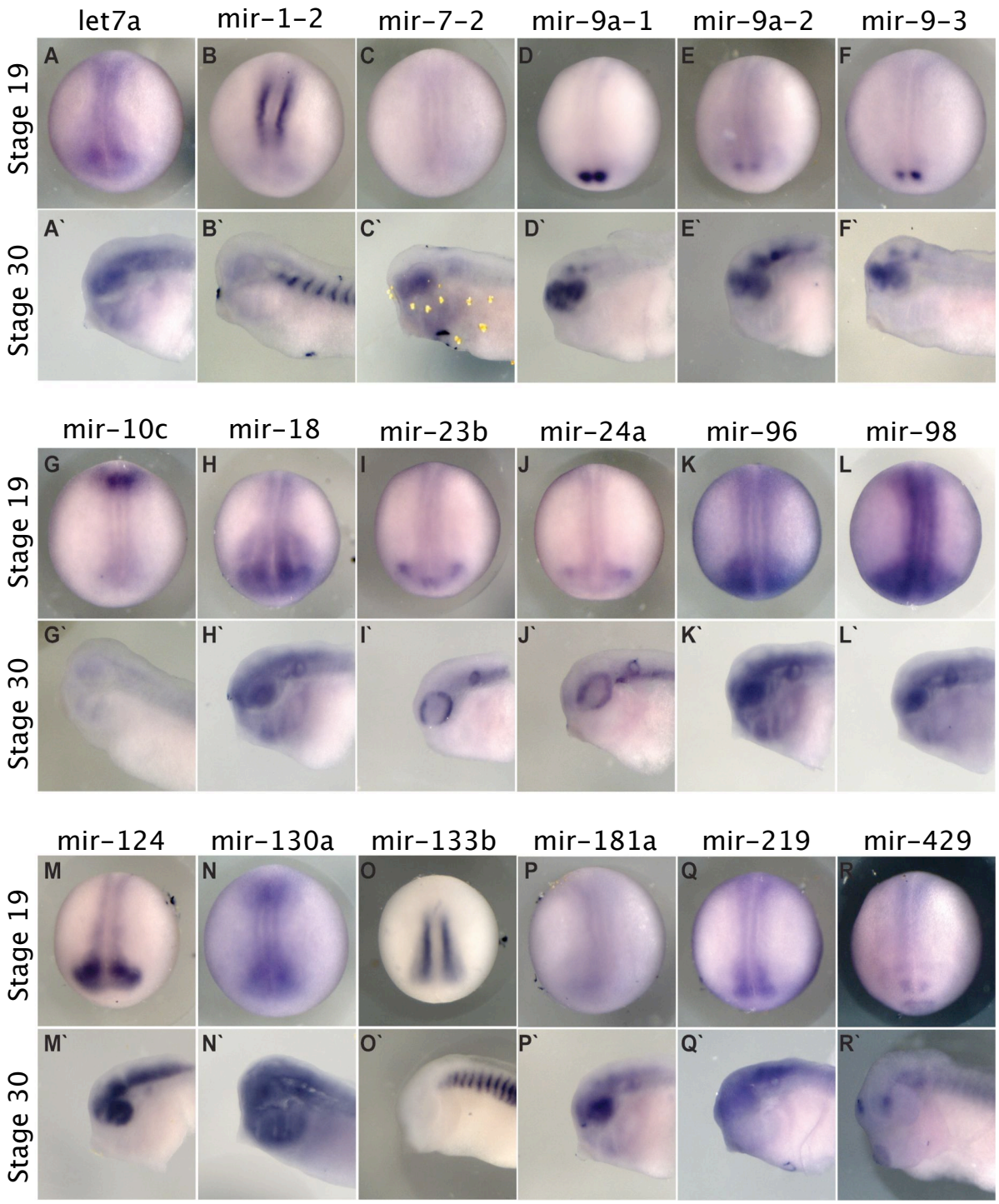
let7a
mir-1-2
mir-7-2
mir-9a-1
mir-9a-2
mir-9-3
Stage 19
Stage 30
A
B
C
D
E
F
A`
B`
C`
D`
E`
F`
mir-10c
mir-18
mir-23b
mir-24a
mir-96
mir-98
G
H
I
J
K
L
G`
H`
I`
J`
K`
L`
mir-124
mir-130a
mir-133b
mir-181a
mir-219
mir-429
M
N
O
P
Q
R
M`
N`
O`
P`
Q`
R`

Figure 3.2 *Xenopus* miRNAs exhibit tissue-specific expression patterns.
(A-F) Stage 35 tadpole showing *miR-9a-1* expression in sub-ventricular cells of the brain . (G-L) Stage 24 tailbud embryo showing *miR-23b* expression in the eye primordia and the posterior mesenchyme. (M-R) Stage 35 tadpole showing *miR-124* expression in non-proliferative neural tissue. (S-X) Stage 35 tadpole showing *miR-133b* staining in head mesoderm, migrating hypaxial muscles, and somites. A, G, M, and S are lateral views, anterior to the left. All others are 100uM coronal sections, dorsal at the top.

Figure 3.2

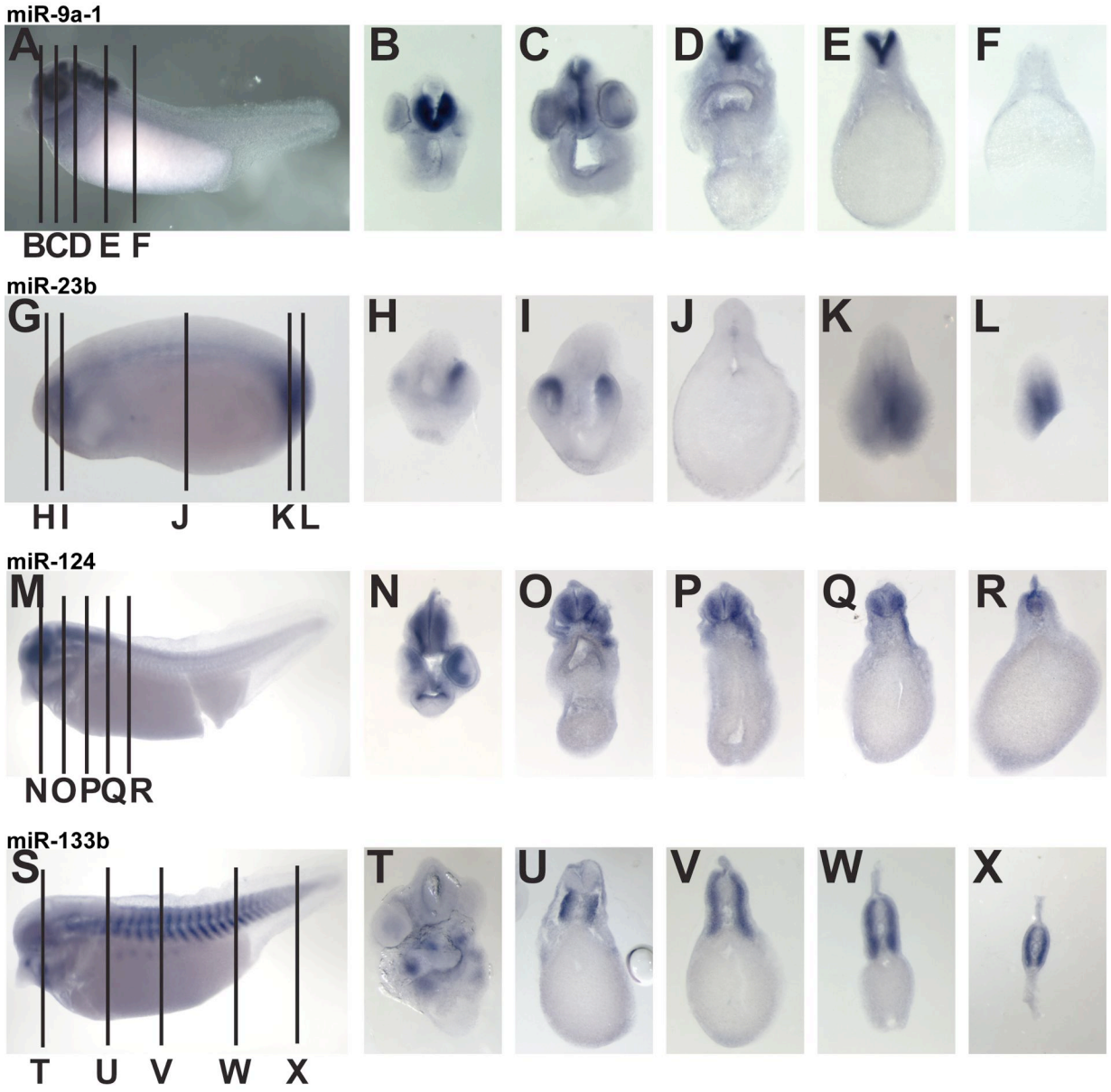
miR-9a-1
A
B
C
D
E
F
BCD E F
miR-23b
G
H
I
J
K
L
HI
J
KL
miR-124
M
N
O
P
Q
R
NOPQR
miR-133b
S
T
U
V
W
X
T
U
V
W
X

Chapter 4

microRNA-24a is required to repress apoptosis in the developing neural retina

Summary

Apoptosis, or programmed cell death, is an important part of the proper development of organs during development. In the retina, precise regulation of apoptosis is necessary for proper morphogenesis and development. However, little is known about the regulatory mechanisms that restrict apoptosis in the retina. I have found that *microRNA-24a* is expressed in the neural retina and is required for correct eye morphogenesis. Inhibition of *mir-24a* during development causes a reduction in eye size due to a significant increase in apoptosis in the retina. I show that *mir-24a* functions as a negative regulator of the pro-apoptotic factors *caspase9* and *apaf1* through interactions with their 3' untranslated regions and that *mir-24a* is sufficient to repress apoptosis induced by hydroxyurea treatment or *caspase9* overexpression. Together my findings demonstrate that *mir-24a* is required during development of the neural retina to repress programmed cell death by targeting *caspase9* and *apaf1*.

Introduction

Apoptosis regulates the size and morphology of developing tissues and organs, and this is particularly true in the developing neural retina, the structure that gives rise to the photoreceptors, retinal ganglion cells and the optic nerve (Lupo et al., 2000). As many as 90% of newborn retinal ganglion cells subsequently die during normal rat retinal development (de la Rosa and de Pablo, 2000; Vecino et al., 2004). In *Xenopus*, spatiotemporal elimination of retinal cells is a key factor in maturation (Gaze and Grant, 1992). Zebrafish also undergo retinal apoptosis, though at lower levels (Biehlmaier et al., 2001). In the chick, caspase-dependent apoptosis has been demonstrated in the retina, and inhibition of caspases results in an enlargement of the ganglion cell layer (Mayordomo et al., 2003). Similarly, in mouse, apoptotic factors are highly expressed in the early retina and down-regulated as development proceeds (O'Driscoll et al., 2006; Wallace et al., 2006), and knockdown of caspases results in an overgrown retina (Hakem et al., 1998). However, the factors important for the regulation of caspases and other apoptotic factors in the eye are unknown, although some transcriptional regulation has been postulated (Wallace et al., 2006).

Several miRNAs have been implicated in the regulation of apoptosis in *Drosophila* (Xu et al., 2004). In various forms of cancer, *miR-21* has been shown to be an anti-apoptotic factor (Chan et al., 2005; Cheng et al., 2005) and *miR-34* has been shown to be a downstream target of p53 and an inducer of cell death (He et al., 2007a). However, knowledge is still lacking about the *in vivo* roles of most miRNAs during vertebrate development. Recent work in mice has shown that Dicer inactivation specifically in the retina results in neuronal degeneration (Damiani et al., 2008). Therefore, miRNAs may be important for the regulation of cell death pathways in the retina during development.

In this study, I show through loss-of-function experiments that *mir-24a* is necessary for proper neural retina development. I further demonstrate that knockdown of *mir-24a* results in an increase in apoptosis while proliferation, patterning, and differentiation of the eye remain unchanged. I find that loss of *mir-24a* function leads to an increase in Caspase9 protein levels without altering mRNA levels, and that the miRNA knockdown phenotype is dependent on the function of Caspase9. In addition, I establish that *mir-24a* is capable of repressing the pro-apoptotic factors *apaf1* and *caspase9* by interaction with their 3' untranslated regions. Finally, I show that *mir-24a* is able to prevent Caspase-dependent apoptosis when overexpressed. Together these data indicate that *mir-24a* is an essential regulator of programmed cell death in the developing neural retina.

Results

mir-24a is expressed in the developing neural retina

Previously, I had reported the primary-miRNA expression patterns for several miRNAs during development of *X. tropicalis* (Walker and Harland, 2008) (Chapter 3 of this thesis). One expression pattern that was particularly intriguing was that of *mir-24a*,

which appeared in the eye anlage and the posterior mesenchyme during late neurula stages (Fig. 3.1 and 4.1A). In *X. laevis*, neural retina development begins when the eye anlagen evaginate from the anterior portion of the neural tube and continues as the optic cup invaginates and later differentiates into three nuclear layers (Nieuwkoop and Faber, 1994). Further analysis of the expression of *mir-24a* revealed that this miRNA is expressed specifically in the neural retina throughout the development of the eye until at least stage 40 (Fig. 4.1B-D' and data not shown). RT-PCR experiments confirmed that *miR-24a* was developmentally expressed and that relative transcript abundance was highest at stage 23 and 28, consistent with qualitative transcript levels suggested by in situ hybridization (Fig. 4.1E).

Knockdown of *mir-24a* results in reduced eye size

To determine the function of *mir-24a* during development, I took a knockdown approach using an antisense morpholino oligonucleotide designed to complement both the mature *mir-24a* sequence and some sequence of the adjacent loop in the predicted pri-miRNA structure (24aMO). This design was predicted to prevent processing of the primary miRNA transcript as well as to inhibit the function of the mature miRNA (Yin et al., 2008). Injection of 20ng of 24aMO in one cell at the two-cell stage resulted in a reduction in eye size on the injected side (Fig. 4.2A-F'), which was significant after stage 28 (n=94 sections over 8 stages). On average, eyes injected with 24aMO were reduced 50% in size compared to the uninjected control eye at stage 40 (data not shown). To ensure the specificity of the morpholino, I performed several control experiments. I was able to rescue the morpholino by co-injecting 2ng of duplex *mir-24a* RNA (Fig. 4.2G. In addition, a mismatch morpholino with four base substitutions in the 'seed' region (24ammMO) did not have a phenotype at an equivalent dose (Fig. 4.2G, n=121).

To further ensure that 24aMO was blocking *mir-24a* function, I constructed and injected mRNA for several GFP reporters. These and other GFP reporter constructs were generated by fusing the coding region of a destabilized GFP to a 3' untranslated region containing recognition elements for putative miRNAs. Should the miRNA functionally interact with the recognition element, then the miRNA would repress translation of the GFP and the embryo would lack green fluorescence. RNA coding for RFP without miRNA recognition elements was always coinjected, so that a measure of the repression of GFP by the miRNA could be generated by quantification of the green:red fluorescence ratio. A reporter GFP mRNA with two perfect *mir-24a* recognition elements in its 3' untranslated region (24aMRE), when co-injected with 500pg of duplex *mir-24a*, was translationally repressed (Fig. 4.2H). However, when 10ng of 24aMO was also co-injected, it is able to block the miRNA-induced repression (Fig. 4.2H). This repression was dependent on the *mir-24a* recognition elements, because mutating these elements (mut24aMRE) resulted in no repression by the miRNA (Fig. 4.2H). Together, these results show that 24aMO is able to block the function of *mir-24a in vivo*, and that this leads to a reduction in eye size.

Knockdown of *mir-24a* reduces eye size without disrupting patterning, specification, or differentiation

To determine the molecular effects of knocking down *mir-24a*, I performed a broad analysis looking for changes in marker gene expression. *En-2*, a marker of the midbrain-hindbrain boundary, and *n-tubulin*, expressed in differentiated neurons, were unaffected, indicating that the effect of knocking down *mir-24a* is eye-specific (Fig. 4.3A, n=12 for each marker) (Brivanlou and Harland, 1989; Richter et al., 1988). *Foxg1* marks the ventrolateral, *pax2* the ventral, and *vent2* the dorsal region of the eye (Mariani and Harland, 1998); (Heller and Brandli, 1997; Onichtchouk et al., 1996). Expression of these markers was unchanged in 24aMO-injected embryos, indicating that spatial patterning of the eye is maintained (Fig. 4.3A, n=12 for each marker). Progenitors of neural retina cells express *rx1*, *pax6*, *sox2*, *notch1* and/or *otx2* (Coffman et al., 1990; Grammer et al., 2000; Hartley et al., 2001; Lamb et al., 1993; Mathers et al., 1997). However, injection of 24aMO did not qualitatively change the intensity of expression of any of these progenitor marker genes compared with the uninjected control side (Fig. 4.3B n=12 for each marker). At this stage, the size difference between the uninjected eyes and *mir-24a* knockdown eyes was sometimes apparent but not statistically significant. These data demonstrate that knockdown of *mir-24a* has no effect on the specification of the neural retina.

I then determined the expression patterns of several marker genes of neuronal differentiation, including *neurogenin, neuroD, xic1(p27), MyT1*, and *nrp1*; (Lee et al., 1995; Ma et al., 1996; Richter et al., 1988; Vernon et al., 2003). Although the eye domains were sometimes smaller, consistent with my previous observations (Fig. 4.2B), these also showed no significant change in expression at stage 28 (Fig. 4.3C, n=12 for each marker), leading to the conclusion that knockdown of *mir-24a* has no effect on neural differentiation.

I also examined neural progenitor and neural differentiation gene expression at later stages. At stage 35, expression of progenitor genes was normal in intensity and was limited to the marginal zone, but the field of expression was smaller, consistent with the gross morphological phenotype (Fig. 4.3D, n=12 for each marker). Neural differentiation markers showed similar results (Fig. 4.3E n=12 for each marker), indicating that continued specification and differentiation are not affected in 24aMO-injected embryos, despite the reduced territory of the eye. Terminal differentiation of the neural retina into rods, cones, and ganglia was able to proceed normally, as antibody stains for XAP-1 (rods and cones), XAP-2 (rods) and islet-1 (ganglia) showed (Fig. 4.3F). In sum, these results indicate that while knockdown of *mir-24a* causes a reduction in eye size, there is no disruption in the patterning, specification, or differentiation of the neural retina, and all terminal structures (rods, cones, and ganglia) are present.

Knockdown of *mir-24a* leads to an increase in apoptosis

Since it is evident that the reduction in eye size of miR24a morphants does not arise from a change in the initial specification of the eye field or its subsequent patterning or differentiation, there are two likely explanations for the reduction in size of the eye caused by the knockdown of *mir-24a*: either there is a decrease in proliferation or an increase in apoptosis. To test the former, I performed immunohistochemistry for phosphorylated histone-3, a marker of dividing cells (Martin and Harland, 2006). In this analysis, there was no significant difference between the 24aMO-injected side and the

uninjected side in the number of proliferating cells in the eye (Fig. 4.4A, n=6 embryos per stage, 18 sections per embryo). In contrast, TUNEL staining on 24aMO-injected embryos clearly demonstrated that apoptosis was significantly increased in the eye of *mir-24a* knockdown embryos (Fig. 4.4B, n=6 embryos per stage, 11 sections per embryo). Furthermore, this apoptosis began even before a morphological phenotype was observed, as early as stage 24, and continued through the development of the eye to tadpole stages (Fig. 4.4B and data not shown). These results indicate that *mir-24a* may be a potent negative regulator of members of the apoptotic pathway during eye development.

Knockdown of *mir-24a* causes up-regulation of Caspase9 protein and inhibition of Caspase9 rescues the knockdown phenotype

One of the most important members of the apoptotic pathway during neural development is *caspase9* (Cecconi et al., 2008). Therefore, I examined both *caspase9* mRNA levels by RT-PCR and protein levels by Western blot. In *mir-24a* knockdown embryos, the levels of *caspase9* mRNA were the same as uninjected controls or embryos injected with the mismatch morpholino, 24ammMO (Fig. 4.5A). However, Caspase9 protein levels were significantly increased in embryos with reduced *mir-24a* function, relative to controls (Fig. 4.5B). These data demonstrate that *caspase9* is being regulated post-transcriptionally and may be a direct target of *mir-24a*.

To test whether Caspase9 function was necessary for the *mir-24a* knockdown phenotype, I co-injected several specific Caspase inhibitors with 24aMO and analyzed their effect on eye size. Significantly, the only specific inhibitor I tested that was able to fully rescue the 24aMO phenotype was the Caspase9-specific inhibitor Ac-LEHD-CMK (Fig. 4.5C). An inhibitor to all Caspases was also able to rescue the *mir-24a* knockdown phenotype (Fig. 4.5C). Together, these data suggest that *mir-24a* regulates apoptosis by repressing protein translation of *caspase9* mRNA.

mir-24a* can negatively regulate the pro-apoptotic factors *caspase9* and *Apaf1

I investigated the possibility that members of the apoptotic pathway were direct targets of *mir-24a*. First, I analyzed the 3' untranslated regions of pro-apoptotic genes for putative *mir-24a* binding sites from both *X. tropicalis* and *X. laevis* using miRbase (Griffiths-Jones et al., 2008) as well as RNAhybrid analysis of EST databases (Kruger and Rehmsmeier, 2006). *Caspase9* and apoptosis protease activating factor (*Apaf1)* were identified by this method as potential *mir-24a* targets (Fig. 4.6A). Caspase9 and Apaf1, along with Cytochrome C from the mitochondria, form a complex in the cytosol known as the apoptosome which initiates a catalytic cascade that leads eventually to cell death (Penaloza et al., 2008). *Caspase9* and *apaf1*are both expressed in the neural retina during the time of development when *mir-24a* functions (Fig. 4.7A).

To test whether *mir-24a* is able to regulate *caspase9* and *apaf1* directly, I made reporter constructs with the *X. laevis* 3'UTR of these genes fused to a destabilized GFP. In addition, I mutated two putative *mir-24a* recognition elements in the 3'UTRs as controls (mutCasp9 and mutApaf1). *mir-24a* was able to significantly repress the expression of GFP only when *mir-24a* sites in the 3'UTR of *caspase9* or *apaf1* were

present (Fig. 4.6B). This demonstrates that *mir-24a* can specifically target the *mir-24a* binding sites in the 3'UTRs of both *caspase9* and *apaf1*. *Caspase9* may have more *mir-24a* binding sites than the two identified, as the mutated version is still slightly repressed relative to the no UTR control.

mir-24a is able to prevent hydroxyurea-induced and *caspase9*-induced apoptosis

My loss-of-function studies determined that *mir-24a* is necessary in the eye to prevent apoptosis from occurring, and that depletion of *mir-24a* leads to the development of a smaller eye. To test whether *mir-24a* is sufficient to regulate other modes of apoptosis, I induced apoptosis by soaking embryos in 15mM hydroxyurea; this causes large amounts of Caspase-dependent apoptosis, visible as cell autolysis and loss of adhesion, but only at the onset of zygotic transcription (Stack and Newport, 1997; Takayama et al., 2004). To assess *mir-24a* mediated rescue, I injected 2ng of *mir-24a* into both cells of a two-cell stage embryo and incubated them in 15mM hydroxyurea until early gastrula stages, then analyzed the number of embryos undergoing apoptosis. I found that addition of *mir-24a* significantly reduced the number of embryos undergoing apoptosis, and that this reduction was not seen when embryos were injected with equal amounts of a four base-pair mismatch RNA (*mir-24amm*) (Fig. 4.8A, n=3 trials of >30 embryos each). This apoptosis analysis is qualitative, however, and more rigorous quantitative measures may be necessary in the future. Still, these results indicate that *mir-24a* is able to prevent apoptosis more generally than in the eye, most likely by targeting components of the apoptosis pathway including *caspase9* and *apaf1*.

Similarly, overexpression of *caspase9* is sufficient to cause apoptosis by a similar analysis, and *mir-24a* overexpression is able to rescue this phenotype. I injected *X. tropicalis caspase9* transcript and recorded the incidence of apoptosis at neurula stages. Co-injection with *mir-24a* decreased the incidence of apoptosis significantly (Fig. 4.8B), indicating that *caspase9* may be a direct target of *miR-24a* repression.

Discussion

I have found that *mir-24a* represses apoptosis in the neural retina, likely by down-regulating *apaf1* and *caspase9*. These two proteins are the major components of the apoptosome, the first complex in the protease cascade deployed during programmed cell death. Normally, cytochrome *c* released from the mitochondria binds apaf1 and induces the recruitment of caspase9 to the apoptosome. The interaction between these proteins leads to the activation of caspase9, which then proceeds to cleave and activate downstream caspases, including caspases-3, -6, and –7 (Guerin et al., 2006). My data implicate miRNAs as an important regulator of apoptosis during vertebrate development, and specifically of the apoptosome. Other genes may also be regulated by *mir-24a* in this process and make a contribution to the knockdown phenotype. It is intriguing that miR-23b and miR-27b, the other miRNAs in the cluster with *mir-24a*, are predicted to regulate other genes important for apoptosis, such as the low-affinity NGF receptor or DIABLO, an antagonist of inhibitor of apoptosis proteins (IAPs) (Griffiths-Jones et al., 2007; Guerin et al., 2006).

The target sequences of *caspase9* and *apaf1* that I identified as necessary for *miR-24a* repression are not perfectly complementary to the 'seed sequence' of the microRNA, though they do have extensive pairing along the entire mature microRNA sequence. While this situation conflicts with the dogma in the field (Bartel, 2004), recent evidence suggests that some biologically relevant targets do not follow the seed rule (Didiano and Hobert, 2006; Vella et al., 2004). How prevalent this phenomenon is remains to be seen, but genome-scale biochemical analyses of microRNA:mRNA target interactions promise to provide a much greater data pool from which to draw conclusions.

This chapter also makes clear the importance of proper regulation of apoptosis in the neural retina in *X. laevis*. Mouse knockouts of *caspase9* have an excessive accumulation of neurons throughout the central nervous system, including the retina (Hakem et al., 1998). *Apaf1* knockouts also have retinal overgrowth in addition to forebrain overgrowth and thickening of the hindbrain walls (Cecconi et al., 1998). Here, I show that disrupting a negative regulator of *caspase9* and *apaf1* increases their abundance, resulting in higher levels of apoptosis and a smaller eye. Previous reports have disrupted the transcription of *apaf1* by interfering with histone deacetylation, causing an increase in apoptosis in the developing retina (Wallace and Cotter, 2008). My data argue that post-transcriptional regulation by miRNAs is also a factor in the correct regulation of *apaf1* during normal amphibian development.

Mouse knockouts of *caspase3* can have a similar phenotype to those of *caspase9*, although the phenotype occurs in far fewer animals (10% vs. 97%), and cell death is still seen in the retina (Cecconi et al., 2008). This agrees with my experiments using caspase inhibitors: while caspase-3 inhibitor was able to partially rescue the phenotype caused by depletion of *mir-24a*, it was not significant, indicating that it probably has only a small role in the downstream activity of the caspase cascade.

Remarkably, the loss of a single miRNA is sufficient to release members of the apoptotic pathway from inhibition, resulting in a significant increase in apoptosis and severe morphological disruption of eye structures. This occurs without any disruption in early patterning or specification. This indicates that *mir-24a* is primarily a negative regulator of apoptosis in the neural retina. Similar miRNA regulation may be important for other neural structures that also require precise levels of apoptosis during development, including the brain and spinal cord (De Pietri Tonelli et al., 2008). Further characterization of the functions of neuronally expressed miRNAs should lead to an understanding of how general this mechanism is during development.

Figure 4.1 *mir-24a* is expressed in the developing neural retina.

In situ hybridization on *Xenopus tropicalis* with probe antisense to the primary miRNA shows expression of pri-*mir-24a* in the eye anlagen and posterior mesenchyme (A and B). Expression continues in the neural retina as the optic cup develops and invaginates (C-D'). Sense probe shows no expression (C, inset). RT-PCR for the primary miRNA was performed on cDNA from stages 7-31 (E). *mir-24a* expression begins at stage 19 and is highly expressed throughout the maturation of the neural retina.

Figure 4.1

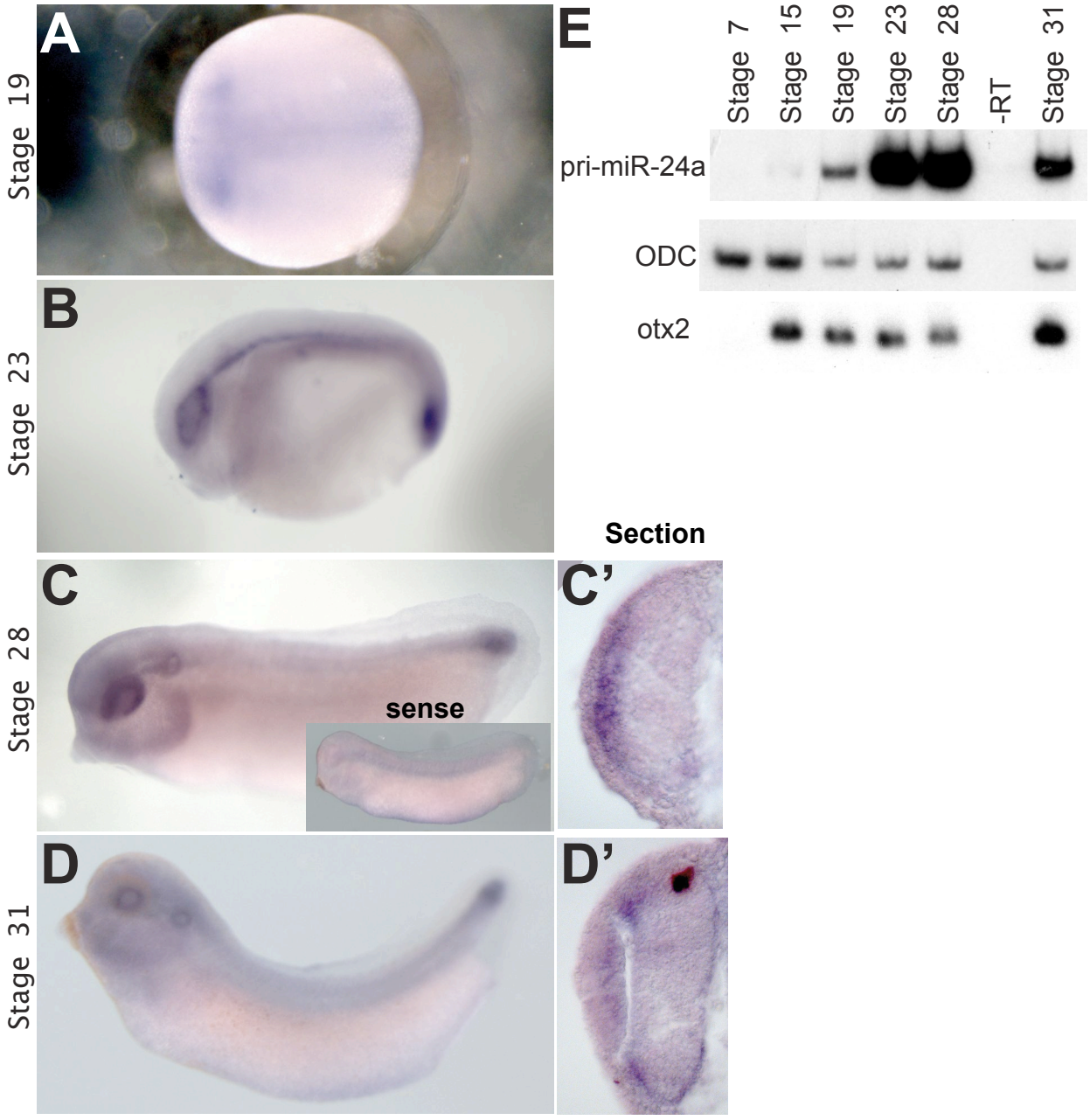
A
Stage 19
B
Stage 23
C
Stage 28
sense
C'
Section
D
Stage 31
D'
E
Stage 7
Stage 15
Stage 19
Stage 23
Stage 28
-RT
Stage 31
pri-miR-24a
ODC
otx2

Figure 4.2 *mir-24a* knockdown results in a reduction in eye size.
(A-F') Hematoxylin and eosin staining of 12μm sections in embryos injected with 20ng of 24aMO in one cell at the two-cell stage, injected half on the right. The knockdown of *mir-24a* causes a reduction in eye size that does not occur until after stage 26 (A) first becoming prevalent at stage 28 (B). The reduction in eye size becomes obvious in stage 31 (C), 34(D), 40(E), and 45(F and F') embryos. (G) The size of the eye was measured at stage 40 and the ratio of the injected eye to the uninjected eye in each embryo was used to classify the severity of phenotypes. *mir-24a* knockdown caused many embryos to have a smaller eye, an effect that was rescuable by co-injection of *mir-24a* duplex RNA. A mismatch morpholino also had no effect on eye size ratio (n=121). (H) 24aMO functionally represses *mir-24a*. A GFP construct with two *mir-24a* recognition elements (24aMRE) when injected alone strongly fluoresces, but shows significantly lower levels of fluorescence when coinjected with duplex *mir-24a* RNA (n=9, error bars are the standard error of the mean). This effect is dependent on the interaction between *mir-24a* and the *mir-24a* recognition elements, because mutating either abrogates the effect. 24aMO is able to rescue fluorescence of 24aMRE by blocking the function of *mir-24a* when coinjected. Similar results were obtained with multiple experiments. RFP without *mir-24a* recognition elements was always coinjected, so that a measure of GFP repression was expressed as the relative fluorescence of GFP/RFP.

Figure 4.2

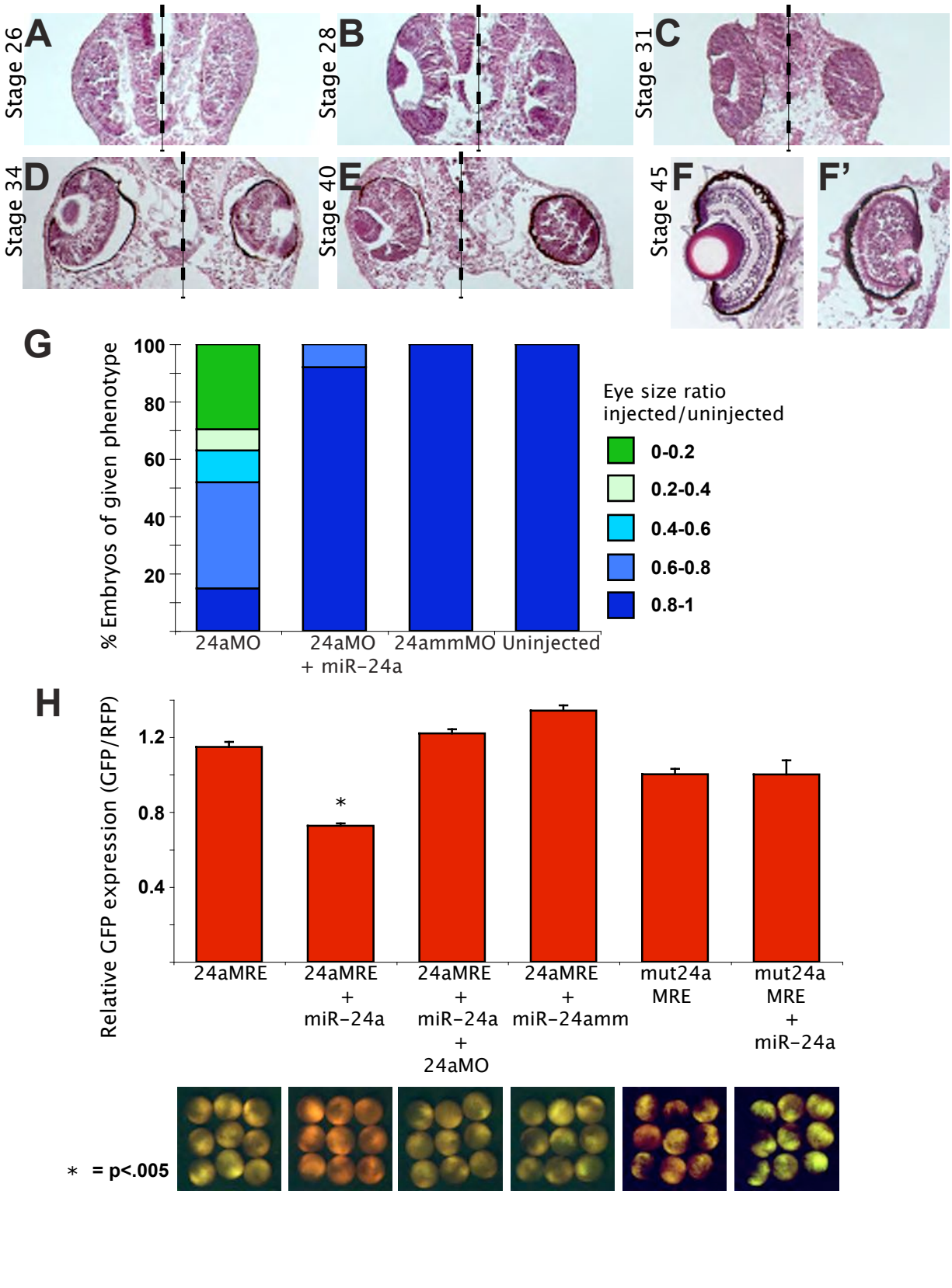
Stage 26
A
Stage 28
B
Stage 31
C
Stage 34
D
Stage 40
E
Stage 45
F
F'
G
% Embryos of given phenotype
100
80
60
40
20
24aMO
24aMO + miR-24a
24ammMO
Uninjected
Eye size ratio injected/uninjected
0-0.2
0.2-0.4
0.4-0.6
0.6-0.8
0.8-1
H
Relative GFP expression (GFP/RFP)
1.2
0.8
0.4
*
24aMRE
24aMRE + miR-24a
24aMRE + miR-24a + 24aMO
24aMRE + miR-24amm
mut24a MRE
mut24a MRE + miR-24a
* = p<.005

Figure 4.3 *mir-24a* knockdown has no effect on patterning, specification, or differentiation of the eye.

(A) Marker gene expression for *en-2* and *n-tubulin*, which denote the midbrain-hindbrain boundary and differentiating cranial neurons, respectively, shows that knockdown of *mir-24a* has no effect on other aspects of the nervous system. The expression patterns of *foxg1*, *pax2*, and *vent2* show that no alteration in patterning dorsal-ventral or anterior-posterior regions of the eye occurs in 24aMO-injected embryos at stage 28. (B) Marker gene expression for neural progenitors in the eye is unchanged at stage 28 after knockdown of *mir-24a*. (C) Marker gene expression for neuronal differentiation genes is unchanged at stage 28 after knockdown of *mir-24a*. (D) At stage 35, expression of neural progenitor markers is disrupted in *mir-24a* knockdown eyes, but the levels of expression at the margin remain high. (E) Similarly, expression of neuronal differentiation genes is disorganized at stage 35, but clearly still persists. (F) Immunohistochemistry for ganglion cells (isl1, in red), rod photoreceptors (XAP2, in red) and rod and cone photoreceptors (XAP1, in green) shows that knockdown of *mir-24a* does not prevent the terminal differentiation of the neural retina at stage 45 (sections are 12μm thick).

Figure 4.3

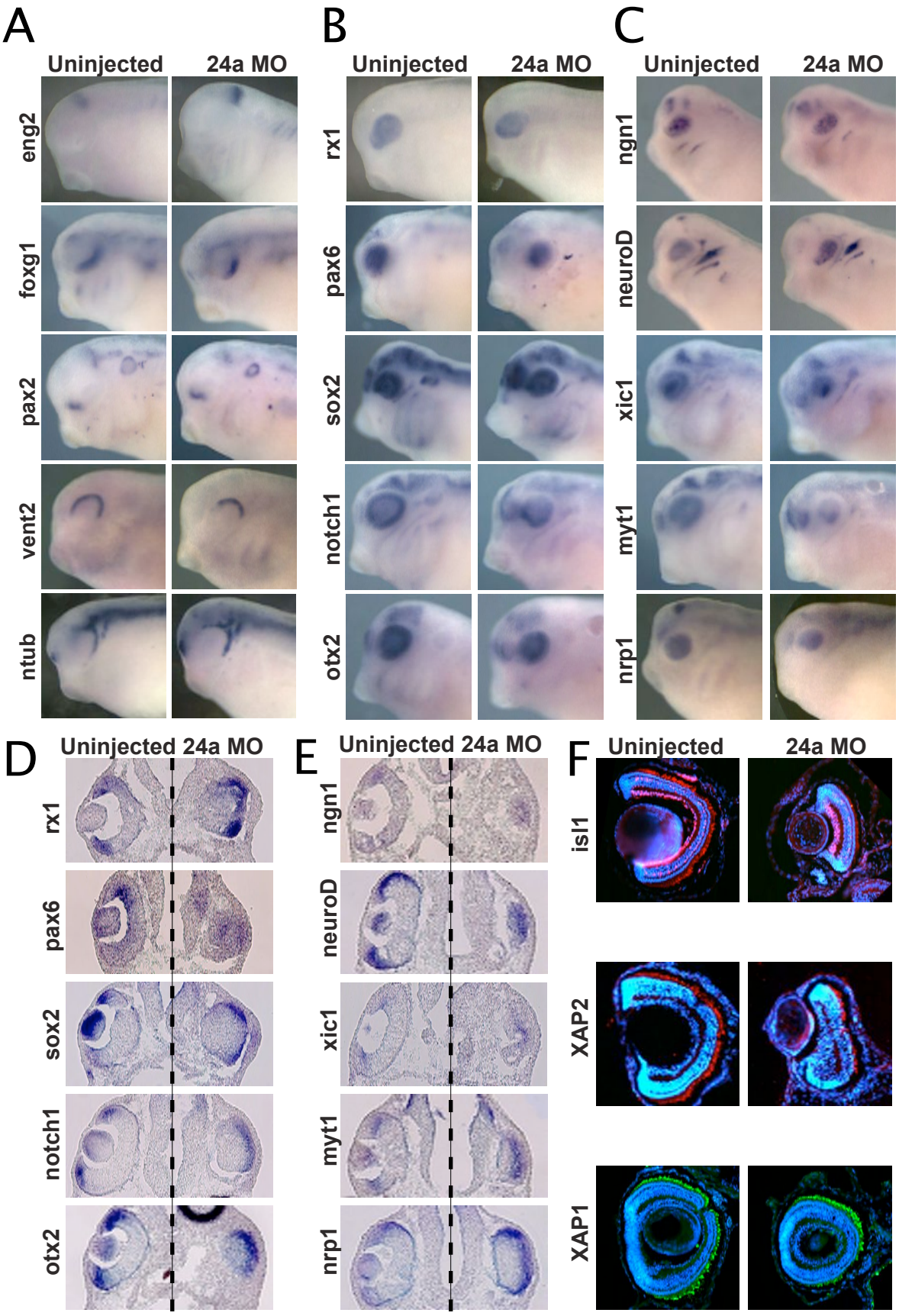
A
Uninjected
24a MO
eng2
foxg1
pax2
vent2
ntub
B
Uninjected
24a MO
rx1
pax6
sox2
notch1
otx2
C
Uninjected
24a MO
ngn1
neuroD
xic1
myt1
nrp1
D
Uninjected 24a MO
rx1
pax6
sox2
notch1
otx2
E
Uninjected 24a MO
ngn1
neuroD
xic1
myt1
nrp1
F
Uninjected
24a MO
isl1
XAP2
XAP1

Figure 4.4 *mir-24a* knockdown has no effect on proliferation but leads to an increase in apoptosis.

(A) Immunohistochemistry for phosphorylated histone-3 (PH3, in red) shows that there is no significant difference in proliferation between control eyes and 24aMO-injected eyes (n=6 embryos per stage, 18 sections per embryo, sections are 12μm, error bars are s.e.m.). (B) Knockdown of *mir-24a* results in a significant increase in apoptosis at all stages assayed, measured by the number of TUNEL-positive nuclei per 20 (n=6 embryos per stage, 11 sections per embryo, error bars are s.e.m.).

Figure 4.4

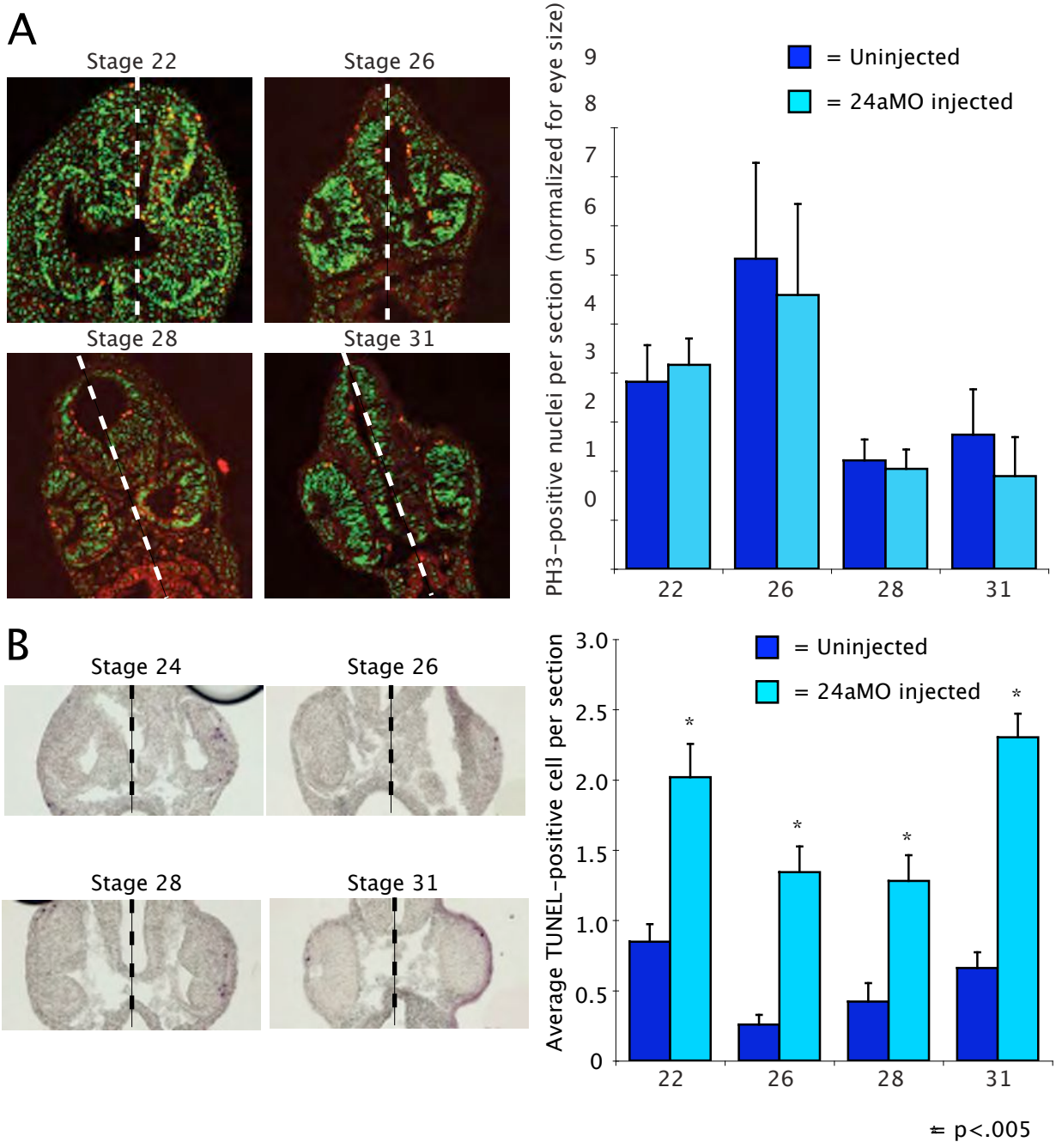
A
Stage 22
Stage 26
Stage 28
Stage 31
PH3-positive nuclei per section (normalized for eye size)
= Uninjected
= 24aMO injected
0
1
2
3
4
5
6
7
8
9
22
26
28
31
B
Stage 24
Stage 26
Stage 28
Stage 31
Average TUNEL-positive cell per section
= Uninjected
= 24aMO injected
0
0.5
1.0
1.5
2.0
2.5
3.0
*
22
26
28
31
= p<.005

Figure 4.5 Knockdown of *miR-24a* causes up-regulation of Caspase9 protein and is rescued by its inhibition

(A) RT-PCR of *caspase9* on stage 28 heads shows no change in mRNA levels between uninjected and *miR-24a* knockdown embryos. (B) Western blot for Caspase9 on stage 28 heads shows a significant increase in protein levels when *miR-24a* function is blocked (n=3 experiments, error bars are s.e.m.). (C) Coinjection of Caspase inhibitors to rescue the *miR-24a* knockdown phenotype. Only a pan-Caspase inhibitor (All) or an inhibitor specific to Caspase9 rescued the reduction in eye size caused by injection of 24aMO (n≥47 for each treatment, error bars are s.e.m.).

Figure 4.5

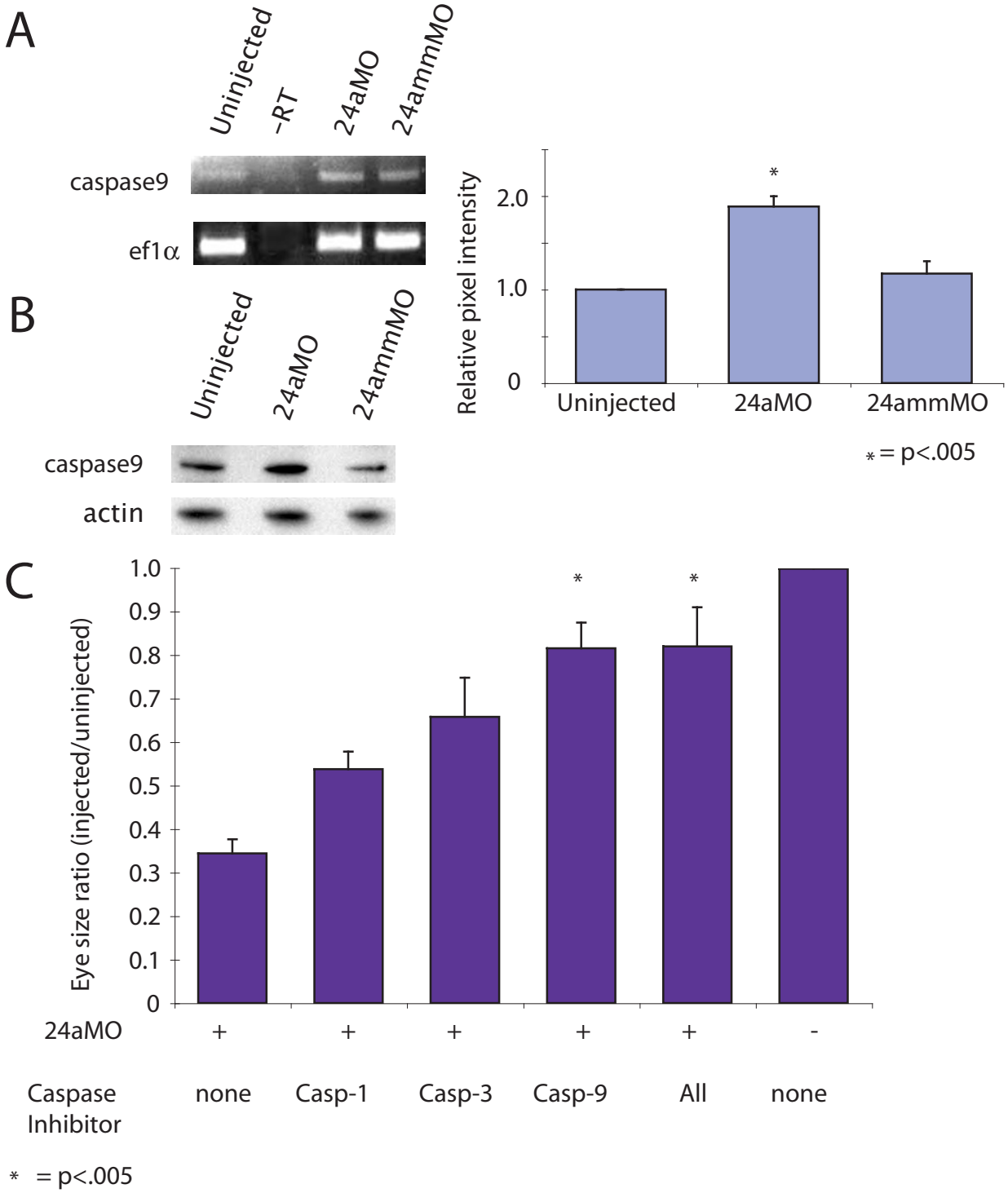
A
Uninjected
-RT
24aMO
24ammMO
caspase9
ef1α
B
Uninjected
24aMO
24ammMO
caspase9
actin
Relative pixel intensity
2.0
1.0
0
*
Uninjected
24aMO
24ammMO
* = p<.005
C
Eye size ratio (injected/uninjected)
1.0
0.9
0.8
0.7
0.6
0.5
0.4
0.3
0.2
0.1
0
*
*
24aMO + + + + + -
Caspase Inhibitor none Casp-1 Casp-3 Casp-9 All none
* = p<.005

Figure 4.6 *mir-24a* targets the 3' untranslated region of *caspase9* and *apaf1*
(A) The 3' untranslated regions of *X. laevis caspase9* and *apaf1* have two putative *mir-24a* binding sites, as measured by RNAhybrid (Kruger and Rehmsmeier, 2006). (B) The addition of *mir-24a* causes GFP reporters with *mir-24a* recognition elements in their 3' untranslated regions to be repressed. GFP reporters with the 3'UTR of *caspase9* and *apaf1* show repression by *mir-24a*. Mutating the putative *mir-24a* binding sites in these constructs (red letters in A, mutCasp9 and mutApaf1) abolishes the repression (n=4 experiments, error bars are s.e.m.).

Figure 4.6

A

Xla Caspase-9

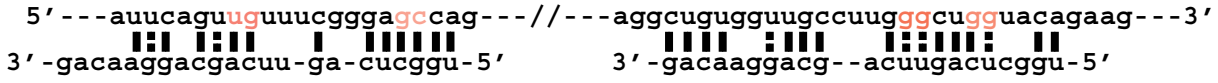

Xtr-miR-24a Xtr-miR-24a

Xla **AP**AF1

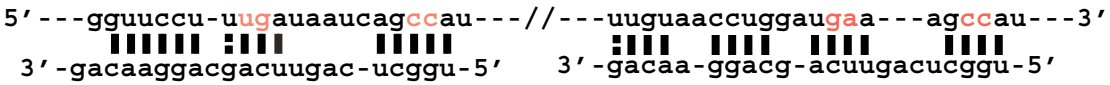

Xtr-miR-24a Xtr-miR-24a

B

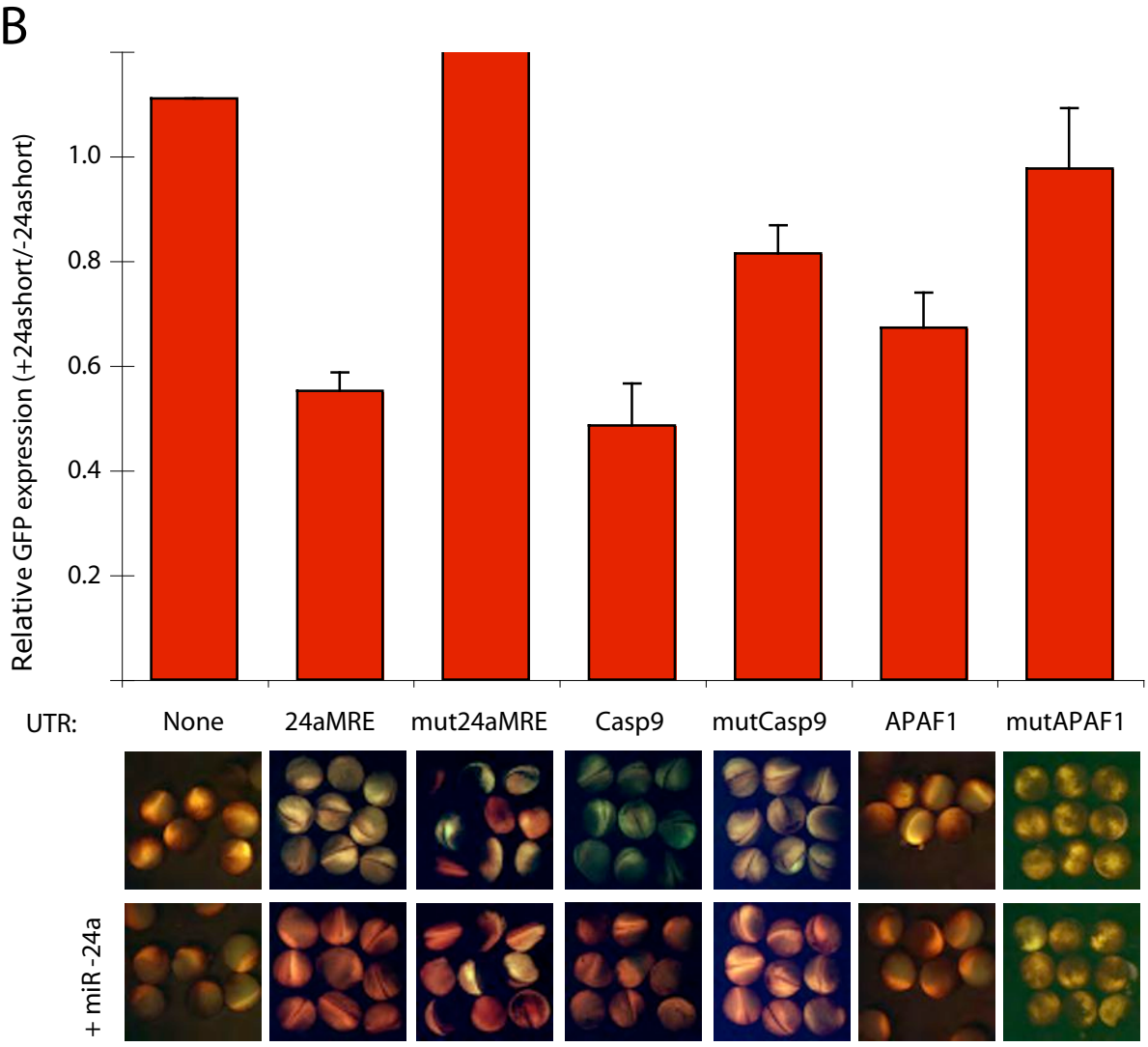

Figure 4.7 *Caspase9* and *apaf1* are expressed in the retina during *Xenopus* development

(A) *In situ* hybridization in *X. laevis* for *caspase9* and *apaf1* at stages 24 and 31, showing expression in the retina during the time of *miR-24a* function.

Figure 4.7

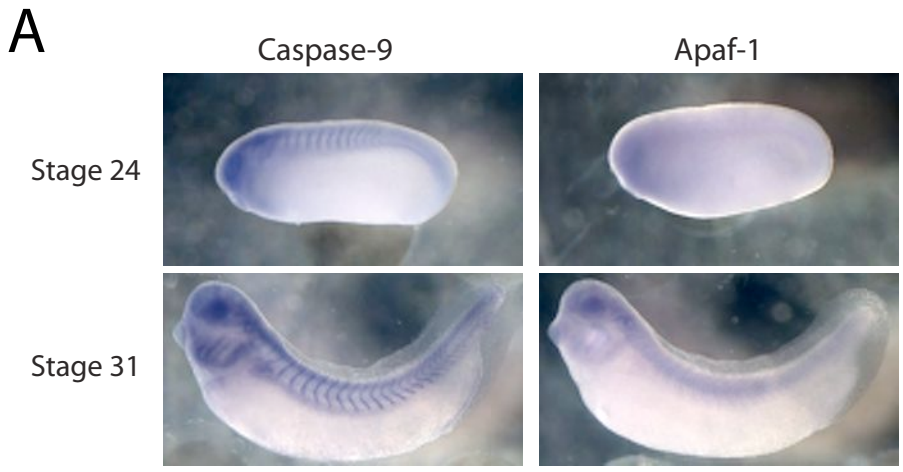

Figure 4.8 Overexpression of *mir-24a* can suppress hydroxyurea-induced and caspase9-induced apoptosis

(A) Embryos injected with 2ng *mir-24a* or *mir-24a*mm or nothing were cultured in 15mM hydroxyurea to induce apoptosis at the onset of gastrulation. Only *mir-24a* was able to significantly repress or delay the onset of apoptosis (n=3 experiments, error bars are s.e.m.). (B) Embryos injected with either 1ng *caspase9* or 1ng *caspase9* and 2ng *miR-24a* were cultured until neurula stages. *miR-24a* was able to significantly repress the amount of apoptosis (n=3 experiments, error bars are s.e.m.)

Figure 4.8

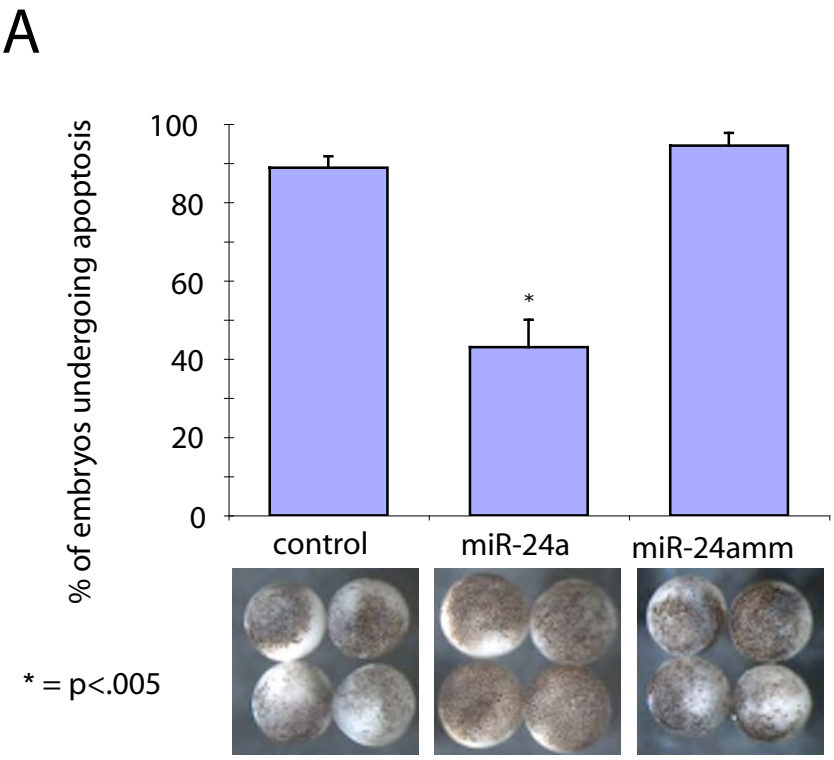
A
% of embryos undergoing apoptosis
100
80
60
40
20
0
*
control
miR-24a
miR-24amm
* = p<.005
B
% of embryos undergoing apoptosis
80
60
40
20
0
*
control
caspase9
caspase9
+
miR-24a
* = p<.005

Chapter 5

miR-133b is required for proper differentiation of hypaxial muscles

Summary

miR-133b is expressed in the developing somites and hypaxial muscle derivatives shortly before terminal differentiation and the formation of myotubes. Functional knockdown of *miR-133b* with antisense morpholinos results in reduced expression of hypaxial muscle differentiation markers, including myoD, p27, and 12-101. Knockdown of *miR-133b* has no effect on proliferation but results in elevated apoptosis late in development. Overexpression of *miR-133b* in hypaxial muscle precursors results in premature differentiation and disrupted migration, but has no effect on proliferation. In animal caps, both activin and myoD are able to induce the expression of *miR-133b*, which provides an in vitro system to search for targets of *miR-133b*. The data presented here strongly suggest that *miR-133b* functions in developing myoblasts and is necessary for the proper differentiation of hypaxial muscles during development in *X. laevis*.

Introduction

MicroRNAs are non-coding RNAs that have been shown to have important developmental functions in a variety of tissues, including the liver, brain, and eye (Damiani et al., 2008; Giraldez et al., 2005; Hand et al., 2009). Several miRNAs show highly conserved expression patterns in developing muscle tissues, including *miR-1*, *miR-206*, and *miR-133* (Kim et al., 2006; Rao et al., 2006; Takaya et al., 2009). Pairs of these miRNAs can even be found on the same primary transcript in different combinations, and so are very likely expressed in the same tissues. Several reports have identified transcriptional regulators for these myogenic-specific miRNAs, including the muscle-specific transcription factors *myoD* and *myogenin* (Rao et al., 2006). Furthermore, when mature miRNAs are eliminated in developing muscle in conditional Dicer mutant mice, the embryos die perinatally and have significantly less muscle mass, poor muscle morphology, and increased levels of muscle-specific apoptosis (O'Rourke et al., 2007). Mouse *miR-133a* knockouts lead to embryos with cardiac muscle defects (Liu et al., 2008). These results clearly indicate that muscle-specific miRNAs are key regulators of proper muscle differentiation, a function that may be conserved across animal taxa.

While most of these muscle-specific miRNAs are expressed in both cardiac and skeletal muscles, I previously reported that *miR-133b* is not expressed in cardiac tissue in *Xenopus*, but rather expressed in skeletal and hypaxial muscle domains in the developing embryo (Walker and Harland, 2008). Hypaxial muscles are derived from myoblasts of the ventrolateral somite and undergo an epithelial-to-mesenchymal transition prior to their migration to the location where they undergo terminal differentiation. In *Xenopus* the migrating hypaxial muscle forms the rectus abdominus, rectus cervicus, and geniohyoideus muscles, among others (Martin and Harland, 2001). These hypaxial myoblasts are specified express *pax3* when specified and require *msx1* and *lbx1* for migration; cells eventually express *miR-133b*, *myf5*, and *myoD* as they differentiate (Martin and Harland, 2001; Martin and Harland, 2006). Because *miR-133b* is the only miRNA so far described to have hypaxial myoblast expression, it may be an important regulator of the myogenesis exhibited by this tissue.

In this study, I investigated the function of *miR-133b* by morpholino knockdown and miRNA overexpression. I confirmed that *miR-133b* is expressed in hypaxial muscles in *X. laevis*, and showed that knockdown of *miR-133b* results in a significant decrease in hypaxial muscle differentiation while early specification and migration markers remain unchanged. Late-stage apoptosis is increased in *miR-133b*-depleted embryos, and as a result, hypaxial-derived muscles are absent or severely reduced. Overexpression of *miR-133b* causes similar reductions in the amount of hypaxial muscle, but premature differentiation appears to be the cause. My results indicate that *miR-133b* likely targets an inhibitor of muscle differentiation, and I present several candidates that have putative *miR-133b* target sites in their 3'UTR.

Results

***miR-133b* is expressed in developing somites and hypaxial muscles**

In Chapter 3, I reported the primary-miRNA expression patterns for several miRNAs during development of *X. tropicalis*. The miRNA with the most robust expression pattern was that of *miR-133b*, which was expressed in somites during and after neurulation and in hypaxial muscle derivatives, including the body wall muscles and several muscles of the head. This was also one of the few miRNAs for which there exist *X. laevis* ESTs, which confirmed its expression and allowed me to create antisense probes against *miR-133b* for in situ hybridization in this species. The expression pattern of *miR-133b* in *X. laevis* is identical to that in *X. tropicalis*; it is expressed in somitic mesoderm and migratory hypaxial muscles (Figure 5.1A, arrowheads and arrows, respectively). To further define the expression pattern relative to other markers of hypaxial muscle migration and differentiation, I compared the expression of *miR-133b* to that of *lbx1*and *myoD*, and 12-101, an antibody to an antigen that is specifically expressed muscles that have undergone myotube formation (Kintner and Brockes, 1984). As Figure 5.1B shows, *miR-133b* is not expressed in the early migratory precursors of hypaxial muscles, unlike *lbx1* and *myoD*. However, *miR-133b* is expressed just prior to hypaxial muscle differentiation in a similar domain to *myoD*, just at the ventral edge of myotube formation of the body wall muscles (arrow). This expression pattern suggests that *miR-133b* may be important for the differentiation of hypaxial muscle cells.

Knockdown of *miR-133b* causes specific loss of hypaxial differentiation markers

To repress the function of *miR-133b*, an antisense morpholino oligonucleotide targeting the stem and loop of pre-*miR-133b* (133bMO) was injected into one cell of embryos at the two-cell stage. Injection of 133bMO had no effect on neural development (as assayed by *sox2* and *n-tubulin* expression) or neural crest development (as assayed by *slug* expression) (data not shown). However, hypaxial muscle development was disrupted specifically on the injected side. As Figure 5.2A shows, knockdown of *miR-133b* causes a decrease in the expression of differentiation markers *myoD*, *p27(Xic1)*, and *myogenin* in the hypaxial muscle domains in which they are normally expressed at stage 35. This repression is found only for markers of late muscle differentiation, because *pax3* and *myf5*, markers for hypaxial specification, and *lbx1*, a marker of migrating hypaxial muscles, are all normal after *miR-133b* knockdown (Figure 5.2A). Tadpole muscles that are hypaxial derivatives are especially reduced when *miR-133b* is knocked down, as show by 12-101 staining (Figure 5.2B). Whole-mount staining of embryos at stage 41 reveals that no body wall muscles or head muscles have differentiated in the absence of *miR-133b* function. At later stages, a ventral view of a representative tadpole shows significant reduction in several hypaxial derivatives, including the rectus abdominus and the hypoglossal muscles (Figure 5.2B).

To confirm that 133bMO was disrupting the function of *miR-133b* in vivo, I generated a GFP sensor that consisted of a destabilized green fluorescent protein with two perfect *miR-133b* recognition elements (MREs) in its 3' untranslated region (133bUTR). When RNA was injected into embryos, robust expression of GFP was seen before the onset of *miR-133b* expression. If duplex *miR-133b* is co-injected, the GFP is translationally repressed, as quantified by pixel intensity (Figure 5.3A). If both *miR-133b*

and 133bMO are injected, the reporter is de-repressed and GFP levels are almost the same as control, demonstrating that 133bMO is able to repress the function of *miR-133b* (n=3 batches, 9 embryos per batch). The repression of the GFP reporter is dependent upon the *miR-133b* sites in the 3'UTR, because mutating four nucleotides of the seed sequence in these sites prevents *miR-133b* from repressing expression. These experiments are further strengthened by the observation that the GFP sensor is sensitive enough to be repressed by endogenous levels of *miR-133b*. In Figure 5.3B, embryos were injected into two cells at the 32-cell stage with RNA for the sensor and RFP, one of ectodermal fate and one of mesodermal fate. When the embryos reached tadpole stage, the RFP tracer was observed in both tissue types, the skin and tail muscles. However, the GFP was observed only in the skin, having been repressed by *miR-133b* in the muscle tissue (n=10). Because the sensor is sensitive even to levels of endogenous miRNA, it serves as a good control for *miR-133b* activity and 133bMO efficacy.

Knockdown of *miR-133b* causes apoptosis during late hypaxial myogenesis

Because hypaxial muscle derivatives were reduced or absent during tadpole stages, I tried to identify if and when programmed cell death was occurring. TUNEL staining showed no significant difference between 133bMO-injected and uninjected embryos in the numbers of apoptotic nuclei in embryos at stage 33 or 37, before and during hypaxial myoblast migration, before most differentiation has occurred (Figure 5.4A-B). However, once significant differentiation should have taken place, the side of the embryo with repressed *miR-133b* function had significantly more cells undergoing apoptosis than the uninjected side, while continuing to have much less differentiated muscle, as marked by 12-101 staining (n>6 embryos per stage).

Another mechanism for muscle loss might be a reduction in proliferative potential by the progenitors of hypaxial muscles. To analyze this possibility, I performed immunostaining for phosphorylated histone-3, a marker of proliferating cells. Throughout the development of the hypaxial musculature, there is no difference between the *miR-133b* knockdown and the control embryos in the amount of proliferation in the hypaxial domain (Figure 5.5A-B, n>9 embryos per stage, 3 stages). This correlates with gene expression data that shows *miR-133b* is expressed in cells that have probably exited the cell cycle, as well as with the knockdown analysis showing no effect on specification or migration of hypaxial muscles. Together these data lead me to propose that *miR-133b* is necessary for the correct differentiation of hypaxial myoblasts into myotubes, and that cells that are unable to complete this transition undergo programmed cell death.

***miR-133b* overexpression disrupts hypaxial muscle differentiation**

To explore the function of *miR-133b* further, I pursued a gain of function strategy by injecting duplex *miR-133b* RNA into the location of the embryo destined to become dorso-anterior mesoderm, from which the hypaxial muscles are derived. Overexpression of *miR-133b* caused a reduction of *myoD* and *p27* without affecting the expression pattern of *pax3*, similar to the knockdown phenotype of *miR-133b* (Figure 5.6A). This counterintuitive result may be explained by premature myoblast differentiation, which would also appear as a disruption in differentiation. Using 12-101 staining as a marker

for differentiation, it appears that the overexpression of *miR-133b* leads to premature myotube formation prior to complete migration (Figure 5.6B) This staining shows differentiated cells near the ventral edge of the paraxial muscle and myotube formation oriented perpendicular to that in normal embryos. Premature differentiation is seen in embryos even at early stages (33, Figure 5.6B) and in embryos in which migration appears to be normal (*pax3*, Figure 5.6A, and *lbx1*, data not shown). One explanation for this apparently normal migration may be that proliferation levels are unchanged between *miR-133b*-injected embryos and control embryos (Figure 5.6C, n>7 embryos per stage, 3 stages). Another possibility is that only small subsets of hypaxial muscle cells have enough exogenous *miR-133b* to overwhelm the migratory program and undergo premature full differentiation and myotube formation. Further investigations into the effects of the exogenous *miR-133b* dose may elucidate the requirement for *miR-133b* to prematurely activate differentiation.

miR-133b is induced by *activin* and *myoD* in animal caps

Animal cap explants are normally fated to become epidermis, but are a naïve enough tissue that they can be induced to form many different tissue types in an embryo (Woodland and Jones, 1987). Previous research has shown that overexpression of *myoD* is able to transiently induce muscle in the animal cap (Hopwood and Gurdon, 1991). Injection of 1ng of *myoD* can induce animal caps to become immunoreactive to 12-101 and to express muscle markers such as *myoD*, *myf5*, *p27*, and *muscle actin* by RT-PCR (Figure 5.7A and data not shown). *MyoD* overexpression also weakly induces pri-*miR-133b* expression.

Previous research has also shown that low levels of Activin can induce animal caps to become mesoderm and then muscle tissue. Injection of 4pg *activin* caused animal caps to elongate and to become immunoreactive to 12-101 (Thomsen et al., 1990) and data not shown), indicating that some differentiated muscle was forming. RT-PCR analysis revealed that expression of pri-*miR-133b* was induced in activin-injected caps (Figure 5.7B). Furthermore, other muscle markers such as myoD, myf 5, p27, and cardiac actin were induced as well. Because both overexpression of myoD and activin induce *miR-133b* expression, I can use these induced caps to further study the function of *miR-133b*.

When 133bMO is co-injected with either *myoD* or *activin*, the levels of pri-*miR-133b* increase in animal caps. This is probably due to the morpholino interfering with the processing of the primary transcript into the mature product, but could also indicate negative feedback in the regulation of *miR-133b*. *miR-133b* knockdown in *activin*-injected caps shows phenotypes similar to those in whole embryos; *myf5* and *pax3* expression is unchanged, but *muscle actin* and *p27* expression is reduced. I hope that recapitulating hypaxial muscle development in animal caps will provide another method to investigate the molecular function of *miR-133b*, particularly regarding putative targets. I expect bona fide targets of *miR-133b* to be up-regulated when 133bMO is present, and conversely, down-regulated when *miR-133b* is overexpressed.

Several candidate target genes for miR-133b are expressed during myogenesis

From both the loss- and gain-of-function experiments described above, conclusions can be drawn about the likely targets for *miR-133b* in vivo. Because *miR-133b* knockdown prevents myotube formation, and *miR-133b* overexpression causes premature differentiation, it is probable that *miR-133b* is responsible for repressing a gene whose function inhibits differentiation. There are many such genes in the literature, and I have refined this list by searching their 3'UTRs for putative *miR-133b* target sites using RNAhybrid (Kruger and Rehmsmeier, 2006). Among the best candidates are inhibitor of differentiation (Id) genes *id2*, *id3* and *id4*, forkhead box (fox) genes *foxC2*, *foxD2*, and *foxK1*, myogenic factors *myogenin* and *serum response factor* (*SRF*) and basic helix-loop-helix genes *sharp-1(dec2)* and *paraxis*. While biochemically isolating in vivo targets would be the preferred method of target identification, there are few published protocols, and much troubleshooting remains to be done (Chapter 6). In lieu of this deficiency, I have begun to determine whether any of these candidates is likely to be the primary target of *miR-133b*. An initial step is to determine the expression patterns in *Xenopus*, which I have done in several cases (Figure 5.8A-J). For the target of *miR-133b*, I would expect muscle expression, ideally in hypaxial muscles, before terminal differentiation. This eliminates the Id genes as candidates, as *id2* is expressed in the brain, kidney, and branchial arches (Figure 5.8A), *id3* is expressed in the eye and the branchial arches (Figure 5.8B), and *id4* is expressed in the kidney and the brain (Figure 5.8C). *FoxD2* is also a poor candidate, as expression is found only in muscles of the head and not in body wall muscles (Figure 5.8E). Conversely, *foxc2*, *foxk2*, *myogenin*, *srf*, *sharp1(dec2)*, and *paraxis* are all expressed in hypaxial muscle domains and are good candidates to be *miR-133b* targets. Experimentally, I would expect overexpression of the target to phenocopy the knockdown of *miR-133b*, either in whole embryos or animal caps. In addition, the 3'UTRs of these genes should confer *miR-133b*-based repression when placed downstream of a destabilized GFP. These experiments are currently being performed with the results forthcoming.

Discussion

The data presented here indicate that *miR-133b* is necessary for proper differentiation of hypaxial muscles during development in *X. laevis*. My results suggest that overexpression of *miR-133b* leads to premature hypaxial muscle differentiation and that knockdown of *miR-133b* leads to delayed differentiation, eventually causing apoptosis and severe reduction in hypaxial muscle derivatives, including the body wall muscles (rectus abdominus and rectus cervicus) and geniohyoideus. These results are in stark contrast to other results published on the role of *miR-133* during myogenesis, however. Chen et al. found that overexpression of *miR-133* in cell culture resulted in a decrease in muscle differentiation and an increase in cell proliferation, and knocking down *miR-133* resulted in an increase in muscle differentiation and a decrease in cell proliferation (Chen et al., 2006). I have found no evidence of *miR-133b* affecting cell proliferation in my analyses. Perhaps the differences between the two sets of experiments reflect a difference in the model system used or the type of muscle cells in which the experiments were performed. To support this possibility, Chen et al. found no significant difference in proliferation when *Xenopus* embryos were injected with *miR-133*. However, the nearly opposite phenotypes observed between Chen at al. and this

report are potentially problematic. Several explanations for the differences could apply. Chen and colleagues did not distinguish between *miR-133a* and *miR-133b*, while my analysis has been on *miR-133b* only. While these miRNAs are different at only a single nucleotide at the 3' end of the sequence, perhaps it is important for the regulatory function of the gene. It is also possible that the role of miR-133 during myogenesis is different between species, and that in mammals it is an inducer of proliferation and a negative regulator of differentiation. I think that it is more likely that the type of experiment is important – the myogenic differentiation program that Chen et al. use *in vitro* may be significantly different than the one that hypaxial muscles are undergoing *in vivo*, leading to repression of different target mRNAs and therefore different phenotypes.

Furthermore, when the authors overexpressed *miR-133b* in *Xenopus* embryos, they found a reduction in anterior structures and defects in somite development, especially in the more anterior and posterior portions of the embryo, and defects in cardiac looping and chamber formation. This collection of phenotypes has never been present in my *miR-133b*-injected embryos, although several caveats apply; my injections were targeted marginally at the two-cell stage, while they performed injections at the one-cell stage. Though both these manipulations should have targeted somites, no somite disruption occurs at the doses of RNA that I have used, doses that are sufficient to block the translation of a GFP sensor construct and rescue the morpholino phenotype. I am convinced that gene knockdown approaches and targeted overexpression are more relevant to determining the *in vivo* function of miRNAs, because off-target effects are highly likely when miRNAs are overexpressed in tissues in which they are normally absent.

In partial support of my conclusions are the results of studies in zebrafish. Yin et al. found that *miR-133b* is repressed as fin regeneration proceeds in an Fgf-dependent manner (Yin et al., 2008). Overexpression of *miR-133b* led to decreased regeneration potential, and blocking *miR-133b* function accelerated regeneration by specifically increasing proliferation. These results are consistent with the role I characterized for *miR-133b* in *Xenopus*, as *miR-133b* is necessary and sufficient for the terminal muscle differentiation phenotype, although I see no role for regulation of proliferation during hypaxial muscle development. Mishima et al. down-regulated *miR-133* in zebrafish embryos and found only minor defects, including a reduction in muscle fiber size and a mild effect on actin bands during sarcomere assembly (Mishima et al., 2009). In line with these data, I have found no somite or sarcomere phenotype in *Xenopus* when *miR-133b* is functionally reduced. Mishima and colleagues, however, found more severe effects on sarcomere organization when they knocked down both *miR-1* and *miR-133*, an experiment that I am also interested in pursuing, as both are expressed in the somites of developing embryos (Chapter 3).

Hypaxial muscle development is a highly regulated process (Martin and Harland, 2006; Martin et al., 2007; Zhao et al., 2007a), and *miR-133b* is a crucial regulator for the correct terminal differentiation of this migratory population. However, *miR-133b* is expressed not just in the hypaxial and cranial muscles that require its function, but also in the developing somites and their fully differentiated trunk muscles. Yet these tissues show no perturbations when *miR-133b* levels are experimentally manipulated in *Xenopus*. This may be an issue of *miR-133* gene family redundancy; there is EST evidence for expression of *miR-133a* and *miR-133d*, and they may be expressed in trunk muscle. It

may also be muscle-specific miRNA redundancy, as it has been shown that *miR-1* and *miR-206* can have overlapping targets with *miR-133* (Shkumatava et al., 2009), and these microRNAs are expressed in non-hypaxial muscle domains. Another possibility is that pri-*miR-133b* is unprocessed in these tissues and actually has no developmental function in them, maturing only in the hypaxial muscles where it can then regulate its target genes. Future experiments exploring the functional roles of the other members of the *miR-133* family and *miR-1/206* may be able to show separable activities of unique miRNAs during muscle differentiation.

Figure 5.1 *miR-133b* is expressed in developing somites and hypaxial muscles

(A) In situ hybridization on *X. laevis* with probe antisense to the primary microRNA shows expression of pri-*miR-133b* in the central compartment of the somites (arrowheads) and paraxial mesoderm early and the hypaxial muscle derivatives of the belly wall (arrows) and facial muscles late. (B) Expression pattern of *miR-133b* in comparison to other hypaxial muscle markers lbx1 (migrating cells), myoD (differentiating cells) and 12-101 (myotube formation marker, in brown). *MiR-133b* is not expressed during early migration of hypaxial muscle cells, but as terminal differentiation occurs, before complete myotube formation.

Figure 5.1

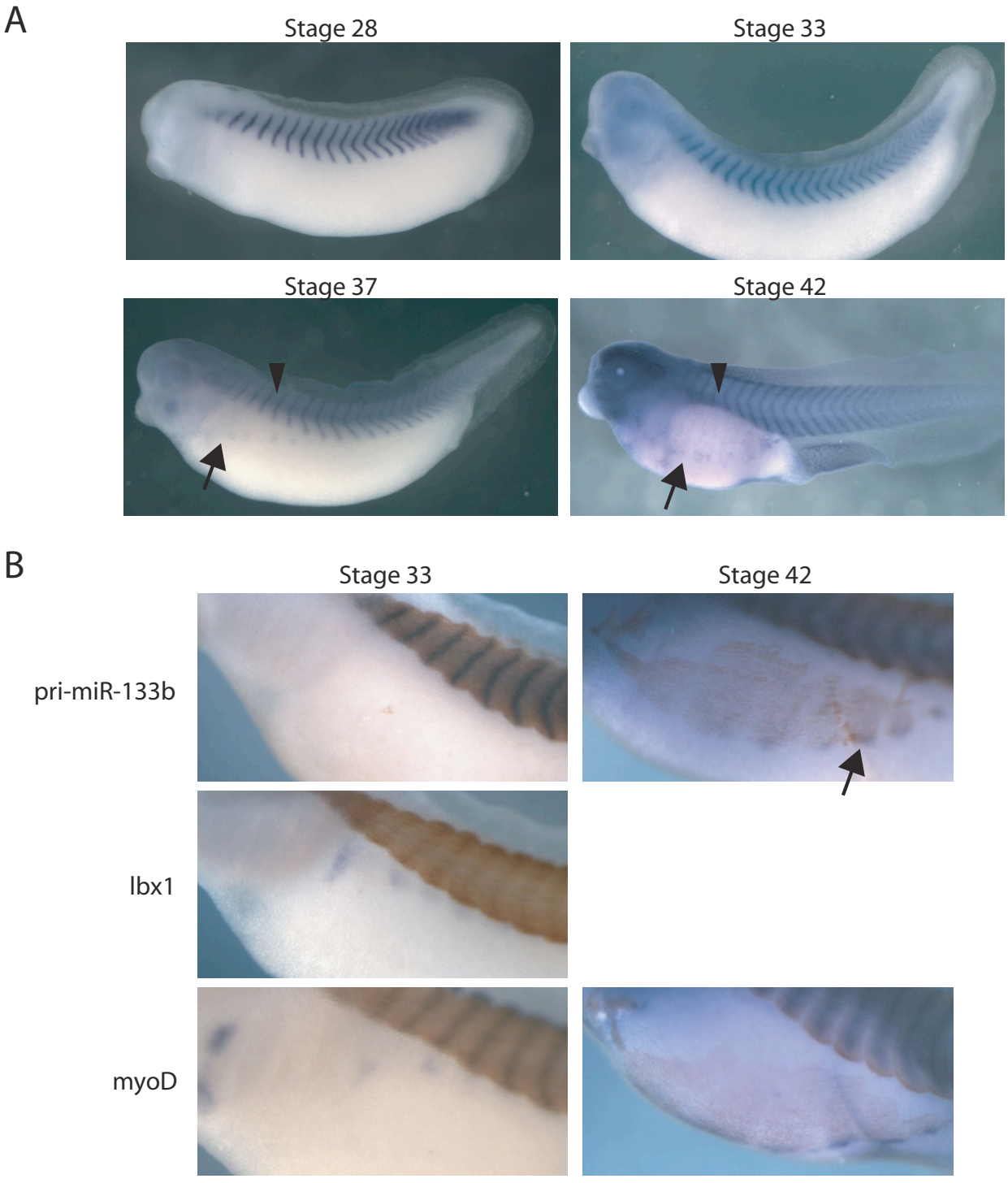
A
Stage 28
Stage 33
Stage 37
Stage 42
B
Stage 33
Stage 42
pri-miR-133b
lbx1
myoD

Figure 5.2 Knockdown of *miR-133b* causes specific loss of hypaxial differentiation markers

(A) Injection of an antisense oligonucleotide to *miR-133b* (133bMO) causes reduction or loss of differentiation markers in the hypaxial muscle territory. (B) The terminal muscle differentiation marker 12-101 shows specific loss of hypaxial muscle derivatives at tadpole stages when *miR-133b* function is reduced. Left panel shows both sides of a representative embryo at stage 37. Middle panel is a section at stage 37 showing loss of hypaxial muscles (arrow). Right panel is a representative embryo at stage 45, showing loss of hypaxial muscle derivatives, especially body wall muscles and the geniohyoideus (arrow and arrowhead, respectively).

Figure 5.2

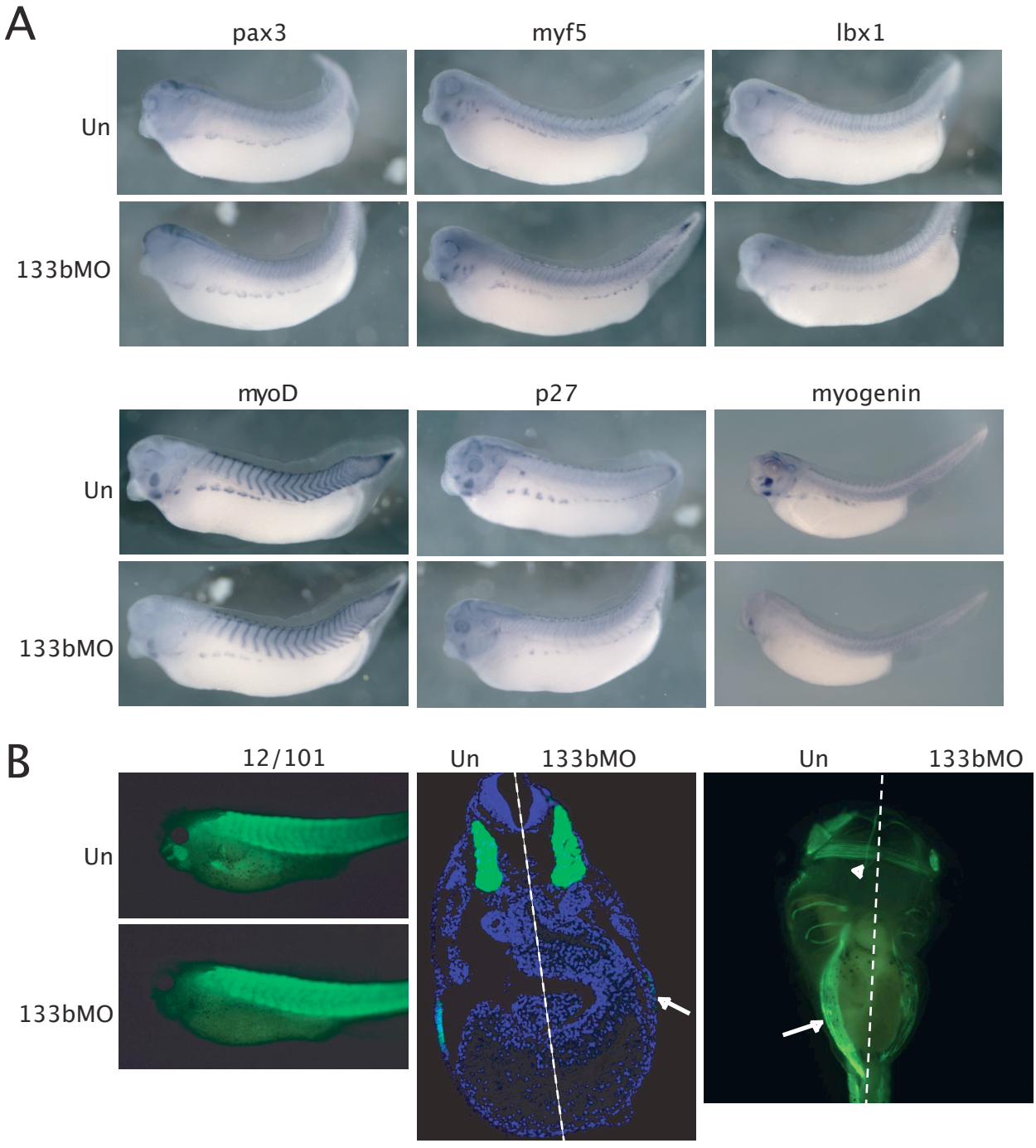
A
pax3
myf5
lbx1
Un
133bMO
myoD
p27
myogenin
Un
133bMO
B
12/101
Un
133bMO
Un
133bMO
Un
133bMO

Figure 5.3 A GFP reporter system for assessing *miR-133b* function
(A) 133bMO functionally represses *miR-133b*. RNA for GFP with two *miR-133b* recognition elements (133bUTR) was co-injected with RFP. When duplex *miR-133b* is coinjected, the levels of green fluorescence are significantly reduced. When antisense morpholino oligonucleotide to *miR-133b* is coinjected, green fluorescence is restored. This effect is dependent on the interaction between *miR-133b* and the *miR-133b* recognition elements (MREs), because mutation of these elements eliminates the repression by *miR-133b* (All situations n=3 batches, 9 embryos per batch, error bars s.e.m.). (B) Endogenous *miR-133b* is able to repress the GFP construct with two perfect *miR-133b* recognition elements. Embryos were injected with 133bUTR and RFP RNA in one ectoderm and one mesoderm cell at the 32-cell stage and were cultured until tailbud stages and photographed for fluorescence in the green and red channels. In ectoderm, where *miR-133b* is not expressed, the reporter maintains translation and green fluorescence is seen. However, in muscle tissues, where *miR-133b* is expressed, the reporter is repressed, and no green fluorescence can be seen.

Figure 5.3

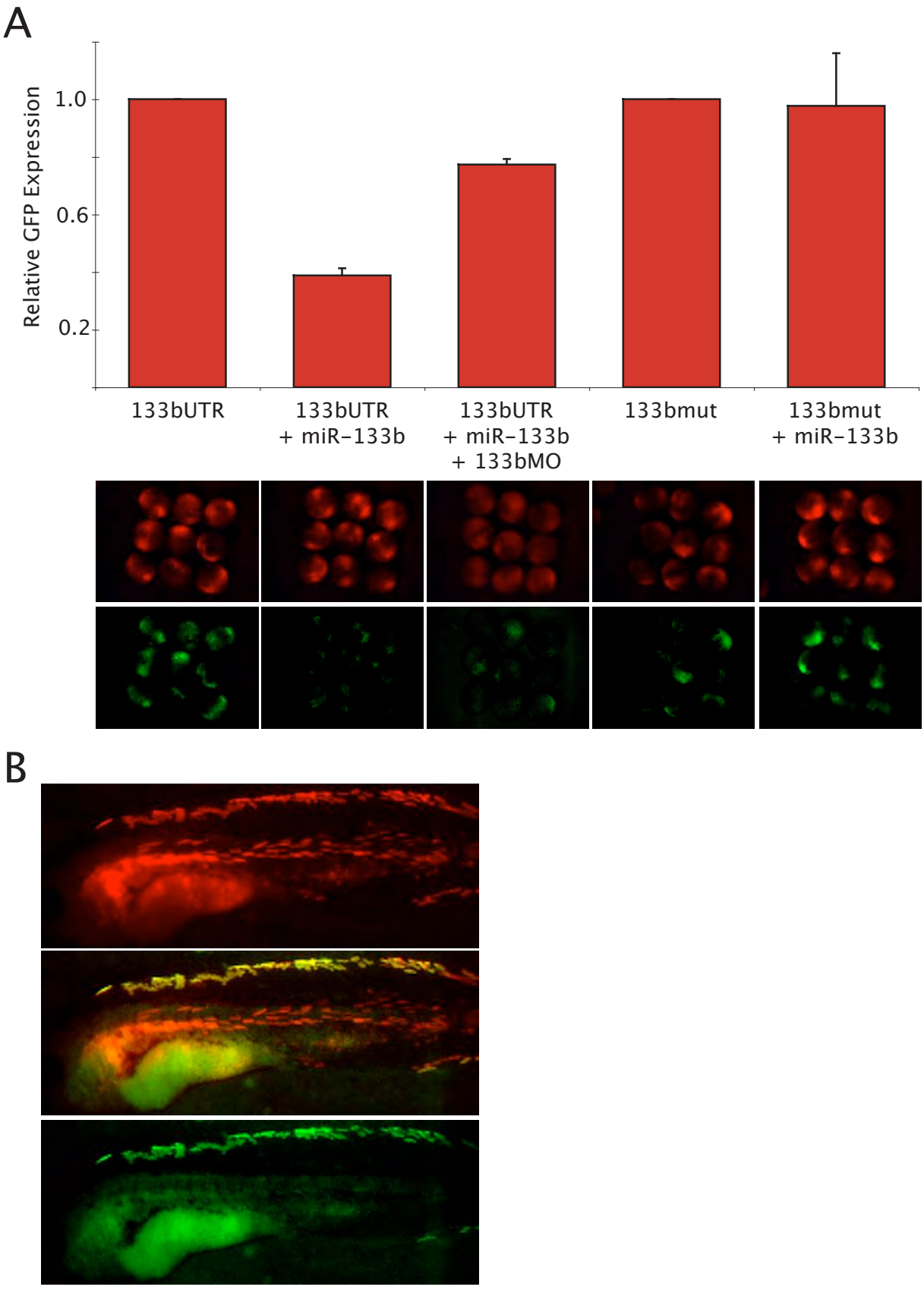
A
Relative GFP Expression
1.0
0.6
0.2
133bUTR
133bUTR + miR-133b
133bUTR + miR-133b + 133bMO
133bmut
133bmut + miR-133b
B

Figure 5.4 Knockdown of *miR-133b* causes apoptosis during late hypaxial myogenesis
(A) Apoptotic nuclei (shown by TUNEL staining, black nuclei) in embryos injected with 133bMO and stained for 12-101 (brown). (B) Quantification of TUNEL-stained embryos. Only at stage 41 is there a significant increase in apoptotic cells in the hypaxial domain, when most mature myotubes have formed in the uninjected control ($n > 6$ embryos per stage, * $p < .05$).

Figure 5.4

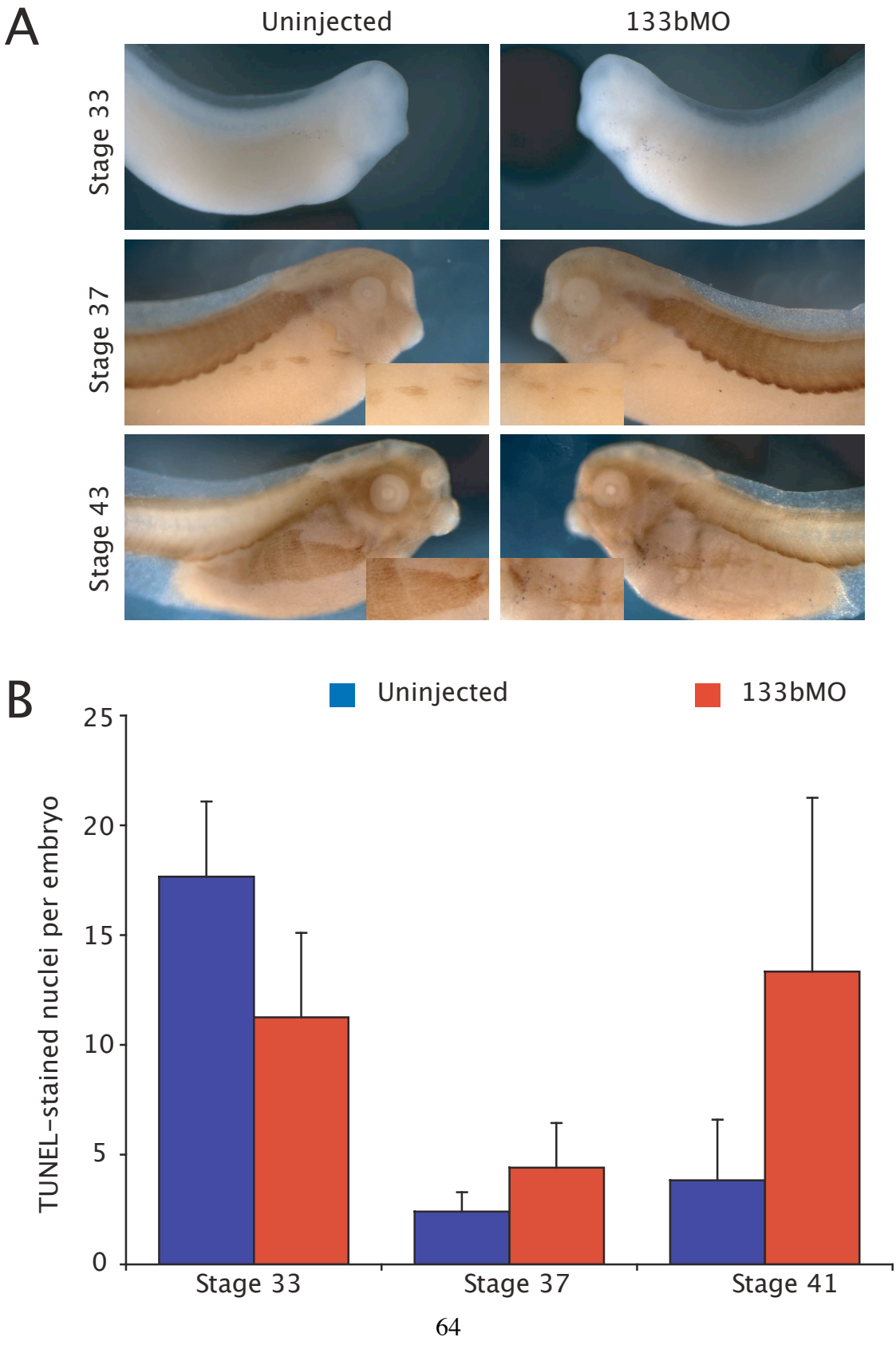
A
Uninjected
133bMO
Stage 33
Stage 37
Stage 43
B
Uninjected
133bMO
TUNEL-stained nuclei per embryo
25
20
15
10
5
0
Stage 33
Stage 37
Stage 41

Figure 5.5 Knockdown of *miR-133b* has no effect on proliferation during hypaxial myogenesis
(A) Proliferating cells (shown by phospho-histone 3 staining, black nuclei) in embryos injected with 133bMO and stained for 12-101 (brown). (B) Quantification of phospho-histone 3-stained cells in the hypaxial domain of injected embryos. There is no significant difference between the 133bMO-injected side and the uninjected control side ($n > 9$ embryos per stage).

Figure 5.5

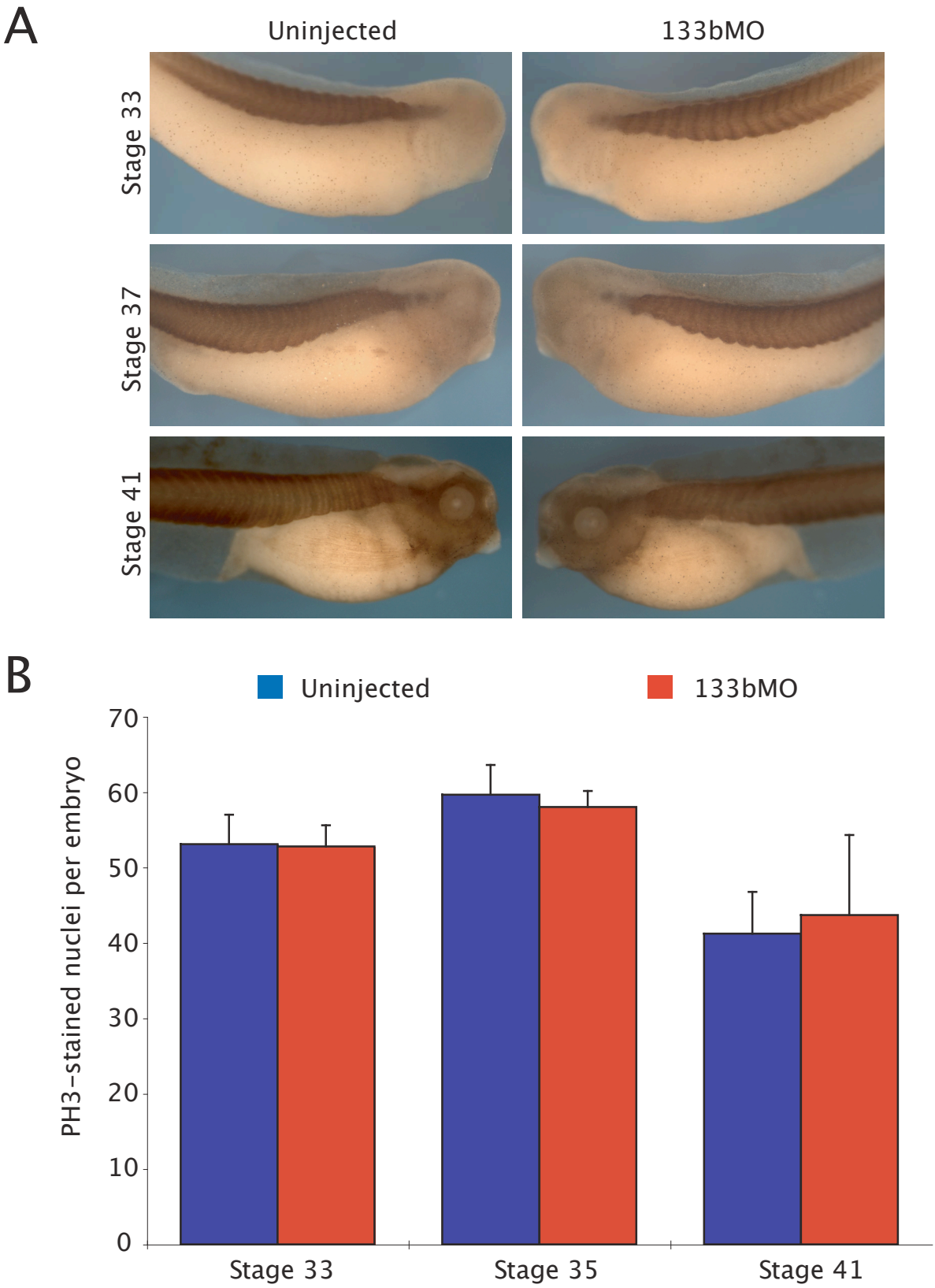
A
Uninjected
133bMO
Stage 33
Stage 37
Stage 41
B
Uninjected
133bMO
PH3-stained nuclei per embryo
0
10
20
30
40
50
60
70
Stage 33
Stage 35
Stage 41

Figure 5.6 *miR-133b* overexpression disrupts hypaxial muscle differentiation
(A) Injection of duplex *miR-133b* leads to a reduction in hypaxial muscle differentiation markers *myoD* and *p27* without disrupting precursor *pax3* expression. Red stain is LacZ lineage tracer. (B) Proliferating cells (shown by phospho-histone 3 staining, black nuclei) in embryos injected with *miR-133b* and stained for 12-101 (brown). Note that differentiated hypaxial myotubes are located much nearer to the somites from which they migrated, and are disrupted in organization. Red stain is LacZ lineage tracer. (C) Quantification of phospho-histone 3-positive nuclei in hypaxial domain. There is no significant difference between the *miR-133b*-injected side and the uninjected control side ($n > 7$ embryos per stage).

Figure 5.6

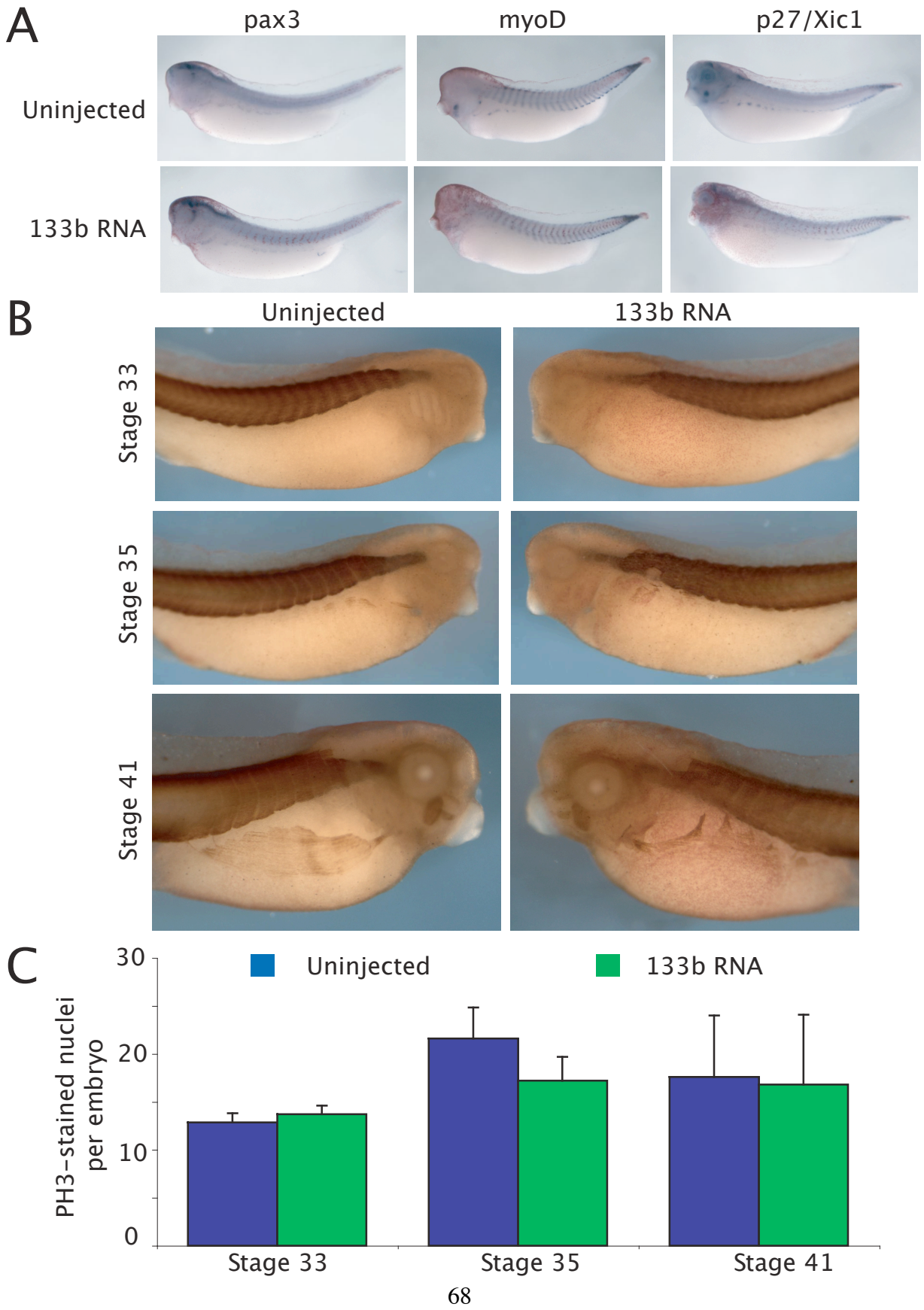
A
pax3
myoD
p27/Xic1
Uninjected
133b RNA
B
Uninjected
133b RNA
Stage 33
Stage 35
Stage 41
C
Uninjected
133b RNA
PH3-stained nuclei per embryo
30
20
10
0
Stage 33
Stage 35
Stage 41

Figure 5.7 Animal cap experiments may lead to insights into *miR-133b* function
(A) Animal cap explants injected with myoD can induce *miR-133b* as shown by RT-PCR for the pri-*miR-133b* transcript. In addition, coinjection with133bMO leads to more pri-*miR-133b*, indicating that processing is likely disrupted. (B) Animal cap explants injected with activin can induce pri-*miR-133b*.

Figure 5.7

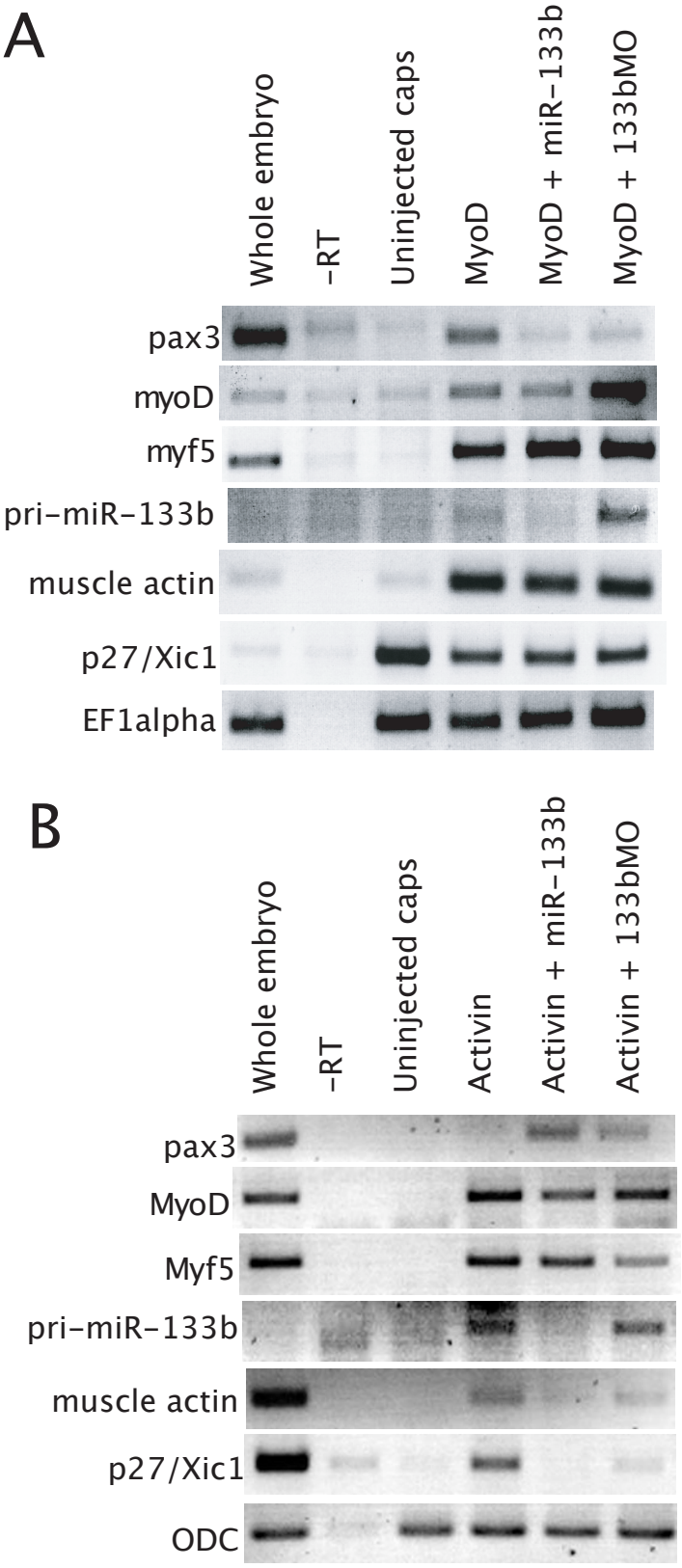
A
Whole embryo
-RT
Uninjected caps
MyoD
MyoD + miR-133b
MyoD + 133bMO
pax3
myoD
myf5
pri-miR-133b
muscle actin
p27/Xic1
EF1alpha
B
Whole embryo
-RT
Uninjected caps
Activin
Activin + miR-133b
Activin + 133bMO
pax3
MyoD
Myf5
pri-miR-133b
muscle actin
p27/Xic1
ODC

Figure 5.8 *In situ* hybridization of potential *miR-133b* target genes
(A) *In situ* hybridization of *id2* in *X. laevis* at stage 35. (B) *In situ* hybridization of *id3* in *X. laevis* at stage 33. (C) *In situ* hybridization of *id4* in *X. laevis* at stage 35. (D) *In situ* hybridization of *foxc2* in *X. tropicalis* at stage 33. (E) *In situ* hybridization of *foxd2* in *X. laevis* at stage 35. (F) *In situ* hybridization of *foxk1* in *X. laevis* at stage 35, as reported by Pohl and Knochel (2004). (G) *In situ* hybridization of *myogenin* in *X. laevis* at stage 37. (H) *In situ* hybridization of *srf* in *X. laevis* at stage 37. (I) *In situ* hybridization of *sharp1(dec2)* in *X. tropicalis* at stage 37. (J) *In situ* hybridization of *paraxis* in *X. laevis* at stage 31, as reported by Tseng and Jamrich (2004).

Figure 5.8

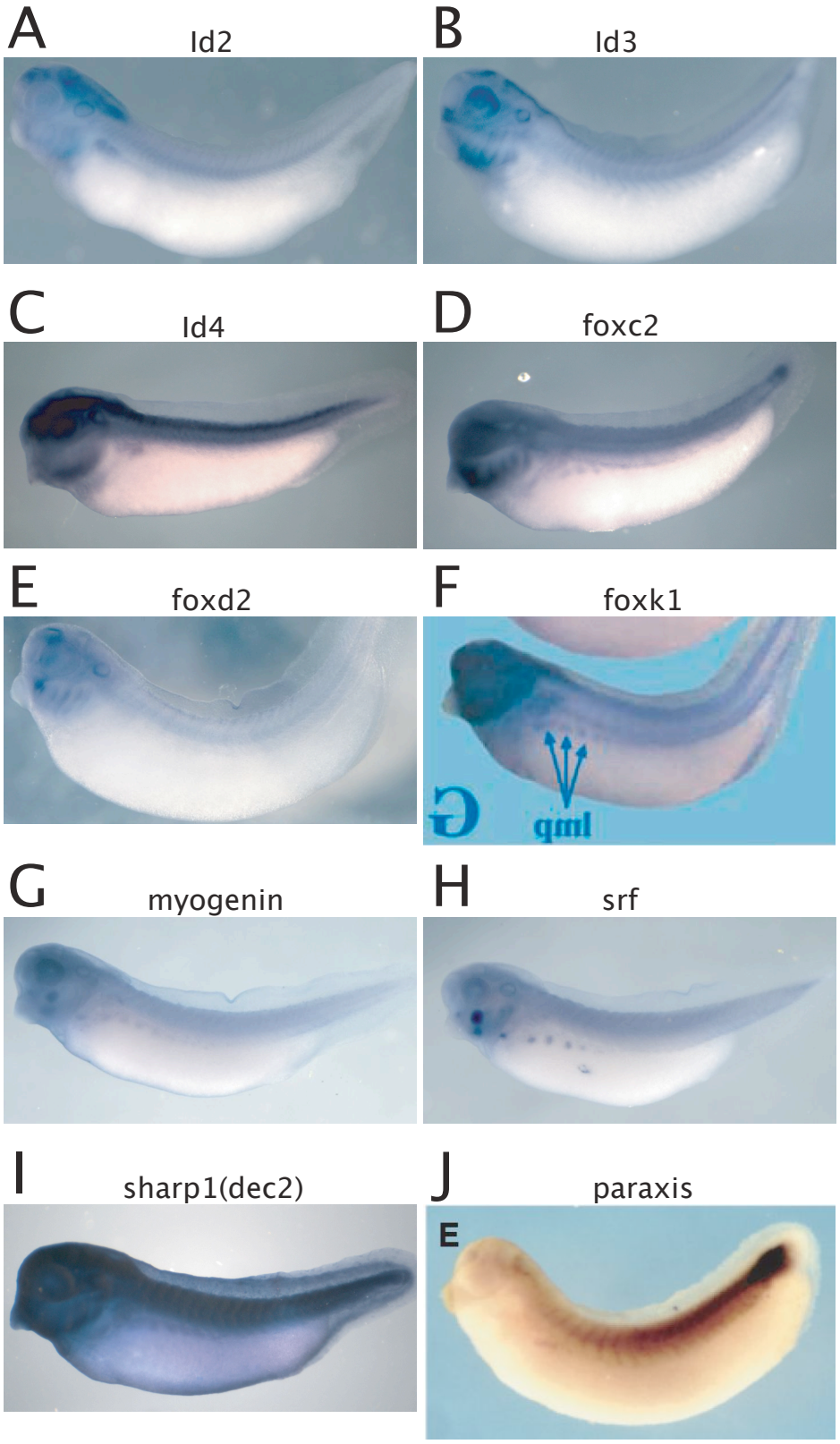
A
Id2
B
Id3
C
Id4
D
foxc2
E
foxd2
F
foxk1
G
myogenin
H
srf
I
sharp1(dec2)
J
paraxis

Chapter 6

Methods for biochemical isolation of microRNA targets

Summary

Computational methods for identifying putative microRNA targets have many failings. To eliminate the need to rely on these resources, several biochemical methods have recently been published with the goal of finding bona fide microRNA targets from tissue samples. I have attempted two of these methods in *Xenopus* with varying levels of success. I found that protocols using the endogenous microRNA as a primer for reverse transcription from its target are difficult to perform and yielded no target information. Alternatively I have utilized labeled mature microRNAs to immunopurify control target mRNA, and I have begun to optimize the protocol to increase the specificity of this reaction, suggesting that this method can be implemented to find in vivo targets of *miR-133b* in the near future.

Introduction

MicroRNAs are transcribed by RNA polymerase II as long primary transcripts and their transcription is regulated in much the same way as coding mRNAs. The functional miRNA forms a characteristic hairpin-loop structure that is the recognized motif for further processing. The primary transcripts are processed first in the nucleus by the enzyme Drosha, which leaves only the stem-loop sequence. After export to the cytoplasm, the pre-miRNA is processed by Dicer, resulting in a double-stranded RNA of ~21 nucleotides with a two-nucleotide overhang on either end. One of these strands is incorporated into the RNA-Induced Silencing Complex (RISC) by a member of the Argonaute family of proteins. The mature, single-stranded miRNA then directs RISC to the 3' untranslated region (UTR) of its target mRNAs, which then undergo translational repression and deadenylation. Most experimentally verified targets show sequences almost perfectly complementary to the second through the eighth nucleotides of the miRNA, the 'seed sequence' (He and Hannon, 2004).

Computational techniques to identify miRNA-mRNA target pairs are primarily based on finding strict seed sequence complementarity in the 3'UTR of transcripts (Watanabe et al., 2007). Some algorithms allow for single- or double-nucleotide insertions in their analysis of UTRs, but this of course increases the number of putative targets (and false positives) immensely. Further weight is given to sequences that share complementarity beyond the seed sequence, and several programs evaluate hybridization energy of putative miRNA-mRNA pairs (Kruger and Rehmsmeier, 2006; Zuker, 2003). Finally, evolutionary conservation of target sites is used to narrow down putative targets to those that have been under (presumed) selective pressure. Various combinations and weightings of each of these factors account for the differences between computational approaches (Watanabe et al., 2007).

Several issues make a purely computational technique to identifying miRNA targets unsatisfying. First, the sheer volume of putative targets that are predicted means that experimental validation of each for even a single miRNA would require a massive effort. Furthermore, even the most stringent algorithms have high false-positive rates (Jiang et al., 2009), and these algorithms are likely to be missing targets due to their very stringency. Several experimentally verified targets have poor seed sequence complementarity, and recent work has shown that secondary seed sequences may be important for a subset of miRNA targets (E. Samal, personal communication). Therefore, such mRNAs would be missing from most computationally predicted target datasets. In addition, species-specific targets would be ignored if conservation of miRNA target sites across evolutionary divergence is used as a key factor in target determination. Bioinformatic target identification is also extremely sensitive to the quality of 3'UTR annotation, which in the case of *X. tropicalis* is frequently simply the 2kb of sequence after the stop codon (Griffiths-Jones et al., 2008). These annotations can be wrong if there is splicing of the 3'UTR, and I have found that they often includes repeat sequences from the genome, and are therefore of insufficient quality for the task of whole-genome microRNA target predictions. It is because of these limitations that biochemical approaches for identifying bona fide *in vivo* targets are so important.

The biochemical approaches presented to date can be organized into three broad categories: reverse transcription on the target mRNA using the miRNA to prime the reaction (Andachi, 2008; Vatolin and Weil, 2008); immunoprecipitation with labeled

miRNAs (Hsu et al., 2009); and immunoprecipitation with argonaute proteins (Chi et al., 2009; Easow et al., 2007). Each technique has advantages and disadvantages, depending on the goal of the researcher and the manipulations that can be made with the starting tissue.

The first technique, described by Andachi, takes advantage of the complementarity of the miRNA and the 3'UTR of the mRNA (Andachi, 2008). The protocol describes a method whereby RISC-miRNA-mRNA complexes from cytoplasmic extracts are combined with a detergent at low temperature to destabilize proteins yet the miRNA-mRNA duplex is kept intact. The extract is then incubated in a reverse-transcription reaction buffer to synthesize a first-strand cDNA using the miRNA as a primer. After collection of double-stranded polynucleotides, a second-strand synthesis is performed that makes a DNA complementary to both the first strand cDNA and the miRNA. The resulting cDNAs are then cloned as a recombinant DNA library by standard procedures, with the exception that an amplification step occurs by PCR with a miRNA-specific primer. When Andachi performed this analysis on a miRNA with a known target gene (*lin-4* and *lin-14*, respectively), he found almost 75% of his miRNA-positive clones were from the known genetic target. When he examined a different miRNA, however, only 159 out of 672 clones actually bore the miRNA signature, showing that there is a high degree of non-miRNA priming (76%) (Andachi, 2008). This method has some promise to be useful for identifying targets of a single miRNA, though it remains to be seen how useful the method is in other systems. A similar protocol has been presented that uses a gene-specific primer for the second strand cDNA synthesis, which vastly reduces the likelihood of false positives, but eliminates the possibility of finding novel targets (Vatolin et al., 2006).

The second class of techniques is a purification of target RNAs whereby labeled exogenous miRNA is added to cellular extracts to immunoprecipitate miRNA:mRNA target complexes. Hsu et al. use a stem-loop pre-miRNA that is digoxigenin-labeled (Hsu et al., 2009). This dig-pre-miRNA is mixed with cell extracts where the endogenous Dicer cuts the duplex and generates the mature miRNA, which is then incorporated into the endogenous RISC and targets its complementary mRNAs. The mixture of miRNA-mRNA is then pulled down by anti-DIG antibodies and the RNA used for cDNA synthesis, cloning and/or sequencing (Hsu et al., 2009). It is important in this technique that the pre-miRNA is processed into the miRNA by the cell extracts. E. Samal (personal communication) has bypassed this step and instead incubates extracts with mature miRNA labeled with biotin. Hsu et al. report disappointingly few clones for mRNAs (11 out of 465) but of those, more than half were for the same gene, subsequently verified as a target. Another potential pitfall of these methods is that the labeled miRNA in the RISC is exposed to the total RNA pool of the entire embryo, instead of its more limited endogenous context, so that potentially incorrect miRNA-mRNAs complexes may form and obscure the correct, *in vivo* targets. Samal has tried to address these issues by preparing extracts from only heart tissue for her analysis of *miR-1*. She has also controlled her experiment by comparing pools generated from *miR-1* depleted to wild-type embryos, to eliminate non-specific targets. These kinds of controls are important in evaluating the data obtained from these experiments.

The final class of biochemical techniques to attempt to identify *in vivo* miRNA-mRNA complexes relies on the Argonaute proteins as the catalysts of this process

(Easow et al., 2007). By immunoprecipitating Argonaute, both miRNAs and, to a lesser extent, their mRNA targets can be isolated and purified for subsequent reverse transcription, cloning and sequencing. Some methods use cross-linking to increase the number of protein-RNA complexes they purify (Chi et al., 2009). These methods produce a large amount of sequence or microarray data, because all miRNAs are pulled down indiscriminately. This is a disadvantage if one is focusing on the targets of a single miRNA, unless the miRNA in question is the predominant one in the starting sample. Comparing overexpression, wild-type, and knockdown samples could also address this issue. However, the technique has proven valuable at finding unpredicted targets (Easow et al., 2007).

I have attempted to replicate both the miRNA-primer method and the labeled-miRNA pull-down method in *Xenopus* in order to identify the targets of *miR-133b*, with minimal success. I found the primer method to be very difficult to optimize for the ideal detergent concentration and temperature that would allow first-strand synthesis from the endogenous miRNA primer. In addition, I have been unable to detect pre-miRNA processing in *Xenopus* extracts, which precludes the methods outlined by Hsu et al (2009), though troubleshooting this should be straightforward. Finally, I have attempted to pull-down miRNA-mRNA complexes using biotinylated mature *miR-133b*, but this also results in purification of RNAs that have no *miR-133b* sites. While I have not yet determined the correct stringency conditions that allow binding to only *miR-133b* targets instead of total RNA, I have made some progress by modulating the temperature at which extracts are incubated.

Results and Discussion

The earliest report that suggested a biochemical method for isolating miRNA targets for a specific miRNA was by Andachi (2008), in which he described the protocol for utilizing a miRNA as the primer for reverse transcription of an mRNA template. This process was dependent upon the removal of the RISC protein complex without disrupting the miRNA-mRNA interaction, for which the report suggests "short-term treatment with a strong detergent at low temperature." The first-strand synthesis was followed by reverse transcription of the second strand, whose products were digested by a 4-mer restriction enzyme and ligated to an adapter oligo. Two rounds of PCR amplification then followed, with the forward primer complementary to the 5' adapter and the reverse primer identical to the miRNA of interest. These PCR products were then cloned and sequenced. By modifying a protocol from Andachi (2008) (Chapter 2), I was able to visualize a smear of PCR products of ~1kb after the second PCR step, which is associated with an extending time of one minute (Figure 6.1A), but only with an annealing temperature of 55°C. In all subsequent experiments, PCRs were performed at either 55°C or 50°C. The results of these experiments were highly repeatable no matter the volume of starting material, as shown in Figures 6.1B and 6.1C. However, when these products were cloned into vectors and sequenced, no *X. tropicalis* genes were isolated (0/20). The most common sequence was derived from ligated adapters and/or primers, even though PCR products were purified over a Qiagen column between every step in order to remove un-ligated products.

This result suggests that there was no cDNA in the reactions that led into the PCR, which further indicates the miRNA-directed polymerization failed. Trouble-shooting this crucial step for the ideal temperature, detergent concentration, incubation time, etc. may prove exceedingly difficult and time-consuming, as the only step at which one can evaluate the efficacy of this procedure is when clones are sequenced, which requires numerous preceding steps and a significant investment in resources and time. Because of these difficulties, I decided to focus on other strategies that might identify miRNA targets biochemically.

Utilizing labeled pre-miRNAs to purify in vivo targets is another method I have attempted to reconstitute in *Xenopus*. According to Hsu et al. (2009), digoxigenin-labeled pre-miRNAs are processed and incorporated into RISC in cell extracts, allowing purification of miRNA-mRNA complexes by anti-dig antibodies. This method was intriguing because, unlike the RT-PCR method, it had verifiable results at intermediate steps before the endpoint of the reaction, so the progress of the reaction could be followed and ineffectual steps could be identified. These include analyzing the correct processing of the pre-miRNA into mature, 21-nucleotide product by Northern blot, and the association of dig-miRNA with the RISC complex by a Western blot for Argonaute. Figure 6.2A shows a Northern blot that demonstrates my ability to detect *miR-133b* specifically. However, using this Northern protocol, *miR-133b* cannot be detected in 10ug of total RNA from embryonic lysates. Dig-labeled pre-*miR-133b* does give a signal using this method (Figure 6.2B), and so it should be sufficient for identifying the products of its processing by cellular extracts. By following the procedure outlined in Hsu et al. (2009) with minor changes noted in Chapter 2, in three separate experiments I have never identified mature dig-labeled *miR-133b* processed from the pre-*miR-133b* precursor. This is true whether I blot for *miR-133b* (Figure 6.3C) or for digoxigenin (data not shown).

Several possibilities may explain lack of mature *miR-133b* product. It is possible that the minor changes I made to the protocol were actually major changes, and rendered the cellular extracts enzymatically inactive. In addition, it may be that the dig-labeled pre-*miR-133b* was too large to be correctly processed by the cellular extracts, or that processing takes longer than the allotted incubation time, so that the amount of mature product produced was too small to be detected. To determine if substrate size explains the failure to detect mature product, I will to synthesize a dig-labeled pre-miR-133 that is of shorter length (approximately 100nt), similar to that used in Hsu et al. (2009), for subsequent reactions. However, bypassing this initial step of miRNA processing by incubating with labeled mature miRNA may be just as beneficial.

Based on personal communications with E. Samal at the Gladstone Institute at the University of California, San Francisco, I attempted to purify *miR-133b* targets from extracts using a biotin-labeled mature *miR-133b* RNA. As a positive control, RNA encoding GFP but with perfect *miR-133b* recognition sites (133bUTR) was added to extracts. After incubation, purification, and reverse transcription, PCR analysis was performed in order to determine in which experimental conditions I co-purified control target (GFP) and a non-target RNA, *ornithine decarboxylase* (ODC). Initial results were promising, because 133bUTR was bound by the biotin-labeled *miR-133b* and purified by the streptavidin beads, with no control target ending up in the supernatant fraction (Figure 6.3A). This indicates that the purification of mRNAs with this procedure is possible.

However, the specificity of the reaction was not acceptable, as significant amounts of non-target RNAs were also purified (Figure 6.3A). As a control for sequence specificity, I then compared my perfect target (133bUTR) with a seed region mutated version (mut133bUTR). In ideal reaction conditions, the purification procedure will isolate only targets with near-perfect (or biologically relevant) seed sequences. In reactions performed at 30°C, there is no difference between the amount of 133bUTR and mut133bUTR isolated (Figure 6.3B). In addition, reactions are still co-purifying non-targets such as ODC. To verify this phenomenon of non-sequence-specific purification, the reaction was also performed with a scrambled biotin-labeled *miR-133b*, which should have no affinity for 133bUTR, mut133bUTR, or ODC. However, this scrambled RNA was still capable of isolating all of these RNAs, indicating that the reaction conditions are not resulting in sequence-specific binding, but rather all RNA is being isolated non-specifically (Figure 6.3B). I then tested whether altering the temperature of the reaction would increase the sequence specificity of the purification. I found that temperatures above 37°C were able to eliminate the purification of ornithine decarboxylase, but not of mut133bUTR (Figure 6.3C). This may be because mut133bUTR is still a good *miR-133b* target (only 4/21 nucleotide substitutions), or that there is much more mut133bUTR in the sample than any other single RNA, increasing its likelihood of binding, and therefore purification. Under these temperature conditions, a negative control GFP construct (GFP with miR-24a target sites – 24aUTR) was not purified to the same extent as 133bUTR, indicating more sequence specificity (Figure 6.3D). Interestingly, this sequence specificity requires cytoplasmic extracts, because 24aUTR and ODC are purified in equal amounts to 133bUTR when the reaction is performed in the absence of extracts (data not shown). This indicates that the biotin-labeled miRNA is likely being incorporated into RISC and thus behaving as an in vivo miRNA. Future experiments using these controls and the biotin-labeled scramble RNA will allow me to determine with confidence that the procedure I have developed is purifying only *miR-133b* targets.

Of the techniques I have tried and/or modified, the latter has so far shown the most promise, and shows I am making progress towards a fully outlined procedure for isolating *miR-133b* target mRNAs with little contaminant RNA. Unfortunately, this technique may be the least biologically relevant, because extracts are made from whole embryos and exogenous *miR-133b* is added into the system, which may lead to miRNA-mRNA complexes that do not exist in vivo. There are several ways to decrease or eliminate this potential problem. First, I could inject the biotin-labeled *miR-133b* into embryos and then use them for the subsequent extracts and purification, which would ensure that the complexes were formed in vivo. However, whole-embryo injection would mean that *miR-133b* would then be in tissues in which it is not normally expressed, which might lead to complexes that never exist in wild-type embryos. Alternatively, extracts could be prepared from only muscle tissue, although without a transgenic line this would be a formidable task. Another method might be to compare the RNA profile from wild-type embryos with those injected with *miR-133b* morpholino. This is predicted to increase the levels of *miR-133b* targets in vivo, which would then be reflected in increased RNA representation relative to wild-type extracts. Obviously, any putative targets would have to be verified by overexpression to recapitulate the 133bMO phenotype, or knockdown to rescue it, as well as by 3'UTR analysis.

Once a purification technique can be optimized, an outstanding issue is how best to analyze the miRNA target mRNAs once they are isolated by these techniques. Traditionally, and in the reports described here, RNAs are reverse transcribed into cDNA, which is then subcloned into vectors for sequencing. For comparative analysis between morphants and wild-type embryos, it might be better to hybridize the RNAs to a microarray. However, recent advances in sequencing have made it possible to sequence RNA directly with a huge number of reads, so that one can maximize coverage. RNA-seq is also quantitative because the number of reads reflects the amount of starting RNA, and can therefore be used for comparison between experimental conditions as long as appropriate standards are used (Wang et al., 2009).

Figure 6.1 Analysis of PCR products from miR-133-based RT-PCR
(A) First experiment with 10 starting embryos, PCR2 products run on an agarose gel with primer extension temperatures of 55°C in (Lane 1) and 60°C (Lane 2). (B) Second experiment with 10 starting embryos, PCR products run on an agarose gel from PCR1 and PCR2 with annealing temperature of either 55°C or 50°C. (C) Third experiment with 20 starting embryos, PCR products run on an agarose gel from PCR1 and PCR2 with annealing temperature of either 55°C or 50°C.

Figure 6.1

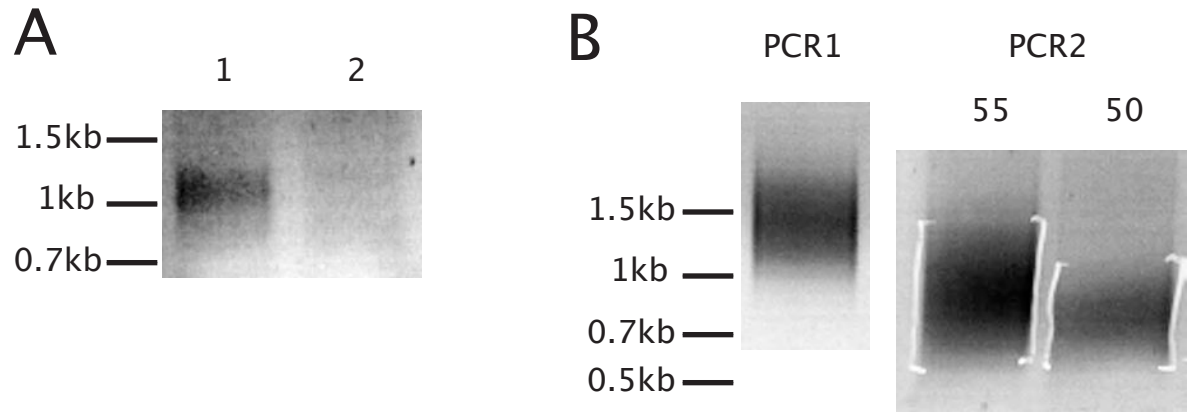
A
1
2
1.5kb
1kb
0.7kb
B
PCR1
PCR2
55
50
1.5kb
1kb
0.7kb
0.5kb
C
Lig
PCR1
PCR2
55
50
2.0kb
1.5kb
1kb
0.7kb
0.5kb

Figure 6.2 Dig-pre-*miR-133b* analysis by Northern blot
(A) Radioactive probe antisense to *miR-133b* hybridizes to *miR-133b* transferred from an agarose gel, but no signal is present from whole embryo RNA preparations (B) Both pre-*miR-133b* and mature miR-133 can be identified by Northern blotting with *miR-133b* probe. (C) There is no evidence of pre-*miR-133b* processing by cytoplasmic extracts.

Figure 6.2

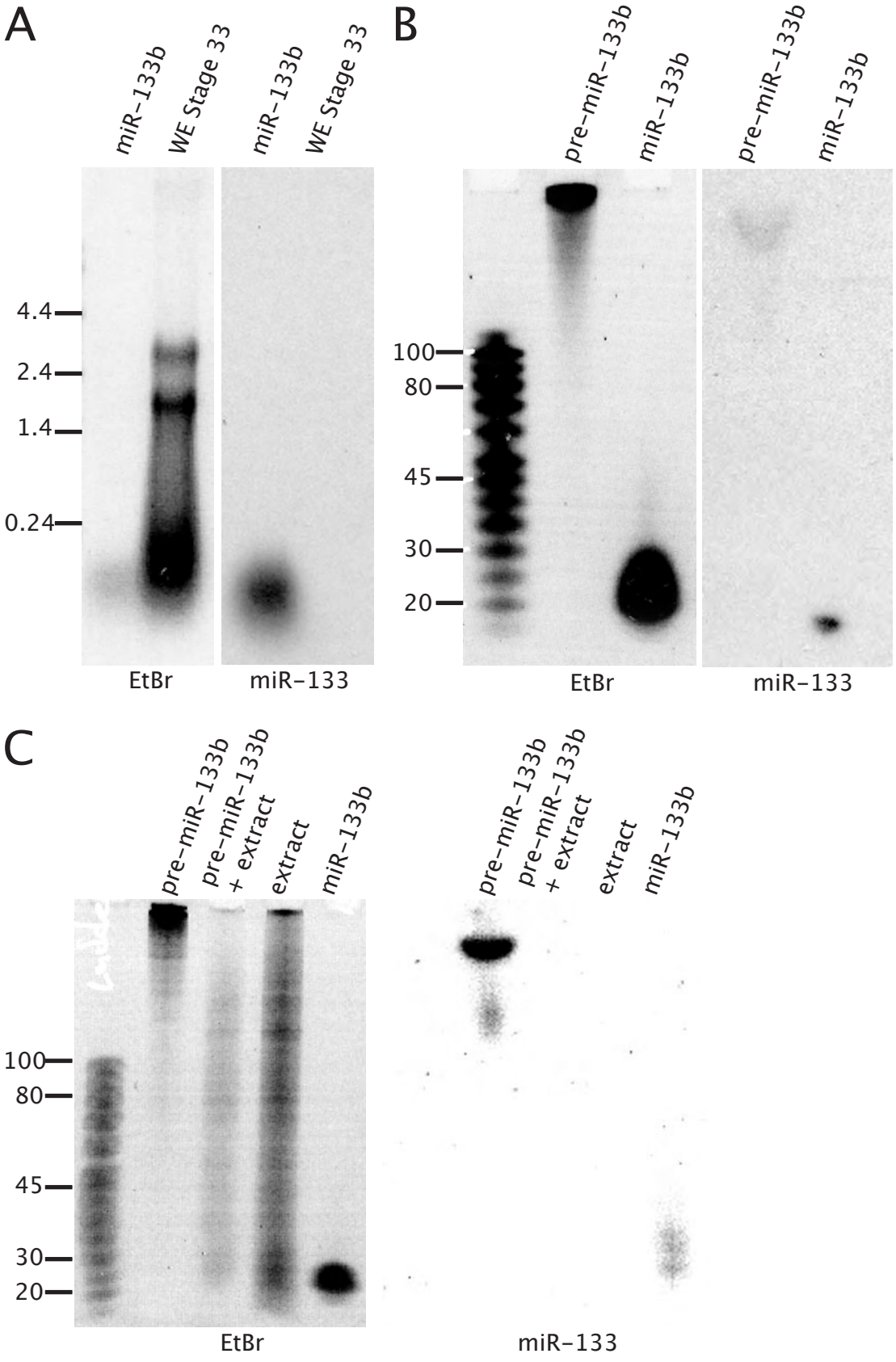
A
miR-133b
WE Stage 33
miR-133b
WE Stage 33
4.4
2.4
1.4
0.24
EtBr
miR-133
B
pre-miR-133b
miR-133b
pre-miR-133b
miR-133b
100
80
45
30
20
EtBr
miR-133
C
pre-miR-133b
pre-miR-133b + extract
extract
miR-133b
100
80
45
30
20
EtBr
pre-miR-133b
pre-miR-133b + extract
extract
miR-133b
miR-133

Figure 6.3 PCR results of biotin-labeled *miR-133b* immunopurification
(A) RNA coding for GFP with *miR-133b* sites in the 3'UTR and for ornithine decarboxylase (ODC) is purified from extracts by biotinylated *miR-133b*. (B) Mutating the *miR-133b* sites in the target RNA or the biotinylated miRNA has no effect on the immunopurification of GFP or ODC. (C) Increasing the temperature of biotin-*miR-133b* incubation with extracts reduces the amount of ODC pulled down by immunopurification. (D) Higher temperatures increase the stringency by which biotin-*miR-133b* immunopurifies GFP RNA with different 3'UTRs.

Figure 6.3

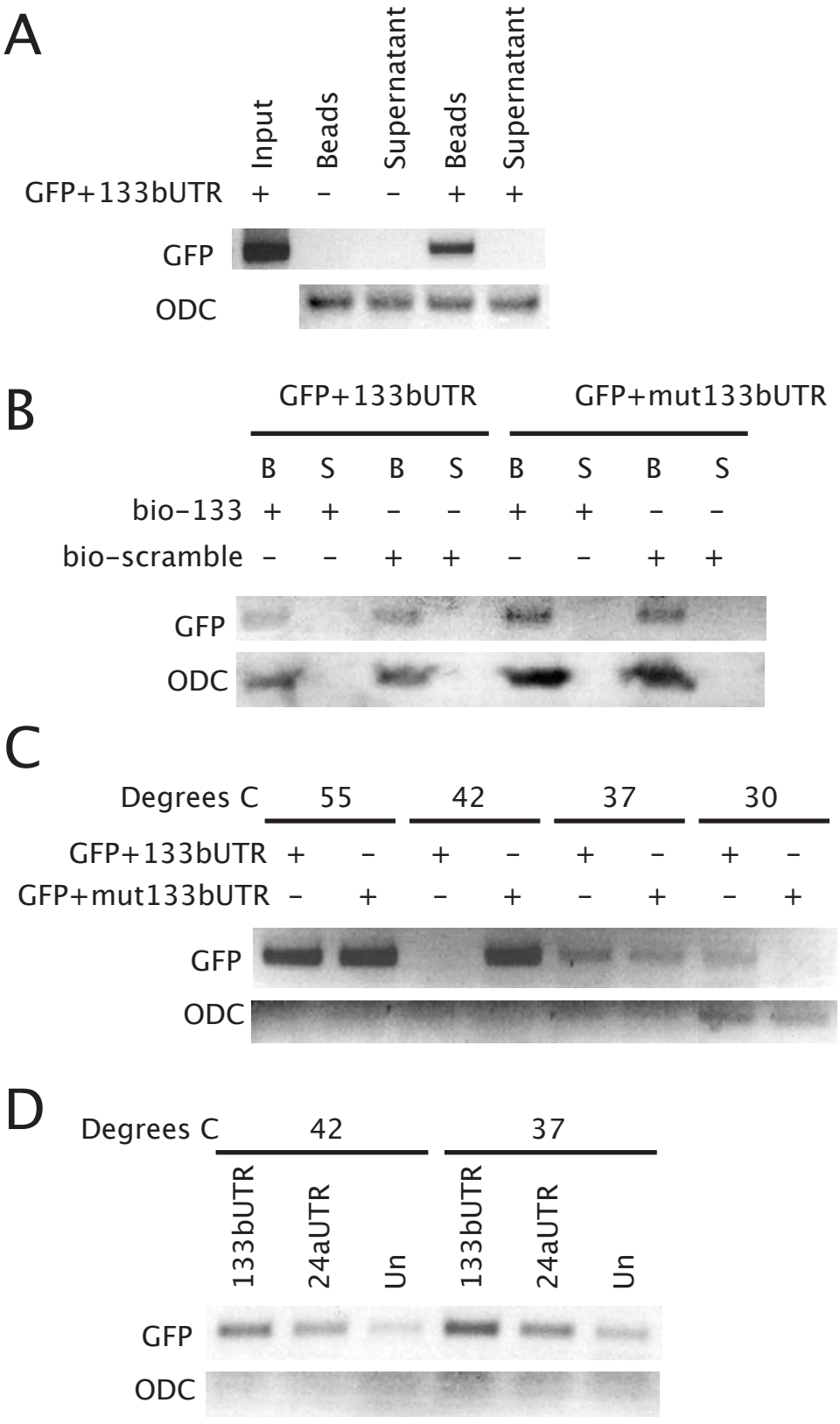
A
+ Input
– Beads
– Supernatant
+ Beads
+ Supernatant
GFP+133bUTR + – – + +
GFP
ODC
B
GFP+133bUTR
GFP+mut133bUTR
B S B S B S B S
bio-133 + + – – + + – –
bio-scramble – – + + – – + +
GFP
ODC
C
Degrees C 55 42 37 30
GFP+133bUTR + – + – + – + –
GFP+mut133bUTR – + – + – + – +
GFP
ODC
D
Degrees C 42 37
133bUTR
24aUTR
Un
133bUTR
24aUTR
Un
GFP
ODC

Appendix I.

Primers used to make pri-miRNA probes

Name	Primer 1	Primer 2
let-7a	TGGCGTTCCACACTTGTTAAGAC	CTCCCCCATCAAAAGCTCAATAAG
let-7c	GCTGCATTGCATTTGCCAAC	TTCACTCAATTAACCTTCCCTCTACTG
let-7e-2	GTCACTTTGTGGCACTGCTGTG	AGGAAAATTCCCTCCCCAATG
let-7f	CAACATCCTCCGTGCCTGTATC	CCCCTCCCTTTCGAGAGAAATC
let-7g	GGGAAAACATCTTCCTGAACG	TTGCTAGGGATTTAGTTGACCTTAC
let-7i	GTGTGCAAAAATTAGAGCATGACAG	CAGTCTGTGCCCCTTTACTTTG
mir-1a-1	GGAAACATCTTACCTTACAGC	CGGCATTTCCACGGAGGCAGG
mir-7-1	GCGCAGCCTCATTATGTAAGG	GTAACACTGAGAAAACTAGGC
mir-7-2	GGAGAAAGAAGGTACAGTG	GGCTACAAATGATATTGAAGTG
mir-9a-1	CACACGGGATTCTGGGAATC	GATCCAATCAGATGACTATG
mir-9a-2	GGAATTGTAGTCTGGGTTTTAG	GTCACTTTGGACTGGAATGGG
mir-9-3	CACACGGGATTCTGGGAATC	GATCCAATCAGATGACTATG
mir-9b	GTGTGCCTGTTTGTTTCTGC	GATATTTGAGGAAGGGAAGATG
mir-10b	GGGTTTGCTTTTCACATGG	CTCCTATTGTTCTATCCTGG
mir-10c	TGCCCTTAGCCTTCTGTCCTTATC	TAGCCTAAATGTGCCAGCGG
mir-16c	GGGGAGGATACAAAGATGGCTTC	GCTAAGGCATGTGAGAGAACTGGC
mir-18a	GATAATCCCAAGCATCCTAAAC	GAGCAAACAGTGAGTGTCC
mir-20a	CTTTCAGTATGTTTCAGTAGAG	GGTGATAATAGTCTAAGCTG
mir-22	TGCTTGATGTGTTGCTTCTCTCC	CCACCCTGGGACAATATGGTAGTC
mir-23a	GTGAACAGGTGCGAGAGTGAC	GTTCTCTGATAAATCTGTGGACTG
mir-23b	GCCTTCCATCCTTTCTGCTG	CACATGATAACTGCTGGGATG
mir-24a	CTTAGCTGATTGGTGAACAGTG	GGTAACGGAGGGAGAACTGG
mir-26a	GTGTTTTGTGTGACTGTGAC	CAGTGGAGATAGAGGGAAC
mir-29d	GCCCTTAGTCAATGGATATGC	CACGGTGTGTACCTCTAATCTGTAG
mir-30b	GAGGCACAATGCACTGAGATGG	TGACCACAGAAGCACAATGTTAGAG
mir-30c-1	CTGTGGCTGAGCTATGATAATCTG	GGAAACTTTGGCTAGGAATCAAG
mir-34a	TGCCTGCCGTTTTAATTCAGTC	ACAGTTAGCACCAACCATTGGG
mir-34b-3	TTCTGGTAAACGGAATCACTACACC	GCCATTTCCTGCAATTTTTAAGTGC
mir-34b-4	TTCAGAATACCTGGGACCTGGGTC	ACAACACTTTGGATCTAAATGCCAG
mir-92a-1	GTGTTACTGTTCCTTTAAGAG	CACTTGTAGCATTATATTGAC
mir-96	CAGCACCACAGAAGAAGAATACTGC	TGGAGGATGGATTAAGGGGC
mir-98	AAGCATCTGAATCCTCTGCTCG	GAATACCCCATTTGAACTGAGCC
mir-99	GACTCTCAAGCATTTCCCAACG	CATTGCCCTTTTTTCCCCTG
mir-100	TAAACACCGTAGCCAGAGCACC	TTCCACCAAGAGCAGAACAAAGTC
mir-103-1	GCCATTTGACCAGTAATCCAGTG	CCATGTTGGGTGTGGTTTAGTGC
mir-103-2	GGGCTCCTTACTGTCCTGTGTATG	AATGGCTGGGTTGCTGATGG
mir-124	GGGGATTGGGCAGGTGCGATTG	CACTGATGCAGATTTGTGGATAG
mir-125a	GGTGAATCCAGTCCATACACACGTAG	GGGGATGCAAAGCACAAGATATAAG
mir-125b-1	GGTGCTAAATGCAGCCGATG	GCGTTCAATAACCGATATGCAGTC
mir-125b-2	GGATCTTAAAACGCAAGGCAGC	TTCACTCTCGCAGACAACAGACAG

mir-129-2	TGAGTAAATGTGCCCCCTAGTGC	TCAGAAGAAAATCCTCCCTCGC
mir-130a	CCCATGTGCCAAAAAGCATAGC	CATGCTCTGTGTATTCTGGGCAG
mir-133b	GGAGCTGCTGCACCTTTGTG	CCCATTCACCTTTCCCTGCC
mir-135-1	CAGTGTATAACACAGGAAATGGCG	TGGCTTCCATCCCTACATGAGAC
mir-137-2	GCAAATTCCCCAACCATAGAAGG	TGCAAGCAGGAAAGAAGACATGAG
mir-143	TGGAAGCAGAGGAAATTGCG	CCAGCCATTATGGATTGCTCTC
mir-153-1	TGTTATTATCTAGGGGGTGCCTGTC	TAGGGACACTGGGAATGTTCGG
mir-153-2	GAAGGAGAACATCAAATTGGTGGC	GCACAGACAATAAATCAGCAGTGC
mir-181a-2	GCACACAATATGCTAAGACACTTTC	GTAAGGTAACCCAATCCTACAAAAC
mir-194-2	GCTGTGAGGATAGCCTGATGTAGTG	TCATATAGACGTTTCTGCCTGTGC
mir-196	ACCATGCCTTGCAGTCAGACAG	GAAAACCTAATGTCATTGCCCCAC
mir-199a	GTAGGGTGCGATATGAAAGCTGTAG	CTGGCTTGAAGATGAAATGACTGC
mir-200a	CTAGTGTTTGAATCCTCTGGGGAG	AGGCAAGGTGTTACAATGCTGTG
mir-210	CCCACCTGATTTATGTGTG	CAGCATCTGTCATTTTGTC
mir-214	CATAATCTCTTTGGCTTTGG	GCACTTAAACATAGGTTCAC
mir-217	TGAAGCCATTCCCACTAACGG	ATTGGTAGACCTTGCGGAGAGG
mir-218	AGCCAACGGAAAAGTTGCTTC	GACATCCCTGGTTTGTGTAACGAC
mir-219	GGAAGAGAACTGATGGCAATGACTG	GGAAGAGAACTGATGGCAATGACTG
mir-222	CATGCGATTTGCTTCAGGGG	CCAGCAGACAATGTAGCTGTTGC
mir-338-1	CATCTCTGGAACCATGAATAAG	CTGGGACTGTGTGCGTATTG

References

Aboobaker, A. A., Tomancak, P., Patel, N., Rubin, G. M. and Lai, E. C. (2005). Drosophila microRNAs exhibit diverse spatial expression patterns during embryonic development. *Proc Natl Acad Sci U S A* **102**, 18017-22.
Agrawal, R., Tran, U. and Wessely, O. (2009). The miR-30 miRNA family regulates Xenopus pronephros development and targets the transcription factor Xlim1/Lhx1. *Development* **136**, 3927-36.
Andachi, Y. (2008). A novel biochemical method to identify target genes of individual microRNAs: identification of a new Caenorhabditis elegans let-7 target. *RNA* **14**, 2440-51.
Andreatta, C., Nahreini, P., Hovland, A. R., Kumar, B., Edwards-Prasad, J. and Prasad, K. N. (2001). Use of short-lived green fluorescent protein for the detection of proteasome inhibition. *Biotechniques* **30**, 656-60.
Arora, A., McKay, G. J. and Simpson, D. A. (2007). Prediction and verification of miRNA expression in human and rat retinas. *Invest Ophthalmol Vis Sci* **48**, 3962-7.
Bagga, S., Bracht, J., Hunter, S., Massirer, K., Holtz, J., Eachus, R. and Pasquinelli, A. E. (2005). Regulation by let-7 and lin-4 miRNAs results in target mRNA degradation. *Cell* **122**, 553-63.
Bartel, D. P. (2004). MicroRNAs: genomics, biogenesis, mechanism, and function. *Cell* **116**, 281-97.
Bartel, D. P. (2009). MicroRNAs: target recognition and regulatory functions. *Cell* **136**, 215-33.
Bernstein, E., Kim, S. Y., Carmell, M. A., Murchison, E. P., Alcorn, H., Li, M. Z., Mills, A. A., Elledge, S. J., Anderson, K. V. and Hannon, G. J. (2003). Dicer is essential for mouse development. *Nat Genet* **35**, 215-7.
Biehlmaier, O., Neuhauss, S. C. and Kohler, K. (2001). Onset and time course of apoptosis in the developing zebrafish retina. *Cell Tissue Res* **306**, 199-207.
Brennecke, J., Stark, A., Russell, R. B. and Cohen, S. M. (2005). Principles of microRNA-target recognition. *PLoS Biol* **3**, e85.
Brivanlou, A. H. and Harland, R. M. (1989). Expression of an engrailed-related protein is induced in the anterior neural ectoderm of early Xenopus embryos. *Development* **106**, 611-7.
Carmell, M. A., Xuan, Z., Zhang, M. Q. and Hannon, G. J. (2002). The Argonaute family: tentacles that reach into RNAi, developmental control, stem cell maintenance, and tumorigenesis. *Genes Dev* **16**, 2733-42.
Cecconi, F., Alvarez-Bolado, G., Meyer, B. I., Roth, K. A. and Gruss, P. (1998). Apaf1 (CED-4 homolog) regulates programmed cell death in mammalian development. *Cell* **94**, 727-37.
Cecconi, F., Piacentini, M. and Fimia, G. M. (2008). The involvement of cell death and survival in neural tube defects: a distinct role for apoptosis and autophagy? *Cell Death Differ* **15**, 1170-7.
Chan, J. A., Krichevsky, A. M. and Kosik, K. S. (2005). MicroRNA-21 is an antiapoptotic factor in human glioblastoma cells. *Cancer Res* **65**, 6029-33.

Chen, J. F., Mandel, E. M., Thomson, J. M., Wu, Q., Callis, T. E., Hammond, S. M., Conlon, F. L. and Wang, D. Z. (2006). The role of microRNA-1 and microRNA-133 in skeletal muscle proliferation and differentiation. *Nat Genet* **38**, 228-33.
Cheng, A. M., Byrom, M. W., Shelton, J. and Ford, L. P. (2005). Antisense inhibition of human miRNAs and indications for an involvement of miRNA in cell growth and apoptosis. *Nucleic Acids Res* **33**, 1290-7.
Chi, S. W., Zang, J. B., Mele, A. and Darnell, R. B. (2009). Argonaute HITS-CLIP decodes microRNA-mRNA interaction maps. *Nature* **460**, 479-86.
Coffman, C., Harris, W. and Kintner, C. (1990). Xotch, the Xenopus homolog of Drosophila notch. *Science* **249**, 1438-41.
Damiani, D., Alexander, J. J., O'Rourke, J. R., McManus, M., Jadhav, A. P., Cepko, C. L., Hauswirth, W. W., Harfe, B. D. and Strettoi, E. (2008). Dicer inactivation leads to progressive functional and structural degeneration of the mouse retina. *J Neurosci* **28**, 4878-87.
Davis, T. H., Cuellar, T. L., Koch, S. M., Barker, A. J., Harfe, B. D., McManus, M. T. and Ullian, E. M. (2008). Conditional loss of Dicer disrupts cellular and tissue morphogenesis in the cortex and hippocampus. *J Neurosci* **28**, 4322-30.
de la Rosa, E. J. and de Pablo, F. (2000). Cell death in early neural development: beyond the neurotrophic theory. *Trends Neurosci* **23**, 454-8.
De Pietri Tonelli, D., Pulvers, J. N., Haffner, C., Murchison, E. P., Hannon, G. J. and Huttner, W. B. (2008). miRNAs are essential for survival and differentiation of newborn neurons but not for expansion of neural progenitors during early neurogenesis in the mouse embryonic neocortex. *Development* **135**, 3911-21.
Decembrini, S., Andreazzoli, M., Barsacchi, G. and Cremisi, F. (2008). Dicer inactivation causes heterochronic retinogenesis in Xenopus laevis. *Int J Dev Biol* **52**, 1099-103.
Deo, M., Yu, J. Y., Chung, K. H., Tippens, M. and Turner, D. L. (2006). Detection of mammalian microRNA expression by in situ hybridization with RNA oligonucleotides. *Dev Dyn* **235**, 2538-48.
Didiano, D. and Hobert, O. (2006). Perfect seed pairing is not a generally reliable predictor for miRNA-target interactions. *Nat Struct Mol Biol* **13**, 849-51.
Easow, G., Teleman, A. A. and Cohen, S. M. (2007). Isolation of microRNA targets by miRNP immunopurification. *RNA* **13**, 1198-204.
Erwin, D. H. and Davidson, E. H. (2002). The last common bilaterian ancestor. *Development* **129**, 3021-32.
Eulalio, A., Huntzinger, E. and Izaurralde, E. (2008). GW182 interaction with Argonaute is essential for miRNA-mediated translational repression and mRNA decay. *Nat Struct Mol Biol* **15**, 346-53.
Eulalio, A., Huntzinger, E., Nishihara, T., Rehwinkel, J., Fauser, M. and Izaurralde, E. (2009). Deadenylation is a widespread effect of miRNA regulation. *RNA* **15**, 21-32.
Gaze, R. M. and Grant, P. (1992). Spatio-temporal patterns of retinal ganglion cell death during Xenopus development. *J Comp Neurol* **315**, 264-74.
Giraldez, A. J., Cinalli, R. M., Glasner, M. E., Enright, A. J., Thomson, J. M., Baskerville, S., Hammond, S. M., Bartel, D. P. and Schier, A. F. (2005). MicroRNAs regulate brain morphogenesis in zebrafish. *Science* **308**, 833-8.

Giraldez, A. J., Mishima, Y., Rihel, J., Grocock, R. J., Van Dongen, S., Inoue, K., Enright, A. J. and Schier, A. F. (2006). Zebrafish MiR-430 promotes deadenylation and clearance of maternal mRNAs. *Science* **312**, 75-9.
Grammer, T. C., Liu, K. J., Mariani, F. V. and Harland, R. M. (2000). Use of large-scale expression cloning screens in the Xenopus laevis tadpole to identify gene function. *Dev Biol* **228**, 197-210.
Griffiths-Jones, S. (2006). miRBase: the microRNA sequence database. *Methods Mol Biol* **342**, 129-38.
Griffiths-Jones, S., Grocock, R. J., van Dongen, S., Bateman, A. and Enright, A. J. (2006). miRBase: microRNA sequences, targets and gene nomenclature. *Nucleic Acids Res* **34**, D140-4.
Griffiths-Jones, S., Saini, H. K., Dongen, S. V. and Enright, A. J. (2007). miRBase: tools for microRNA genomics. *Nucleic Acids Res*.
Griffiths-Jones, S., Saini, H. K., van Dongen, S. and Enright, A. J. (2008). miRBase: tools for microRNA genomics. *Nucleic Acids Res* **36**, D154-8.
Guerin, M. B., McKernan, D. P., O'Brien, C. J. and Cotter, T. G. (2006). Retinal ganglion cells: dying to survive. *Int J Dev Biol* **50**, 665-74.
Hakem, R., Hakem, A., Duncan, G. S., Henderson, J. T., Woo, M., Soengas, M. S., Elia, A., de la Pompa, J. L., Kagi, D., Khoo, W. et al. (1998). Differential requirement for caspase 9 in apoptotic pathways in vivo. *Cell* **94**, 339-52.
Hand, N. J., Master, Z. R., Eauclaire, S. F., Weinblatt, D. E., Matthews, R. P. and Friedman, J. R. (2009). The microRNA-30 family is required for vertebrate hepatobiliary development. *Gastroenterology* **136**, 1081-90.
Hartley, K. O., Hardcastle, Z., Friday, R. V., Amaya, E. and Papalopulu, N. (2001). Transgenic Xenopus embryos reveal that anterior neural development requires continued suppression of BMP signaling after gastrulation. *Dev Biol* **238**, 168-84.
He, L. and Hannon, G. J. (2004). MicroRNAs: small RNAs with a big role in gene regulation. *Nat Rev Genet* **5**, 522-31.
He, L., He, X., Lim, L. P., de Stanchina, E., Xuan, Z., Liang, Y., Xue, W., Zender, L., Magnus, J., Ridzon, D. et al. (2007a). A microRNA component of the p53 tumour suppressor network. *Nature* **447**, 1130-4.
He, L., He, X., Lowe, S. W. and Hannon, G. J. (2007b). microRNAs join the p53 network--another piece in the tumour-suppression puzzle. *Nat Rev Cancer* **7**, 819-22.
He, L., Thomson, J. M., Hemann, M. T., Hernando-Monge, E., Mu, D., Goodson, S., Powers, S., Cordon-Cardo, C., Lowe, S. W., Hannon, G. J. et al. (2005). A microRNA polycistron as a potential human oncogene. *Nature* **435**, 828-33.
Heller, N. and Brandli, A. W. (1997). Xenopus Pax-2 displays multiple splice forms during embryogenesis and pronephric kidney development. *Mech Dev* **69**, 83-104.
Hensey, C. and Gautier, J. (1997). A developmental timer that regulates apoptosis at the onset of gastrulation. *Mech Dev* **69**, 183-95.
Hino, K., Fukao, T. and Watanabe, M. (2007). Regulatory interaction of HNF1-alpha to microRNA-194 gene during intestinal epithelial cell differentiation. *Nucleic Acids Symp Ser (Oxf)*, 415-6.
Hopwood, N. D. and Gurdon, J. B. (1991). Gene activation in the amphibian mesoderm. *Dev Suppl* **1**, 95-104.

Hsu, R. J., Yang, H. J. and Tsai, H. J. (2009). Labeled microRNA pull-down assay system: an experimental approach for high-throughput identification of microRNA-target mRNAs. *Nucleic Acids Res* **37**, e77.
Humphreys, D. T., Westman, B. J., Martin, D. I. and Preiss, T. (2005). MicroRNAs control translation initiation by inhibiting eukaryotic initiation factor 4E/cap and poly(A) tail function. *Proc Natl Acad Sci U S A* **102**, 16961-6.
Hutvagner, G., McLachlan, J., Pasquinelli, A. E., Balint, E., Tuschl, T. and Zamore, P. D. (2001). A cellular function for the RNA-interference enzyme Dicer in the maturation of the let-7 small temporal RNA. *Science* **293**, 834-8.
Jiang, Q., Feng, M. G. and Mo, Y. Y. (2009). Systematic validation of predicted microRNAs for cyclin D1. *BMC Cancer* **9**, 194.
Kapsimali, M., Kloosterman, W. P., de Bruijn, E., Rosa, F., Plasterk, R. H. and Wilson, S. W. (2007). MicroRNAs show a wide diversity of expression profiles in the developing and mature central nervous system. *Genome Biol* **8**, R173.
Khvorova, A., Reynolds, A. and Jayasena, S. D. (2003). Functional siRNAs and miRNAs exhibit strand bias. *Cell* **115**, 209-16.
Kim, H. K., Lee, Y. S., Sivaprasad, U., Malhotra, A. and Dutta, A. (2006). Muscle-specific microRNA miR-206 promotes muscle differentiation. *J Cell Biol* **174**, 677-87.
Kintner, C. R. and Brockes, J. P. (1984). Monoclonal antibodies identify blastemal cells derived from dedifferentiating limb regeneration. *Nature* **308**, 67-9.
Kiriakidou, M., Tan, G. S., Lamprinaki, S., De Planell-Saguer, M., Nelson, P. T. and Mourelatos, Z. (2007). An mRNA m7G cap binding-like motif within human Ago2 represses translation. *Cell* **129**, 1141-51.
Kloosterman, W. P., Wienholds, E., de Bruijn, E., Kauppinen, S. and Plasterk, R. H. (2006). In situ detection of miRNAs in animal embryos using LNA-modified oligonucleotide probes. *Nat Methods* **3**, 27-9.
Koralov, S. B., Muljo, S. A., Galler, G. R., Krek, A., Chakraborty, T., Kanellopoulou, C., Jensen, K., Cobb, B. S., Merkenschlager, M., Rajewsky, N. et al. (2008). Dicer ablation affects antibody diversity and cell survival in the B lymphocyte lineage. *Cell* **132**, 860-74.
Krichevsky, A. M., Sonntag, K. C., Isacson, O. and Kosik, K. S. (2006). Specific microRNAs modulate embryonic stem cell-derived neurogenesis. *Stem Cells* **24**, 857-64.
Kruger, J. and Rehmsmeier, M. (2006). RNAhybrid: microRNA target prediction easy, fast and flexible. *Nucleic Acids Res* **34**, W451-4.
Lamb, T. M., Knecht, A. K., Smith, W. C., Stachel, S. E., Economides, A. N., Stahl, N., Yancopolous, G. D. and Harland, R. M. (1993). Neural induction by the secreted polypeptide noggin. *Science* **262**, 713-8.
Lee, J. E., Hollenberg, S. M., Snider, L., Turner, D. L., Lipnick, N. and Weintraub, H. (1995). Conversion of Xenopus ectoderm into neurons by NeuroD, a basic helix-loop-helix protein. *Science* **268**, 836-44.
Lee, R., Feinbaum, R. and Ambros, V. (2004). A short history of a short RNA. *Cell* **116**, S89-92, 1 p following S96.
Lee, Y., Jeon, K., Lee, J. T., Kim, S. and Kim, V. N. (2002). MicroRNA maturation: stepwise processing and subcellular localization. *EMBO J* **21**, 4663-70.

Liu, J., Rivas, F. V., Wohlschlegel, J., Yates, J. R., 3rd, Parker, R. and Hannon, G. J. (2005). A role for the P-body component GW182 in microRNA function. *Nat Cell Biol* **7**, 1261-6.
Liu, N., Bezprozvannaya, S., Williams, A. H., Qi, X., Richardson, J. A., Bassel-Duby, R. and Olson, E. N. (2008). microRNA-133a regulates cardiomyocyte proliferation and suppresses smooth muscle gene expression in the heart. *Genes Dev* **22**, 3242-54.
Lund, E., Guttinger, S., Calado, A., Dahlberg, J. E. and Kutay, U. (2004). Nuclear export of microRNA precursors. *Science* **303**, 95-8.
Lund, E., Liu, M., Hartley, R. S., Sheets, M. D. and Dahlberg, J. E. (2009). Deadenylation of maternal mRNAs mediated by miR-427 in Xenopus laevis embryos. *RNA*.
Lupo, G., Andreazzoli, M., Gestri, G., Liu, Y., He, R. Q. and Barsacchi, G. (2000). Homeobox genes in the genetic control of eye development. *Int J Dev Biol* **44**, 627-36.
Lynn, F. C., Skewes-Cox, P., Kosaka, Y., McManus, M. T., Harfe, B. D. and German, M. S. (2007). MicroRNA expression is required for pancreatic islet cell genesis in the mouse. *Diabetes* **56**, 2938-45.
Lytle, J. R., Yario, T. A. and Steitz, J. A. (2007). Target mRNAs are repressed as efficiently by microRNA-binding sites in the 5' UTR as in the 3' UTR. *Proc Natl Acad Sci U S A* **104**, 9667-72.
Ma, Q., Kintner, C. and Anderson, D. J. (1996). Identification of neurogenin, a vertebrate neuronal determination gene. *Cell* **87**, 43-52.
Mansfield, J. H., Harfe, B. D., Nissen, R., Obenauer, J., Srineel, J., Chaudhuri, A., Farzan-Kashani, R., Zuker, M., Pasquinelli, A. E., Ruvkun, G. et al. (2004). MicroRNA-responsive 'sensor' transgenes uncover Hox-like and other developmentally regulated patterns of vertebrate microRNA expression. *Nat Genet* **36**, 1079-83.
Mariani, F. V. and Harland, R. M. (1998). XBF-2 is a transcriptional repressor that converts ectoderm into neural tissue. *Development* **125**, 5019-31.
Martello, G., Zacchigna, L., Inui, M., Montagner, M., Adorno, M., Mamidi, A., Morsut, L., Soligo, S., Tran, U., Dupont, S. et al. (2007). MicroRNA control of Nodal signalling. *Nature* **449**, 183-8.
Martin, B. L. and Harland, R. M. (2001). Hypaxial muscle migration during primary myogenesis in Xenopus laevis. *Dev Biol* **239**, 270-80.
Martin, B. L. and Harland, R. M. (2006). A novel role for lbx1 in Xenopus hypaxial myogenesis. *Development* **133**, 195-208.
Martin, B. L., Peyrot, S. M. and Harland, R. M. (2007). Hedgehog signaling regulates the amount of hypaxial muscle development during Xenopus myogenesis. *Dev Biol* **304**, 722-34.
Mathers, P. H., Grinberg, A., Mahon, K. A. and Jamrich, M. (1997). The Rx homeobox gene is essential for vertebrate eye development. *Nature* **387**, 603-7.
Mayordomo, R., Valenciano, A. I., de la Rosa, E. J. and Hallbook, F. (2003). Generation of retinal ganglion cells is modulated by caspase-dependent programmed cell death. *Eur J Neurosci* **18**, 1744-50.
Mishima, Y., Abreu-Goodger, C., Staton, A. A., Stahlhut, C., Shou, C., Cheng, C., Gerstein, M., Enright, A. J. and Giraldez, A. J. (2009). Zebrafish miR-1 and miR-133

shape muscle gene expression and regulate sarcomeric actin organization. *Genes Dev* **23**, 619-32.
Murchison, E. P., Stein, P., Xuan, Z., Pan, H., Zhang, M. Q., Schultz, R. M. and Hannon, G. J. (2007). Critical roles for Dicer in the female germline. *Genes Dev* **21**, 682-93.
Nagasawa, Y., Matthiesen, S., Onuchic, L. F., Hou, X., Bergmann, C., Esquivel, E., Senderek, J., Ren, Z., Zeltner, R., Furu, L. et al. (2002). Identification and characterization of Pkhd1, the mouse orthologue of the human ARPKD gene. *J Am Soc Nephrol* **13**, 2246-58.
Nieuwkoop, P. D. and Faber, J. (1994). Normal table of Xenopus laevis (Daudin) : a systematical and chronological survey of the development from the fertilized egg till the end of metamorphosis. New York: Garland Pub.
O'Driscoll, C., Donovan, M. and Cotter, T. G. (2006). Analysis of apoptotic and survival mediators in the early post-natal and mature retina. *Exp Eye Res* **83**, 1482-92.
O'Rourke, J. R., Georges, S. A., Seay, H. R., Tapscott, S. J., McManus, M. T., Goldhamer, D. J., Swanson, M. S. and Harfe, B. D. (2007). Essential role for Dicer during skeletal muscle development. *Dev Biol* **311**, 359-68.
Olsen, P. H. and Ambros, V. (1999). The lin-4 regulatory RNA controls developmental timing in Caenorhabditis elegans by blocking LIN-14 protein synthesis after the initiation of translation. *Dev Biol* **216**, 671-80.
Onichtchouk, D., Gawantka, V., Dosch, R., Delius, H., Hirschfeld, K., Blumenstock, C. and Niehrs, C. (1996). The Xvent-2 homeobox gene is part of the BMP-4 signalling pathway controlling [correction of controling] dorsoventral patterning of Xenopus mesoderm. *Development* **122**, 3045-53.
Papalopulu, N. and Kintner, C. (1996). A posteriorising factor, retinoic acid, reveals that anteroposterior patterning controls the timing of neuronal differentiation in Xenopus neuroectoderm. *Development* **122**, 3409-18.
Penaloza, C., Orlanski, S., Ye, Y., Entezari-Zaher, T., Javdan, M. and Zakeri, Z. (2008). Cell death in mammalian development. *Curr Pharm Des* **14**, 184-96.
Pillai, R. S., Bhattacharyya, S. N., Artus, C. G., Zoller, T., Cougot, N., Basyuk, E., Bertrand, E. and Filipowicz, W. (2005). Inhibition of translational initiation by Let-7 MicroRNA in human cells. *Science* **309**, 1573-6.
Place, R. F., Li, L. C., Pookot, D., Noonan, E. J. and Dahiya, R. (2008). MicroRNA-373 induces expression of genes with complementary promoter sequences. *Proc Natl Acad Sci U S A* **105**, 1608-13.
Qiu, R., Liu, Y., Wu, J. Y., Liu, K., Mo, W. and He, R. (2009). Misexpression of miR-196a induces eye anomaly in Xenopus laevis. *Brain Res Bull* **79**, 26-31.
Rao, P. K., Kumar, R. M., Farkhondeh, M., Baskerville, S. and Lodish, H. F. (2006). Myogenic factors that regulate expression of muscle-specific microRNAs. *Proc Natl Acad Sci U S A* **103**, 8721-6.
Rehwinkel, J., Behm-Ansmant, I., Gatfield, D. and Izaurralde, E. (2005). A crucial role for GW182 and the DCP1:DCP2 decapping complex in miRNA-mediated gene silencing. *RNA* **11**, 1640-7.
Richter, K., Grunz, H. and Dawid, I. B. (1988). Gene expression in the embryonic nervous system of Xenopus laevis. *Proc Natl Acad Sci U S A* **85**, 8086-90.

Rosa, A., Spagnoli, F. M. and Brivanlou, A. H. (2009). The miR-430/427/302 family controls mesendodermal fate specification via species-specific target selection. *Dev Cell* **16**, 517-27.
Ruby, J. G., Jan, C. H. and Bartel, D. P. (2007). Intronic microRNA precursors that bypass Drosha processing. *Nature* **448**, 83-6.
Ruvkun, G., Wightman, B. and Ha, I. (2004). The 20 years it took to recognize the importance of tiny RNAs. *Cell* **116**, S93-6, 2 p following S96.
Sempere, L. F., Freemantle, S., Pitha-Rowe, I., Moss, E., Dmitrovsky, E. and Ambros, V. (2004). Expression profiling of mammalian microRNAs uncovers a subset of brain-expressed microRNAs with possible roles in murine and human neuronal differentiation. *Genome Biol* **5**, R13.
Shkumatava, A., Stark, A., Sive, H. and Bartel, D. P. (2009). Coherent but overlapping expression of microRNAs and their targets during vertebrate development. *Genes Dev* **23**, 466-81.
Sive, H. L., Grainger, R. M. and Harland, R. M. (2000). Early development of Xenopus laevis : a laboratory manual. Cold Spring Harbor, N.Y.: Cold Spring Harbor Laboratory Press.
Smirnova, L., Grafe, A., Seiler, A., Schumacher, S., Nitsch, R. and Wulczyn, F. G. (2005). Regulation of miRNA expression during neural cell specification. *Eur J Neurosci* **21**, 1469-77.
Stack, J. H. and Newport, J. W. (1997). Developmentally regulated activation of apoptosis early in Xenopus gastrulation results in cyclin A degradation during interphase of the cell cycle. *Development* **124**, 3185-95.
Takaya, T., Ono, K., Kawamura, T., Takanabe, R., Kaichi, S., Morimoto, T., Wada, H., Kita, T., Shimatsu, A. and Hasegawa, K. (2009). MicroRNA-1 and MicroRNA-133 in spontaneous myocardial differentiation of mouse embryonic stem cells. *Circ J* **73**, 1492-7.
Takayama, E., Higo, T., Kai, M., Fukasawa, M., Nakajima, K., Hara, H., Tadakuma, T., Igarashi, K., Yaoita, Y. and Shiokawa, K. (2004). Involvement of caspase-9 in execution of the maternal program of apoptosis in Xenopus late blastulae overexpressed with S-adenosylmethionine decarboxylase. *Biochem Biophys Res Commun* **325**, 1367-75.
Tang, G. Q. and Maxwell, E. S. (2008). Xenopus microRNA genes are predominantly located within introns and are differentially expressed in adult frog tissues via post-transcriptional regulation. *Genome Res* **18**, 104-12.
Thomsen, G., Woolf, T., Whitman, M., Sokol, S., Vaughan, J., Vale, W. and Melton, D. A. (1990). Activins are expressed early in Xenopus embryogenesis and can induce axial mesoderm and anterior structures. *Cell* **63**, 485-93.
Vatolin, S., Navaratne, K. and Weil, R. J. (2006). A novel method to detect functional microRNA targets. *J Mol Biol* **358**, 983-96.
Vatolin, S. and Weil, R. J. (2008). Chapter 17. Extension of endogenous primers as a tool to detect micro-RNA targets. *Methods Enzymol* **449**, 357-71.
Vecino, E., Hernandez, M. and Garcia, M. (2004). Cell death in the developing vertebrate retina. *Int J Dev Biol* **48**, 965-74.
Vella, M. C., Reinert, K. and Slack, F. J. (2004). Architecture of a validated microRNA::target interaction. *Chem Biol* **11**, 1619-23.

Vernon, A. E., Devine, C. and Philpott, A. (2003). The cdk inhibitor p27Xic1 is required for differentiation of primary neurones in Xenopus. *Development* **130**, 85-92.
Walker, J. C. and Harland, R. M. (2008). Expression of microRNAs during embryonic development of Xenopus tropicalis. *Gene Expr Patterns* **8**, 452-6.
Wallace, D. M. and Cotter, T. G. (2008). Histone deacetylase activity in conjunction with E2F-1 and p53 regulates Apaf-1 expression in 661W cells and the retina. *J Neurosci Res*.
Wallace, D. M., Donovan, M. and Cotter, T. G. (2006). Histone deacetylase activity regulates apaf-1 and caspase 3 expression in the developing mouse retina. *Invest Ophthalmol Vis Sci* **47**, 2765-72.
Wang, Z., Gerstein, M. and Snyder, M. (2009). RNA-Seq: a revolutionary tool for transcriptomics. *Nat Rev Genet* **10**, 57-63.
Watanabe, T., Takeda, A., Mise, K., Okuno, T., Suzuki, T., Minami, N. and Imai, H. (2005). Stage-specific expression of microRNAs during Xenopus development. *FEBS Lett* **579**, 318-24.
Watanabe, Y., Tomita, M. and Kanai, A. (2007). Computational methods for microRNA target prediction. *Methods Enzymol* **427**, 65-86.
Woodland, H. R. and Jones, E. A. (1987). The development of an assay to detect mRNAs that affect early development. *Development* **101**, 925-30.
Wu, L., Fan, J. and Belasco, J. G. (2006). MicroRNAs direct rapid deadenylation of mRNA. *Proc Natl Acad Sci U S A* **103**, 4034-9.
Xu, P., Guo, M. and Hay, B. A. (2004). MicroRNAs and the regulation of cell death. *Trends Genet* **20**, 617-24.
Yang, W. J., Yang, D. D., Na, S., Sandusky, G. E., Zhang, Q. and Zhao, G. (2005). Dicer is required for embryonic angiogenesis during mouse development. *J Biol Chem* **280**, 9330-5.
Yin, V. P., Thomson, J. M., Thummel, R., Hyde, D. R., Hammond, S. M. and Poss, K. D. (2008). Fgf-dependent depletion of microRNA-133 promotes appendage regeneration in zebrafish. *Genes Dev* **22**, 728-33.
Zhao, H., Rebbert, M. L. and Dawid, I. B. (2007a). Myoskeletin, a factor related to Myocardin, is expressed in somites and required for hypaxial muscle formation in Xenopus. *Int J Dev Biol* **51**, 315-20.
Zhao, Y., Ransom, J. F., Li, A., Vedantham, V., von Drehle, M., Muth, A. N., Tsuchihashi, T., McManus, M. T., Schwartz, R. J. and Srivastava, D. (2007b). Dysregulation of cardiogenesis, cardiac conduction, and cell cycle in mice lacking miRNA-1-2. *Cell* **129**, 303-17.
Zuker, M. (2003). Mfold web server for nucleic acid folding and hybridization prediction. *Nucleic Acids Res* **31**, 3406-15.